ERASMUS UNIVERSITEIT ROTTERDAM
ERASMUS SCHOOL OF ECONOMICS

transtrend

Master's Thesis in Quantitative Finance

The Efficiency of Opening Auctions: An Econometric Approach

Author:
van der Ham, R., 434028

Supervisor ESE:
Prof. dr. C. Zhou

Date:
January 15, 2020

Supervisor Transtrend:
MSc. D. Stolwijk

Abstract

This paper tests different auction designs within the call auction class using around the clock 5-minute price dynamics of stocks listed on the FTSE or S&P/ASX 200 index. We propose a structural model that allows for various features in high frequency time series for stock prices, including unobserved price dynamics, multiple persistent stochastic volatility factors, correlated jumps across prices and volatilities, the leverage effect, daily patterns, Monday open effects, and heavy-tailed error distributions. We show that the Australian Security Exchange (ASX) utilises a superior auction design over the Johannesburg Stock Exchange (JSE) in terms of reducing opening price volatility, reducing over-weekend price uncertainty, pre-open market price discovery, and auction price efficiency. We, however, show that none of the two auction designs is sufficient in producing a consensus and stable opening price. Lastly, enticing more active auction participants is a key factor in managing an effective call auction.

Keywords— Call Auction Efficiency, Price Dynamics Modelling, Multi-Factor Stochastic Volatility, Leverage Effect, Bayesian Inference

Author's email address: 434028rh@student.eur.nl

Contents

1 Introduction

Before the emergence of electronic trading technology, traders participated in a visually, and often chaotic, live securities auction process, known as an open outcry. Buyers and sellers of certain securities assembled on the trading floor before the opening of the market and evolved an accurate idea of securities' opening prices. The trading world sustained leading developments ever since due to the rise of new technologies. The most prominent change has been the switch from physical to online trading, where market participants, nowadays, enter orders through an online platform. Although it has the advantage of matching buyers and sellers globally, which is assumed to increase market efficiency, it also raises the problem of inaccurate openings prices at the market open. Without having market participants gathering on trading floors, before actual transactions start, sentient price discovery has disappeared.

Nowadays, the majority of exchanges offer an electronic call auction prior to the market open. In contrast with continuous trading, it is an order-driven platform that batches numerous orders for simultaneous execution at a single price. The actual execution, also referred to as the uncrossing phase, occurs at a predetermined point in time, utilised by a predetermined matching algorithm. Market openings are important in particular, as the fundamental prices must be discovered, preferably before trading resumes, after the overnight close. However, the number of auction participants is rather low and market prices fluctuate heavily shortly after market open. Hence, it is questionable whether auction algorithms perform adequately in serving its main goal of realising stable opening prices.

In this paper, we examine the efficiency of two types of auction mechanisms, which are utilised by the Johannesburg Stock Exchange (JSE) and the Australian Securities Exchange (ASX). In particular, we study to which extent the determined auction price accurately reflects the underlying market price and whether existing call designs realise sufficient pre-open price discovery and opening price stability. We define an efficient auction as a platform that attracts sufficient active participants, where a stable equilibrium price is determined prior to the opening of the market, which represents the true security's value. Analytically, an efficient call produces opening prices that (i) have no significant increase in early market open price volatility, (ii) absorbed a large proportion of daily price discovery during the auction time span, and (iii) accurately reflect the underlying market price. In addition, we analyse which of the two auction procedures is superior in all three targets. Knowledge about the performance of auction mechanisms on opening price efficiency would benefit any market participant concerned with price informativeness. This also includes traders and policymakers exploring determinants of efficient price processes. Moreover, many financial institutions, such as market makers, hedge funds, and exchanges, opt for "fair" prices for their customers. Insight in opening auctions and their efficiency

would shed more light on the fairness of opening prices and whether these indeed maximise the trades in a supply and demand equilibrium.

We exploit the price volatility that arises at the market open by building a flexible model that enables us to fit the complexities that characterise high-frequent intraday data. We propose an Extended Unobserved Components model including stochastic diffusion terms, which are often present in intraday return data. This model captures two important features; (i) the the underlying latent price evolution and (ii) the increase in price volatility during the market open. We use the first to test whether the observed stock prices converge to fundamental values before the market opens. The second we use to test the opening price stability. Both provide us with evidence of auction efficiency.

Our study focuses on stocks listed on either the FTSE or S&P/ASX 200 index. The first sample summarises the Johannesburg Stock Exchange, while the second encompasses the Australian Security Exchange. We find strong evidence of multiple volatility components and complicated shocks. Fitting the model on our sample data gives a few striking results. Existing auction designs are not sufficient in realising accurate and stable consensus opening prices. The volatility shortly after market open increases by 18 and 25 percent for the ASX and JSE, respectively, implying opening price instability. Second, over-weekend effects significantly increases price uncertainty. Lastly, not all necessary information is incorporated in the opening price and the auction price does, on average, not converge to the true underlying market price. We, however, find that the ASX auction process is superior in (i) finding a more stable opening price, (ii) discovering a larger proportion of total price discover before the opening of the market, and (iii) accurately reflecting the true underlying market price.

Since markets implement call auction designs to determine opening and/or closing prices, researchers examined the benefits of a call auction relatively to continuous markets. Pagano and Schwartz (2003) show that a call auction mechanism may benefit conform reducing trading costs and would enhance price discovery. Corresponding to this study, Ellul et al. (2005) and Barclay and Hendershott (2008) show that pre-open trading contributes to the efficiency of opening prices. However exchanges opt for volume maximisation, Mccormick (2001) shows that this might not be appropriate, as only a small percentage of all orders entered during the pre-open phase execute. He relates these depressing execution numbers to rising frustrations of traders, such that the price discovery process is rather meaningless.

Additionally to the matching algorithm of the auction process, transparency is another important feature in call auction designs and may influence opening price efficiency. Economides and Schwartz (1995), Pagano and Röell (1996), and Domowitz and Madhavan (2001) discuss the impact of transparency and argue that deficiency in transparency may attract cognisant traders, which could reduce liquidity and increase price volatility. Moreover, they argue that redundant price transparency would

diminish opening call auction efficiency, as market participants have the anxiety of revealing their information by placing orders. This arises as a trade-off between encouraging liquidity by increasing transparency and preventing traders from deterring by doing the opposite.

Although the majority of exchanges utilise similar call auction designs, small differences could have a significant impact on price efficiency. Market participants seek for nimble trading strategies and could misrepresent their true supply and demand to influence the opening price in their favour. Therefore, strategic entering of orders may obscure price discovery and reduce the accuracy of opening prices (see e.g. Rustichini et al., 1994, Biais et al., 1999, and Medrano and Vives, 2001).

Existing literature has frequently exploited variance ratios and standard unbiasedness regressions to test the impact of auction algorithms on return volatility and opening price efficiency, respectively (see for example Comerton-Forde and Rydge, 2006 and Amihud and Mendelson, 1991). These analyses are convenient to examine the effect of changes in auction mechanisms within a specific market. Compared to these studies, we argue that our method is more robust for auction efficiency tests and comparisons across markets.

While several papers examined the efficiency of call auctions or studied the impact of changes in opening auctions designs on price discovery within specific markets, there are no published papers that empirically examine the dissimilarities in auction mechanisms across different exchanges. We propose an efficient framework which can be used by analysts to test auction performances. We do not assume that observed exchange prices converge to their true underlying market price, which is assumed for conveniences in other studies. Second, our framework enables researchers and practitioners to analyse market heterogeneity in terms of auction processes. The main difficulty of matching distinctive markets is that their securities are often not listed on multiple exchanges. The aforementioned studies make use of simple, but generally strong, price efficiency testing methods. These can not be applied for our purpose in comparing unique call designs.

Studies by Bates (2000), Duffie et al. (2000), Eraker et al. (2003), and Todorov (2011) highlight the importance of considering stochastic volatility and stochastic jumps, in both observed security prices and its volatility. Systematic Markov Chain Monte Carlo simulations are established for stochastic volatility models (see e.g. Omori et al., 2007, Nakajima and Omori, 2009, and Stroud and Johannes, 2014). We extend these methods by including latent price processes. Moreover, we adopt such an extensive model to test the efficiency of opening auctions. We, therefore, extend the current literature not only by introducing an improved method to measure efficiency discrepancies across markets but also by giving a detailed description of sampling procedures for our extended stochastic volatility model.

The remainder layout of this paper is as follows. In Section 2 we describe the different auction

processes we study in this paper and summarise institutional details of the JSE and ASX. In Section 3 we discuss the data. Section 4 gives a detailed description of our proposed model, its estimation algorithm, and prove its validation by a simulation study. Section 5 tests and compares the auction design efficiencies. These tests are subdivided into three main categories: opening price stability, pre-open price discovery, and auction price efficiency. All three pin down to the performance of call designs. Lastly, Section 6 concludes.

2 Preliminaries and Institutional Backgrounds

In the recent ten to twenty years, the single price batch auction, more generally referred to as a call auction, is a trading mechanism that has been implemented by, to our knowledge, almost all exchanges around the globe. During the pre-open of the market, orders can be entered or modified, but no matching or physical trading occurs. Market participants quote different prices for all types of securities listed on the exchange and enter such orders before the market open. The exchange uses the order book to set an auction price on which the security will open. The main goal is to find a fair and stable opening price and to reduce the chance that a single order could raise or lower the opening price exceedingly, which enables a market participant to be the arbitrator of the price. In this research, we examine whether the determined opening valuation is indeed a good reflection of the true underlying market price. Economides and Schwartz (1995) already shows that the use of a call auction enhances price discovery and reduces price volatility after a non-trading period. However, their research is in comparison with alternative auction mechanisms, but it does not examine the contrast within the class of call auction designs.

Due to its efficiency, relative to other mechanisms, call auctions are implemented by exchanges all around the world and are argued to attract a large proportion of intraday trading activities. Biais et al. (1999) and Madhavan and Panchapagesan (2000) show that one-tenth of the average daily trade value is traded at the market open for the Paris Bourse and New York Stock Exchange (NYSE), respectively. Therefore, the opening price is important for many financial institutions. Given that call auctions are more effective than alternative structures, it raises the question whether there are efficiency differences within the class of call auction designs. In this study, we consider the opening price settlement algorithms of the ASX and JSE. Both differ in call auction procedures, which could lead to disparities in the opening price evolution. We expect the Australian exchange to have a superior auction algorithm, which is more likely to produce efficient opening prices. However, we also believe that call designs are not sufficient in finding stable and accurate opening prices. To underpin our hypothesises, we describe both auction algorithms in more detail.

In 1997, the ASX was one of the first markets to incorporate a call auction to determine opening and closing prices. Since then, the process has undergone some substantial changes. Nowadays, its price-setting process follows four basic principles. Principle 1 determines the maximum trading value. If more than one price maximises the matching quantity of the order book, the process considers principle 2. Principle 2 considers the prices that maximise the trading volume and picks the price, within this range, that minimises the order imbalances. That is the price where the difference between the cumulative sum of bids and offers, sorted on price, is minimised. If there is more than one price in the order book that minimises the non-matching quantity, principle 3 is included. Principle 3 considers the prices within the range of trading value maximisation and order-imbalances minimisation and sets the auction price at the highest of these prices if the order imbalances attract buy volume, and vice versa. Hence, if there are more cumulative bids than offers in the subset, then the highest price is chosen and vice versa. If an equivalent buy and sell surplus are present at the aforementioned range, principle 4 is considered. Principle 4 settles the opening price that is closest to the reference price, which is the previous closing price. If the reference price is within the range of these considered prices, the auction price is set to the reference price. An example of the full procedure is given in Appendix A and considers all four principles for more clarity.

Similar to the ASX, the JSE conducts a volume maximising algorithm to determine the opening price. However, the details are quite different from the aforementioned basic principles. As there could be multiple price levels that maximise the trading volume, the JSE auction process seeks multiple price equilibria. The ASX solves this difficulty by including the remaining three principles. Alternatively, the JSE utilises a time ordering priority. The first entered bid (offer) will be filled if an entered offer (bid) crosses the subset of prices that maximise trading volume. An example of the JSE's opening price settlement algorithm is given in Appendix B. Time priority in the auction process could speed up the price discovery process. Market participants are encouraged to place orders rather sooner than later because their placed orders will have a higher probability of getting actual filled for their prespecified market price. However, this opening price could be rather biased. Consider a security that has two price equilibria during its auction process. The order of the lower price has been entered prior to the higher price, but the latter one has a large bid order imbalance. The security opening is set with a low valuation, such that many buy orders are remaining at the market open for a higher price. This could lead to an aggressive price increase shortly after the market open. The ASX partially solves this problem by including principle 2. Therefore, one could expect that the ASX produces more stable opening valuations.

One could predict that the ASX' matching algorithm is expected to contribute to enhancing opening auction efficiency. The four principles jointly maximise trading volume and minimise supply

and demand imbalances. Similar to the JSE, the first principle reduces the price impact of individual orders as the auction price moves towards the valuation where the plurality of orders is executed. At the Johannesburg's stock market, a large and biased order has the capacity to move the auction price substantially if it is submitted on time, decreasing stable price evolution shortly after the market open. The ASX on the other hand, adjusts prices towards the order imbalance, enhancing price efficiency.

The above principles are established to discover a true consensus opening price, conditioning on having sufficient auction participants. The consistent existence of many auction traders is, however, doubtful. The call can only promise to be an efficient price discovery environment when attracting adequate volume. Therefore, it is important to identify which auction details withhold traders to participate or which incentives could encourage participation. We discuss the three main technicalities: Type of orders, transparency, and order amendment rules during the opening auction.

Both the ASX and JSE accept Limit Orders (LO) and Market Orders (MO) during the opening auction. An LO contains a specific quantity and price, while an MO contains a quantity only. Such orders do not contain information regarding price discovery processes and are, therefore, not valuable for the auction process. Moreover, it could even lead to an unsuccessful auction process. Market Orders accept to buy or sell the security against any price level. For explanatory purposes, consider a situation where the book is filled with multiple sell orders, for which at least one is aggressive, and a market order arrives with a volume that exceeds the aggregated contra-side volume. According to the first principle, the clearing price is set to the most aggressively priced offer, which can be fallacious high. This would lead to an inefficient opening price and a deficit of the auction mechanism. However, both the ASX and JSE reside MOs during the call session until the uncrossing phases. These type of orders can, therefore, not influence the clearing price. However, it does affect the depth of the order book and, hence, could cause price instability.

Second, both exchanges publish an indicative auction price (IAP) and the corresponding surplus volume real-time. This implies high transparency, which permits price discovery to evolve during the pre-open phase. As the auction process matures, merging liquidity attracts order flow from both the buy- and sell-side. In a virtuous circle, additional liquidity and competitive order prices are in turn attracted. Transparency allows participants to observe order imbalances and to respond accordingly to offset it. Hence, one could expect that this level of transparency attracts traders to participate in the auction process.

Nevertheless, the lack of opacity hatches the possibility of increasing market impact. Particular participants, especially big institutions, are reluctant to post orders, as it exposes their trading information and intentions when the topic is thin. Moreover, aggressively priced orders, especially during the early stage of pre-open book building, could induce market manipulation. This brings us to the

third point, where order amendments and cancellations are allowed throughout the entire auction process for both markets. An aggressive buy order could lead other auction participants to raise their prices and, subsequently, produce a higher opening price. On the contrary, an aggressively priced sell order could generate the opposite effect. As a consequence, a participant could bluff such an aggressive order to either make the auction price rise or fall, which he cancels and replaces with an inverse order just before the opening of the market. A similar analysis is conducted by Madhavan (1992), who argues that high transparency is associated with the increasing visibility of noise. This problem discourages big institutions and fundamental traders to participate and delays order revelation.

The Australian exchange undertakes this problem by randomising the uncrossing phase. Order cancellation or amendments just before market open puts the aggressive trader at risk of his orders being executed. Additionally, if you wait too long, you can lose out entirely. Therefore, noise should diminish closing to the market open and informative orders, that are intended to trade, dominate the auction order book and facilitate price discovery. Adopting a random open, therefore, gets true auction orders in an earlier stage. We, therefore, expect that the ASX attracts more order volume during the pre-open phase than the JSE.

All things considered, one could expect that both matching algorithms find an adequate consensus price, conditional on sufficient auction participants. Second, we expect that the ASX produces more stable and efficient consensus opening prices than the JSE. This holds if (i) there is no larger increase in price volatility during the start of actual trading, (ii) a larger proportion of true price discovery appears before the market open, and (iii) if the opening price reflects the underlying market price more accurately. This hypothesis relies on the basis that the three principles might increase market depth, which preserves price stability, and that the ASX‘ design encourages more parties to participate in their auction. The latter should increase market depth through the book-building phase and increase pre-open price discovery and efficiency. For both auctions, we do not expect participation to be populous, as the auctions lack incentives to participate in the first place. This could cause overall auction inefficiency. Nevertheless, we do expect that the size of auction participation is greater in the Australian market, as the random open excludes the existence of a gaming environment. This may deter strategic traders from entering unrepresentative orders a few minutes before the open, improving true price evolution.

3 Data

This paper uses two datasets for our analysis. The first dataset contains the 40 most liquid stocks listed on the Johannesburg Stock Exchange FTSE index. Second, we consider the top 40 stocks included in

the S&P/ASX 200 index, which are stocks listed on the Australian Securities Exchange. Both datasets encompass stocks with the highest market-capitalisation within the Exchange. We obtain 5-minute intraday data from the Bloomberg intraday history database, covering a period from January 3, 2019, through July 17, 2019. The datasets consist of 562,338 and 488,605 observations over 134 and 135 trading days for the JSE and ASX, respectively. Each observation includes the Bloomberg Ticker, date, timestamp, traded closing price, traded volume, closing bid price, closing ask price, and their corresponding bid and ask volumes.

A regular trading week consists of five tradings days from Monday to Friday. Each trading day can be divided into three main time periods: Pre-open hours, continuous trading hours, and the closing hours. The pre-open hours can again be subdivided into two subdivisions, a pre-open phase and an opening auction. Similarly, the closing hours are subdivided into the closing auction and the post-close. For the JSE, the pre-open phase runs from 07:00 through 08:30 (local time), which is followed up by a 30-minute opening auction. During the pre-open hours, incoming orders enter the order book, but no actual trading happens until the uncrossing phase, which starts at 09:00. The uncrossing algorithm carries out the execution of all orders in the current order book at the opening price. Consecutive to the opening auction, the continuous trading period starts, which concludes at 16:45. The closure of the market at 17:00 is preceded by a 15-minute enduring closing auction. During the closing auction, orders can be submitted, but no instant trading is realised. If buy and sell offers are crossed, a similar uncrossing algorithm to the opening auction executes all orders in the order book at 17:00 at the settlement. The final post-closing phase runs from 17:00 up to 18:15. Non-executed orders that were entered during the trading day can be cancelled and orders that are validated and approved roll on to the next trading day.

Similar to the JSE exchange, the ASX opens in the morning with a pre-open phase at 07:00 (local time) through 09:30, which is followed up by a 30 minutes opening auction. At the uncrossing, the market opens in five batches of stocks between 10:00 and 10:09. Each batch opens randomly with a range of approximately 15 seconds from its prespecified opening time. The opening price is determined by the uncrossing algorithm of the ASX, based on the current order book. From the random open up to 16:00, continuous trading takes place. Preceded to the random close, which occurs between 16:05 and 16:11, a closing auction is included, where orders may be entered, amended, and cancelled without restrictions. Similar to the JSE, an uncrossing phase determines the closing price based on the current order book. Subsequently, the post-closing phase runs from the random close through 18:50.

In order to account for the changing and random opening across the ASX stocks, each time interval is measured as if the actual opening starts at 10:00 exact. Due to dissimilar opening times, stocks across the ASX have unequal lengths in the continuous trading session and differ for various trading

days. For our analyses and parameter estimation, we need equal lengths of traded price observations within a particular security. To save informative information, we avoid truncation of tradings days which have the majority of data points. We do so by forcing the opening time at 10:00 and the closing time at 16:10 and to interpolate additional traded closing prices between 12:30-12:35 and/or 14:00-14:05. Desirably, this preserves the volatility structure at the start and end of the trading day and it marginally reduces the volatility in the middle, for which we already expect low price dynamics.

A general trading day at the JSE consists of 95 traded price observations, considering the continuous session from 09:00 through 17:00, excluding the closing auction between 16:45 and 17:00. Similarly, the ASX' continuous session runs from 10:00 through 16:10, excluding the closing auction between 16:00 and 16:10, providing 74 intraday transaction prices. We eliminate all tradings days that miss over 95% of daily trade price observations, such that we carry a sufficient amount of 5-minute data points inter-day. Subsequently, we maintain all stocks that cover at least 85% of its original number of trading days. This results in 413,869 observations over 30 stocks for the JSE, containing 116 to 133 tradings day, including at least 23 Monday opens. For the ASX, we retain 487,880 observations over all 40 stocks, containing 133 to 135 tradings day from which at least 24 are Monday opens. Appendix C gives an overview of all considered stocks in our sample.

The combined JSE stocks in our sample have an average trading value of ZAR 5.62 trillion (around $382 billion), while the ASX stocks average a total trading value of AUD 10.2 billion (around $7.11 billion).[1] On average, the JSE executes 2.34% of its 129 million incoming orders on a daily basis. The ASX stocks only average 5.70 million transactions per day from a daily 467 million incoming orders, which is around 1.22%. Table 1 shows the average daily incoming orders of both the JSE and ASX in Panel A and Panel B, respectively. The panels are divided into three main time periods, as specified in Section 2: Pre-open hours, normal trading hours, and the closing hours. The pre-open hours are further divided into the pre-open and the opening auction. Likewise, the closing hours includes the closing auction and the post-close. In addition, we subdivide the normal trading hours into the first 30 minutes after the market open and the remainder of the continuous trading session. Each panel and time subdivision is branched into three tertiles based on relative order entering. For each stock and trading day, we compute the total incoming orders during the pre-open hours, divided by the remainder of the total incoming orders that day. Within a particular exchange, we sort all stocks on the relatively incoming order flow median, which is subtracted over all considered trading days. Consequently, the tertile "high" contains stocks that are relatively active during the opening auction for the majority of trading days. Similarly, the tertile "low" includes stocks that have relatively low order flows before the market open. The tertiles are equal-sized, such that the three tertiles consists

[1] Converting local currencies to dollars is based on the average of exchange rates over our sample period. This is approximately 0.068 ZAR/USD and 0.70 AUD/USD for the South African Rand and Australian Dollar, respectively.

of 10 stocks each for the JSE sample and is 13-14-13 distributed for the ASX. Appendix C reports all stocks, sorted on the relative incoming order flow median. Separating the total sample in these three segments enables us to test the efficiency of auctions conditional on the fact that there are relative many participants in the opening auction in contrast to few auction participants.

Table 1: Summary of Incoming Orders

Pre-open volume	Pre-open hours		Normal trading hours		Closing hours	
tertile	Pre-open	Auction open	Market open	Intermediate	Auction close	Post-close
Panel A: JSE						
High	6,112	716,780	2,493,000	43,500,620	22,784,135	252,492
Middle	4,960	395,858	1,507,725	26,434,360	34,384,868	82,990
Low	28,908	1,285,802	5,090,033	125,688,139	121,696,244	906,109
Panel B: ASX						
High	97,157	2,036,946	8,968,181	159,179,128	1,053,797	457,019
Middle	144,939	3,978,125	25,264,982	428,149,480	1,380,277	420,653
Low	218,834	5,357,052	30,795,163	730,941,213	2,722,414	1,321,069

NOTE: This table presents incoming order activity during a full trading day. Panel A and B report the average number of the conjoint incoming bid and ask orders between the 3rd of January 2019 and 17th July 2019 for the JSE and ASX, respectively. Both panels, the sample stocks are sorted and ranked into three different tertiles. Tertile high contains one-third of all stocks with the highest number of relative incoming orders during the pre-open hours and tertile low contains the same amount of lowest relative incoming order flow during the pre-open hours. The panels are also divided into three main periods: pre-open hours, normal trading hours, and the closing hours. Each time division is again subdivided into two subdivisions. The pre-open consists of the pre-open, from 07:00-08:30 (JSE) or 07:00-09:30 (ASX), and the opening auction from 08:30-09:00 (JSE) or 09:30-10:00(+/-10min) (ASX). The normal trading hours includes the market open, during 09:00-09:30 (JSE) or 10:00(+/-10min)-10:30 (ASX), and the intermediate phase 09:30-16:45 (JSE) or 10:30-16:00 (ASX). The closing hours phase is divided into the closing auction, from 16:45-17:00 (JSE) or 16:00-16:05(+/-5min) (ASX), and the post-close running from 17:00-18:15 (JSE) or 16:05(+/-5min)-18:50 (ASX).

Both panels show that the high tertile stocks average at least two times fewer incoming orders across a whole trading day than low tertile stocks, for each time segment. The combined daily number of incoming orders for the high tertile stocks is 4.35 and 4.49 times larger than the low tertile stocks for the JSE and ASX, respectively. Further, a large amount of the total daily orders occur during the closing auction for JSE listed stocks. Approximately 46.19% appears during the 15-minute closing auction. In contrast, this only yields 0.37% for the ASX stocks, while 98.63% of the intraday orders are being entered during the continuous trading phase. This implies that the majority of market participants try to transact JSE listed stocks at the settlement.

Table 2 reports the number of daily realised transactions for each tertile and time segment. The auction open and auction close realised trades are the crossed orders that are executed during the uncrossing phase. Generally, a larger amount of incoming orders for a particular sub-sample is followed by more actual executions. However, considering the proportions of executed orders across time divisions show quite interesting, but yet consistent, results. Although the proportions of incoming orders during the continuous sessions and closing hours are substantially different across the two

exchanges, it does not apply to the actual transactions. In contrast to the aforementioned percentages of incoming orders during the closing auction, 21.56% and 24.98% of the daily trades are executed on the closing settlement price for the JSE and ASX, respectively. For the JSE, this suggests that the majority of entered closing auction orders will not be executed, while the opposite applies for the Australian Exchange. During the opening auction, proportional executions are rather different across the two markets. Considering the ASX, the relative number of actual trades during the opening uncrossing phase is at least 6 times as large as for the JSE, regardless of the tertile. The disparity in proportional incoming orders during the pre-open hours is of a much lower degree. Therefore, relatively more orders are filled at the uncrossing phase. This points to the direction that the ASX opening auction is superior in finding a fair price before market open.

Table 2: Summary of Realised Transactions

Pre-open volume	Pre-open hours		Normal trading hours		Closing hours	
tertile	Pre-open	Auction open	Market open	Intermediate	Auction close	Post-close
Panel A: JSE						
High	–	10,311	66,503	1,100,898	248,515	–
Middle	–	9,302	87,280	1,314,940	372,618	–
Low	–	34,226	273,296	4,203,730	1,330,380	–
Panel B: ASX						
High	–	144,742	237,648	1,624,915	832,240	–
Middle	–	308,256	673,043	4,244,576	1,554,472	–
Low	–	248,051	585,878	4,398,360	1,764,822	–

NOTE: This table presents average daily trading activity. Panel A and B report the average number of realised trades between the 3rd of January 2019 and 17th July 2019 for the JSE and ASX, respectively. Both panels, the sample stocks are sorted and ranked into three different tertiles and subdivided into six different time segments. For further details, we refer to the notes in Table 1.

Figure 2 plots the relative trade size per 5-minute interval for the ASX (upper figure) and JSE (lower figure), considering the three relative incoming order flow tertiles. We exclude the closing auction transactions because these relative trade size values are rather high and would clutter the figure. All ASX stocks show a large relative trade size during the opening of the market. The high tertile stocks average a market open relative trade size of approximately 3.8, while this yields around 2.6 for the low tertile stocks. These values decline quickly during the first 20 minutes and decrease towards 0.75 after an hour for all ASX stocks. This suggests that many market participants respond to the opening price shortly after the market open. After 20 minutes, a stable price is found and the relative number of executions has decreased sharply, implying that a large proportion of daily price discovery occurs during the pre-open phase and first 20 minutes of normal trading hours. Additionally, the sharp increase in executions during the final minutes represents the desire of traders to execute their orders before the closure of the market.

The shape of the average relative number of trades during a trading day is considerably different for JSE listed stocks. There is no significant difference across the three tertiles during the market open. Moreover, the vast minority of executions during a trading day occur along with the first half-hour. There is a small spike at 10:00 where the number of relative trades increases. This can be explained by the fact that during winter periods the South-African exchange and alternative (European) exchanges open by an hour difference. These traders place orders at their local exchange opening, such that there is an increase of orders for JSE listed stocks at 10:00. Around two hours before market closure, the trades size starts increasing. The average relative trade volume rises sharply when approaching the closing auction. One could, therefore, expect that price discovery is shifted from the opening auction towards the continuous trading session.

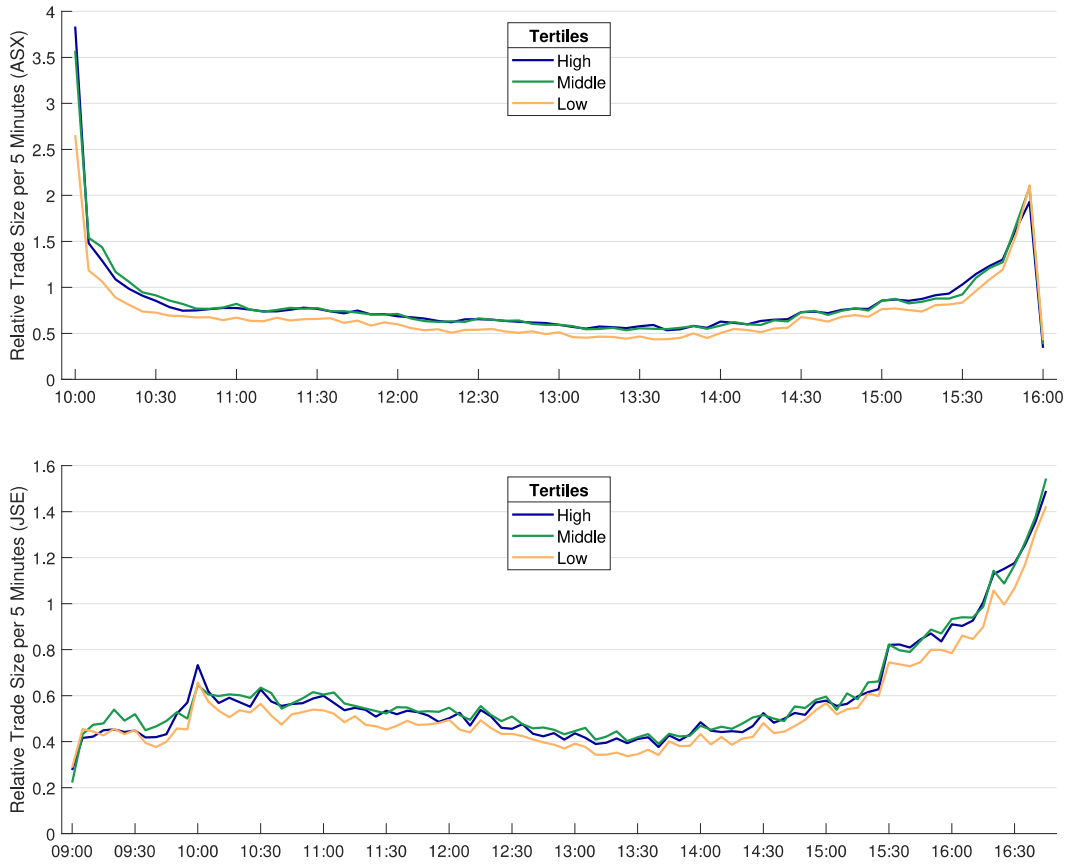

Figure 2: This figure shows the relative daily trading volume per 5 minutes. The average number of transaction, relatively to the rest of the trading day, is computed for each 5-minute interval and tertile. The upper panel corresponds to the ASX and the lower panel with the JSE listed stocks. The time covered is from the market open up to the start of the closing auction.

The trend in traded volume provides an indication for a U-shaped trend in volatility. Barclay and Hendershott (2003) shows that there is a high level of correlation between the trade size volume and volatility during NASDAQ intraday trading. Similar to what we find for the ASX listed stocks, they record the largest trading volume for the first half-hour at the open and the final 30 minutes of

the trading day. However, all orders entered during the pre-open phase are executed at the opening price. A condition of a successful auction inhabits the determination of a stable and fair opening price. Hence, the volatility during the first 30-minutes market open should not show contrast with the remainder of the trading day, disregarding the magnitude of relative trade sizes.

A supplementary requirement for an efficient auction process is the existence of sufficient participants concerning order entering. More participants imply quicker price discovery, as more information is included in the price evolution process. Table 3 presents opening call auction descriptive statistics for the considered ASX and JSE stocks. The table distinguishes non-Monday and Monday-only trading days for each of the three order entry tertiles. Panel A indicates that the overall relative order entry is 1.38 and 1.02 per cent for the ASX and JSE listed stocks, respectively. The difference of 0.36 per cent is significant at the 0.01 level. This large difference is mainly caused by high tertile stocks. The ASX high tertile stocks average a relative order entry of 2.27, while this yields 1.27 per cent for the JSE stocks, a significant difference at the 0.01 level. The low tertile ASX stocks, on the other hand, have an average of 0.06 per cent (insignificant) lower than the low tertile JSE stocks. If the call auction process operates during Monday opens, the relative order entry declines for the ASX, but increases for the JSE listed stocks. Hence, ASX market participants rather delay a larger portion of their total order entries than fully participate in the auction process after a weekend. The contrary holds for the JSE stocks.

Table 3: Opening Call Auction Descriptive Statistics

Relative	Non-Monday trading days				Monday trading days			
volume	JSE	ASX	Diff.	t-stat.	JSE	ASX	Diff.	t-stat.
Panel A: Relative order entry								
Overall	1.02	1.38	0.36	4.34**	1.16	1.31	0.15	1.18
High	1.27	2.27	1.00	6.94**	1.52	2.26	0.74	2.45*
Middle	0.95	1.13	0.18	2.41*	1.12	0.99	−0.12	−1.15
Low	0.83	0.77	−0.06	−0.94	0.83	0.69	−0.14	−1.88
Panel B: Relative trading volume								
Overall	0.61	4.81	4.20	8.26**	0.64	3.66	3.02	17.28**
High	0.68	5.40	4.72	8.20**	0.75	4.13	3.38	17.73**
Middle	0.53	5.04	4.51	9.24**	0.52	3.83	3.31	15.24**
Low	0.63	3.98	3.35	7.12**	0.65	3.01	2.37	14.39**

NOTE: This table presents relative order entry and relative trading volume descriptive statistics for non-Monday and Monday trading days. Panel A reports the total volume of orders entered during the pre-open phase, divided by the total daily incoming orders (excluding the pre-open phase) in percentages. Panel B presents the total volume of executions at the opening uncrossing phase, divided by the total trades executed over the day (excluding the pre-open phase) in percentages. The first two columns (both non-Monday and Monday trading days only) report the relative order entry and relative trade volume for the JSE and ASX, respectively. The third column presents the difference between the two and column four presents a t-statistic to test for significant differences in relative order entry and trading volume across the JSE and ASX. The sign *indicates significance at the 0.05 level and **at 0.01. The analysis is performed separately for each quintile and jointly over all stocks.

The more orders are executed at the opening uncrossing phase, the more participants are aligned to trade on the consensus price. This implies that true consensus price discovery has occurred during the auction process. Panel B indicates that relative trading volume is significantly higher for, and therefore in favour of, the ASX market. The relative trading volume is measured by using the total orders that are filled during the opening auction uncrossing phase divided by the total number of orders executed during the remainder of the trading day. For each tertile, the ASX' relative trading size is at least 6 times larger than the JSE. All differences are highly significant, both for the non-Monday and Monday opening auctions. This implies that the ASX executes significantly more, in proportion to the rest of the trading day, at the opening price than the JSE. This is in line with Figure 2. Analogously to the relative order entry pattern, the relative trading volume decreases for the ASX stocks on Monday opening auctions, while increasing for the JSE stocks. However, the ASX remains superior in opening call auction trade volume across all tertiles.

Figure 3 shows the relative order entry per 5 minutes for each tertile. The upper panel corresponds to the ASX, while the lower panel resembles the JSE listed stocks. We exclude the pre-open period from 07:00 to the opening auction start because order cancellation and amendment activities over this pre-market open time produce minimal changes in the order book volume. For the same reasoning as before, we again omit the closing hours from this analysis. For all stocks, some order entries are registered for the first 20 minutes of the opening auction. However, compared to the rest of the trading day, these orders are rather negligible. Approximately 10 minutes prior to the market open, the relative order size increases sharply for all stocks, up to (a few minutes after) the opening of the market. Considering the ASX stocks, there is a small bump at the uncrossing phase for the high tertile. However, this increase is comparatively small and all other stock entries are relatively constant over time, with a value close to 1. Then the relative order flow increases towards 6 and 4, for the low and high tertile stocks respectively, when approaching the closing auction.

The lower panel of Figure 3 shows that, shortly after the market open, order size starts decreasing. As shown earlier, there is a spike at 10:00, which explains the fast increase in order execution in Figure 2. Subsequently, the relative order entry shows a decreasing trend over an average intraday. This trend preserves until closing the final auction, for which the trend increases sharply. The ASX' opening auction participation, based on order entry volume which is used to determine the opening price, is substantially larger than of the JSE stocks. We could, therefore, expect that the opening prices for ASX stocks (at least the high tertile stocks) have superior price discovery during the pre-open phase, as more information is included in the price determination process. However, even ASX listed stocks have poor auction participation, relatively to the number of order entries during the remainder of the trading day. There is a small favour for the high tertile ASX stocks, but conjointly, we expect

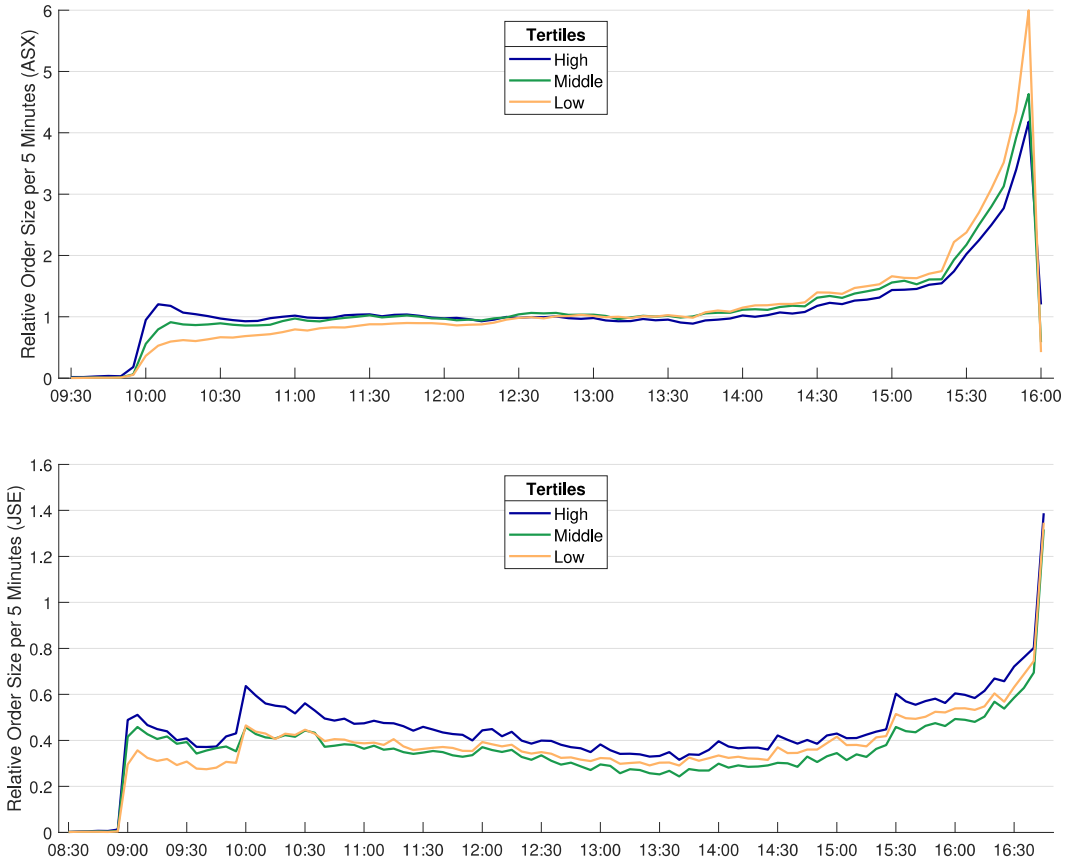

Figure 3: This figure shows the relative order flow per 5 minutes. The average number of incoming orders, relatively to the rest of the trading day, is computed for each 5-minute interval and across all three tertiles. The upper panel corresponds to the ASX and the lower panel with the JSE listed stocks. The time covered is from the opening auction start to the start of the closing auction.

deficiencies in opening price determination during the auction process.

In order to test the efficiency of opening auction processes, we analyse the accuracy of opening prices relative to the true underlying market price and the stability of observed opening prices. For this framework, which is explained in the next section, we make use of actual traded prices. We deal with (scarce) missing traded prices during the continuous trading session by linear interpolation. One could argue that no trading activity during a 5-minute interval would not change the actual stock price. Therefore, one could set a missing price on the previous traded price. However, we assume that the underlying stock price flows gradually over time.[2] We join the two closest discrete data points by a straight line segment. The missing traded price is set to the value of the linear polynomial, corresponding to its specific date-time. Second, we examine the price discovery process during the pre-open. For this purpose, we need indicative opening prices. As our data sets do not contain individual order entries, amendments and cancellations, including market and limit order prices, we

[2]For robustness check, we tried both methods for our analyses. There are no occurrences of significant differences in results or alterations in further conclusions.

can not determine the true indicative auction price (IAP). Alternatively, we compute the IAP by taking the average between the bid and ask price, which, unlike linear interpolation, also preserves the price volatility.[3] We define and underpin our method to test auction inefficiency in the following section. For model estimation, we delete the pre-open hours, as such prices are rather inefficient and biased. Moreover, we exclude the post-close period from model evaluation, except for the traded closing price, determined by the closing auction. The reasoning for that is similar to these of the pre-open phase. By construction, these prices are noisy. However, we observe the settlement price, which is informative as we have shown earlier. Therefore, we use the closing auction price as the final price during a trading day.

4 Methodology

In this section, we describe our methodology to measure auction efficiency. The call's main goal is to find a stable consensus price preceding the market open after the overnight, or over-weekend, close. Throughout the rest of this paper, an efficient auction process contains the three following main conditions: (i) The observed prices after the market open are stable, (ii) a large proportion of the daily price discovery process occurs during the auction period, and (iii) the determined opening price (approximately) corresponds to the true underlying market price. The second condition implies that there is no increase in price volatility during the early stage of continuous trading.

We propose an extended stochastic volatility model to model the underlying security price and price volatility. In this framework, we assume that the observed exchange prices equal the true underlying market price plus an error term and jump a component. That is, for each security and time stamp,

$$\text{Observed Price} = \text{True Price} + \text{Diffusion} + \text{Jump}. \tag{1}$$

The first condition of auction efficiency suggests that the observed opening price should be close to the true price, or put differently, that the diffusion and jump terms are close to zero at the market open. We analyse the speed of price convergence to fundamental values. That is, the time that elapses until the observed price reaches the underlying market price. We test for both auction mechanisms the speed of, and the accuracy of, its price discovery process.

We assume that the diffusion term in Equation (1) is stochastic because empirical price volatility shows dynamic features. We define a volatility model that enables us to capture such dynamics. Second, we add a daily pattern component to capture consistent daily volatility segments. Third, we

[3]The reasoning why a similar approach is not conducted for the missing prices during normal trading hours is because these bid and ask spreads are rather very noisy during continuous trading hours. This leads to very noisy price estimations, which would blur the underlying price volatility.

are interested in the functionality of the auction mechanism when the market has been closed for a longer amount of time than overnight. This period could lead to additional price uncertainty and increase volatility. Therefore, we analyse the impact on price volatility when the market opens on Monday, after being out of business for the weekend. Henceforth, volatility is described by

$$\text{Stochastic Volatility} = \text{Dynamic Volatility} + \text{Daily Pattern} + \text{Monday Open Effect}. \tag{2}$$

As the opening auction participation is rather low, the market's depth becomes shallow. Only a few unexecuted orders structure no solid foundation for price stability. Therefore, we expect that the call is unable to offer stability in intraday price formation shortly after the market open. In addition, preceding the market closing, traders seek opportunities to close their positions, which increases price volatility. Hence, we expect that the daily pattern follows a 'U'-shape over a single trading day. The second condition of auction efficiency suggests, however, that high volatility levels should not persistently occur at the market open. This is satisfied when the daily pattern is close to flat during this time. We refer to the daily pattern as seasonality. The seasonal shapes signify the persistent differences in volatility levels across a trading day. Therefore, we test, and compare, the second auction condition for both the ASX and JSE, by considering the seasonal patterns. Monday open effects are modelled and tested in a similar manner.

The model aids in our auction efficiency analyses as follows. Section 5.1 uses the daily pattern and Monday open effect to find consistent volatility increases in stock prices after the overnight and over-weekend close, respectively. A significant increase would imply unstable opening prices and, therefore, an insufficient auction process. Second, Section 5.2 computes weighted price contributions to display the fraction of daily price evolution explained during the auction phase. A higher value indicates a superior price discovery process, which is an auction's main goal. The measure is model-free and explained in Section 5.2 in more detail. Lastly, we analyse the accuracy of the opening price relatively to the true market price in Section 5.3. We regress the observed opening prices on the model-based true stock prices, which provides us a measure for opening price efficiency. If the opening price does not converge to fundamental values, then the auction price discovery process does not find a true consensus price, implying an insufficient auction procedure. The results of the three analyses are presented in Section 5. Subsections 4.1-4.4 underpin and explain in more detail the definition of our model, describe the estimation procedure, and proof the validation of the model by a simulation study.

4.1 Modeling the Security Prices

In order to evaluate opening price efficiency, we need to study price volatility and deviations from the "true" underlying market price. In our framework, all observed prices, based on a particular security, are driven by a latent efficient price process. This price process represents the unknown underlying market price of its corresponding security. The true market price at time t is defined as the end-of-period value of a security conditional on all publicly available information at time t. We assume that all public information is incorporated into the market price. Then a security's latent price can be modelled as a random walk with stationary innovations $\{r_t\}_{t=1}^{n}$. The observed security price deviates from this latent price as follows. The underlying market price does not make abundant movements in the absence of essential public information. However, observed security price movements are, relatively to the rest of the day, substantially larger around the opening and closing of the market. Therefore, we assume that observed asset prices deviate from underlying latent prices with stochastic error terms. Furthermore, discontinuities, also known as jumps, are proved to be essential in explaining asset prices. For example, Eraker et al. (2003) and Andersen et al. (2002) show that jumps are characteristic in daily S&P500 and/or Nasdaq100 index returns, and Masset (2008) provide strong evidence for intraday jumps in DAX returns.

Mathematically, for each security, our proposed Extended Unobserved Components Model defines the logarithmic observed security price p_t, for each time period t, as

$$p_t = p_t^* + \exp(h_t/2)\epsilon_t^* + J_t Z_t^p, \qquad t = 1, \ldots, n \tag{3}$$

$$p_{t+1}^* = p_t^* + \sigma_r r_t, \qquad t = 1, \ldots, n-1 \tag{4}$$

where p_t^* is the log latent efficient market price, h_t denotes the total non-jump log-volatility, J_t is a jump indicator, which equals one if a jump occurs at time t and zero otherwise, Z_t^p denote the price jump at time t, r_t are the latent price process stationary error terms and are i.i.d. standard normal distributed, $r_t \overset{\text{i.i.d}}{\sim} \mathcal{N}(0,1)$, with σ_r its standard deviation, and ϵ_t^* is assumed to follow a standardised heavy-tailed Student-t distribution with ν unknown degrees of freedom, that is $\epsilon_t^* \overset{\text{i.i.d}}{\sim} t_\nu(0,1)$. In more detail, the jump flag J_t is defined as a Bernoulli random variable such that $P[J_t = 1] = \kappa$ and $P[J_t = 0] = 1 - \kappa$. The price jumps are assumed to be stochastic and follow a normal distribution with constant mean μ_p and volatility σ_p^2, which are unknown and to be estimated, that is $Z_t^p \overset{\text{i.i.d}}{\sim} \mathcal{N}(\mu_p, \sigma_p^2)$. The measurement error ϵ_t^* can be decomposed such that $\epsilon_t^* = \sqrt{\lambda_t}\epsilon_t$, where $\epsilon_t \overset{\text{i.i.d}}{\sim} \mathcal{N}(0,1)$ and $\lambda_t \overset{\text{i.i.d}}{\sim} \mathcal{IG}(\frac{\nu}{2}, \frac{\nu}{2})$. Moreover, for simplicity, we assume that $p_1^* \sim \mathcal{N}(0, c_{p^*}\sigma_r^2)$, where c_{p^*} is set to some large constant.

The dynamics of the unobserved log-volatility is modelled by a stochastic linear model with slow and fast volatility factors. We assume that price volatility can partly be explained by previous volatil-

ity levels and that it is driven by intraday seasonality and additional Monday open uncertainty. Mathematically, h_t is defined by

$$h_t = x_{t,1} + x_{t,2} + s_t + a_t, \tag{5}$$

where $x_{t,1}$ and $x_{t,2}$ are slow and fast stochastic volatility (SV) processes, respectively, and s_t and a_t are seasonal and Monday open components, respectively. The dynamic equations of the SV processes are defined by

$$x_{t+1,1} = \mu + \phi_1(x_{t,1} - \mu) + \sigma_1\eta_{t,1}, \qquad t = 1, \ldots, n-1 \tag{6}$$

$$x_{t+1,2} = \phi_2 x_{t,2} + \sigma_2\eta_{t,2} + J_t Z_t^v, \qquad t = 1, \ldots, n-1 \tag{7}$$

where $\eta_{t,1}$ and $\eta_{t,2}$ are i.i.d and standard normal distributed error terms, $Z_t^v \overset{\text{iid}}{\sim} \mathcal{N}(\mu_v, \sigma_v^2)$ are stochastic jump sizes in the log volatility, and μ is a constant. By definition, the slow volatility is more persistent and relatively flat over time, whereas the fast volatility has quick mean-reverting properties. Therefore, we assume that $0 < \phi_2 < \phi_1 < 1$, such that both processes are stationary. Furthermore, we assume that $x_{1,1} \sim \mathcal{N}(\mu, \sigma_1^2/(1-\phi_1^2))$ and $x_{1,2} \sim \mathcal{N}(0, \sigma_2^2/(1-\phi_2^2))$. Note that the volatility jump occurrences coincident with those in the security prices. This can be understood by the fact that market participants respond on price jump movements, which fluctuates the exchange price and increase the short-term volatility. We capture additional empirical relations between the security price dynamics and its volatility via correlated shocks in security prices and fast volatility, that is $\rho = \text{corr}(\epsilon_t, \eta_{t,2})$. This is also known as the diffusive leverage effect. For further model specifications, we do not assume cross-sectional dependence across λ_t, J_t, r_t, $\eta_{t,1}$, Z_t^p, and Z_t^v.

We model s_t and a_t in Equation (5) by cubic smoothing splines. The seasonal element captures a smooth U-shaped pattern due to intermittent changes in intraday volatility at primary market opening and closing times. We define the periodic component by $s_t = \sum_{k=1}^{K} H_{tk}\beta_k$, where K is the number of periods within a trading day, H_{tk} is an indicator function that equals one if time t corresponds to period k and zero otherwise, and β_k denotes the intraday seasonal effect at period k.

The Monday open factors are modelled similarly. After the market close on Friday evening, the market opens only on Monday morning again. This protracted time in the absence of market trading increases price uncertainty by market participants. Generally, this is likely to generate larger price movements than at regular opening times, which increases volatility. After the Monday open, prices are expected to stabilise expeditiously, because price uncertainty abates during actual market trading. We, therefore, assume that weekly market inaugurations have a short-term impact only, increasing a security's volatility for 5 periods after the new week open. The total time's t Monday open effect

is defined by $\alpha_t = \sum_{l=1}^{5} I_{tl}\alpha_l$, where I_{tl} is an indicator function that equals one if the Monday open occurred at period $t - l + 1$ and zero otherwise, and α_l denotes the week initiation effect, l periods after the Monday open. Similarly to the seasonal components, we make use of cubic smoothing splines to filter and smooth the parameters $\boldsymbol{\alpha} = (\alpha_1, ..., \alpha_5)'$.

Our proposed model aims to capture the main characteristics in observed exchange prices and is more sophisticated than "traditional" stochastic volatility models. Bedendo and Hodges (2004) shows that, by means of daily and 5-minute return autocorrelograms, the stochastic volatility factor has two major features: i) A fast mean-reverting component intraday and ii) a more persistent component, for which its slow decay can be modelled by the sum of AR(1) processes. Our model captures these components by $x_{t,1}$ and $x_{t,2}$. Other than Andersen and Bollerslev (1997), we do not make the assumption of constant intraday stochastic volatility, since both the slow and fast SV factors are affected by intraday shocks through the innovation terms $\eta_{t,1}$ and $\eta_{t,2}$, respectively. Without jumps, seasonal and Monday open segments, and underlying latent price dynamics, this can be seen as a superposition model. These types of models are becoming popular and are argued to be flexible in the SV literature (see e.g. Omori et al., 2007). In contrary to the original superposition model, we restrict to the case that the correlation between ϵ_t and $\eta_{t,1}$ is zero, that is $\text{corr}(\epsilon_t, \eta_{t,1}) = 0$. Our reasoning for this condition is as follows. Foremost, we assume that such price shocks only affect short-term volatility and do not lead to changes in the long-term volatility pattern. This also makes identification of the two volatility dynamics (6) and (7) easier. Second, the estimation of the additional parameter would increase the computational burden substantially. The estimation procedure for all 80 stocks would become considerably slower and rather infeasible.

Our model adds common price and volatility jumps in intraday prices. Price jumps are accompanied with jumps in the short-term volatility, as market participants respond on such price movements, resulting in price instability. Correlated-jump SV models have gained more attention in the recent literature (see e.g. Eraker et al., 2003, Kobayashi, 2005, and Nakajima and Omori, 2009), considering simultaneous jumps in returns and volatilities. Moreover, this model is more flexible in allowing fat-tailed errors terms, instead of assuming normally distributed innovations. Estimation procedures for leveraged, heavy-tailed, and correlated jumped SV models are scarcely developed (see e.g. Omori et al., 2007, and Nakajima and Omori, 2009). We illustrate our sampling approach that conjointly includes these characteristics in Section 4.3.

Similar to Andersen and Bollerslev (1997), Andersen and Bollerslev (1998), Martens et al. (2002), and Engle and Sokalska (2012), we incorporate intraday seasonal effects in our model. Existing studies make either use of an iterative two-step procedure or third-party interday volatility estimates. The first method estimates the daily volatility, assuming volatility to be constant intraday, and subsequently,

estimates the seasonal component. By contrast, our algorithm estimates all parameters and latent states simultaneously in a similar manner to Stroud and Johannes (2014). This avoids the requirement of an inefficient two-step estimation procedure and it makes assumptions conform normally distributed shocks or the absence of jumps nonessential.

Both the seasonal effects and Monday open realisations are modelled by cubic smoothing splines. A similar approach is done by Weinberg et al. (2007) who try to smooth within-day Poisson arrival rates to predict future US commercial bank's call centre calls. As in their approach, $\boldsymbol{\beta} = \{\beta_k\}_{k=1}^{K}$ and $\boldsymbol{\alpha}$ are density functions, such that the sum over all elements, within the two series, should equal one. We adopt an efficient estimation procedure, following the methodology of Kohn and Ansley (1987). They proposed a state-space representation for the coefficients β_k, for $k = 1, \ldots, K$, and α_l, for $l = 1, \ldots, 5$, including a cubic smoothing spline prior. The full procedure for filtering and smoothing the seasonal and Monday open cubic splines is explained in Section 4.3.2.

As mentioned before, this model captures many important characteristics of intraday price data. This underpins the need for this model to measure auction efficiency because it enables us to filter out the underlying latent market price and the latent price volatility that is (approximately) solely due to the opening and closing of the market. Our proposed model, therefore, facilitates us with two important measures for our efficiency analyses: (i) a "true" opening valuation and (ii) a consistent increase in price volatility during the early stage of continuous trading. In case of an efficient auction mechanism, the first should approximately be equal to the observed opening price and the latter should be close to zero.

The full auction efficiency analysis is carried out is Section 5. First, we examine the impact of the call mechanisms on price volatility. Not all market participants that trade during the start of the continuous session participate in the opening auction. The clearing price may, therefore, not equal the consensus price across all traders. When this happens, it triggers traders to enter orders, which heightens accentuated volatility. This indicates opening auction inefficiency. Our model defines volatility as the dispersion between the observed log price and true log security value. More specifically, it provides the intraday volatility free from individual stock dynamics or volatility jumps through $\boldsymbol{\beta}$. This measure determines the consistent increase in volatility during early continuous trading hours compared to its baseline level. We estimate our proposed model for each individual stock. To make it auction specific, instead of stock characteristic, we take a joined $\boldsymbol{\beta}$ measure within an exchange. We could keep the seasonal pattern equivalent within a market, but this would exclude the possibility of parallel programming across all stocks, making the estimation procedure infeasible. Therefore, we model the intraday pattern individually for each stock and average out within each exchange. This provides us with a robust price volatility measure, which consistently occurs during the specific

market open. We use this method to test the differences in price volatility across the ASX and JSE as a consequence of auction price inefficiency. We take a Bayesian approach, which means that we get many simulated $\boldsymbol{\beta}$ vectors, for both the ASX and JSE. For each sample, we take the difference between $\beta_{k,ASX}$ and $\beta_{k,JSE}$, for $k = 1, \ldots, 24$, where $\beta_{k,ASX}$ and $\beta_{k,JSE}$ correspond to the average beta factor for the ASX and JSE, respectively. We compute the standard deviation, that is $\hat{S} = \exp(\beta_{k,diff}/2)$, where $\beta_{k,diff}$ correspond to $\beta_{k,JSE} - \beta_{k,ASX}$. Hence, we get a posterior distribution for the difference in β_k, across the ASX and JSE, on standard deviation scale. A posterior mean significantly higher than one implies that the average volatility increase at time k is significantly higher for the average JSE listed stocks and vice versa. These so-called variance ratios are computed from market open to two hours after, which enables us to test two important features: the difference in (i) opening price stability and (ii) the speed of convergence to a stable equilibrium price. For the first, we test for significant differences for $k = 1$. For the second, we analyse for which k, $\hat{S} = \exp(\beta_{k,diff}/2)$ is not significantly different from one anymore.

Second, to see the performance of the auction mechanisms while the market has been closed for a longer amount of time, we use a similar approach for the $\boldsymbol{\alpha}$ series. A longer time span of market closure increases price uncertainty, which may result in an opening price volatility increase if true consensus price discovery is frittered away during the auction. The variable α_l, for $l = 1, \ldots, 5$, represents the increase in volatility, during the first 20 minutes of continuous trading, due to the market being closed for the weekend. Hence, we compute the difference in $\alpha_{l,ASX}$ and $\alpha_{l,JSE}$, for $l = 1, \ldots, 5$.

Third, in Section 5.2, we evaluate the price discovery process during the auction phase. For the opening call, it is of great importance that overnight information is absorbed into security prices before the opening of the market. If so, participants have come to a consensus price for which the majority is willing to trade.

Lastly, we compare and test the efficiency of auction prices, produced by the call design of the ASX and JSE, in Section 5.3. We use a price efficiency test where we regress the observed price series on the current true value. The main difficulty is the impossibility of observing the true latent value of any asset. For this purpose, we assume p_t^* to be the best quote prevailing at time t. We perform analogous analyses for high and low tertile stocks. This enables us to examine dissimilarities in opening price volatility, pre-open price discovery, and opening price efficiency given the relative number of auction participants. Details of the auction efficiency evaluations are discussed in Section 5.

Additional to this unique method to measure auction efficiency, this paper contributes by developing an efficient MCMC parameter estimation and latent state smoothing method for our proposed model. This includes a multidimensional stochastic volatility model with leverage, correlated jumps, heavy-tailed Student-t errors, intraday seasonal patterns, Monday open effects, and a latent efficient

price process. This is an extension to Nakajima and Omori (2009), Chib et al. (2002), and Stroud and Johannes (2014). The full estimation approach and a simulation study are considered in the following subsections.

4.2 Auxiliary Mixture Sampler

Discrete-time stochastic volatility models, such as our extended framework, bear the difficulty that its likelihood function is not easily derived. A well-known likelihood computation method is established by Del Moral (1996), called a particle filter. However, such a method requires an extensive amount of repetitions to evaluate the likelihood for each set of parameters until a maximum is reached. To overcome such a computational difficulty, we make use of a Bayesian estimation approach including Markov chain Monte Carlo (MCMC) methods to evaluate our proposed model.

For likelihood evaluation, lets define $d_t = I(\epsilon_t \geq 0) - I(\epsilon_t < 0)$ and $\tilde{p}_t = \log(p_t - p_t^* - J_t Z_t^p)^2 - \log\lambda_t$. Nelson (1988) and Harvey et al. (1994) show that the observed price process in Equation (3) can be rewritten as $\tilde{p}_t = h_t + \zeta_t$, where $\zeta_t = \log(\epsilon_t^2)$, such that we have the map $p_t = d_t\sqrt{\lambda_t}\exp(\tilde{p}_t/2) + p_t^* + J_t Z_t^p$. Note that ζ_t is $\log\chi^2$ distributed and inhibits direct and simple inference. Kim et al. (1998) introduces a key idea to approximate the distribution of ζ_t by matching a mixture of normal distributions, which they show to be accurate and efficient in MCMC algorithms. Following Omori et al. (2007), we approximate the bivariate conditional density $(\zeta_t, \eta_{t,2}) \,|\, d_t$, which are correlated through the leverage effect ρ, by a 10-components mixture of bivariate Gaussian densities (see Appendix D for the reformulation steps). That is,

$$g(\zeta_t, \eta_{t,2} \,|\, d_t, \rho, \sigma_2) = \sum_{j=1}^{10} pr_j \mathcal{N}(\zeta_t \,|\, m_j, v_j^2)\mathcal{N}\Big[\eta_{t,2} \,|\, d_t\rho\sigma_2 \exp\Big(\frac{m_j}{2}\Big)(a_j^* + b_j^*(\zeta_t - m_j)), \sigma_2^2(1-\rho^2)\Big], \quad (8)$$

where a_j^*, b_j^*, pr_j, m_j, and v_j^2 are prespecified values that are chosen to minimise the mean square norm to accurately match the $\log\chi^2$ distribution. In addition, we define a set of mixture component indicators $\omega_t \in \{1, ..., 10\}$. The main principle of this approach is that we can accurately approximate $\tilde{p}_t$ and the models (6)-(7), conditional on the indicators, by means of a linear Gaussian state space model:

$$\begin{aligned}
\hat{p}_t &= x_{t,1} + x_{t,2} + m_{\omega_t} + v_{\omega_t} u_{t,1}, && (9)\\
x_{t+1,1} &= \mu + \phi_1(x_{t,1} - \mu) + \sigma_1 u_{t,2}, && (10)\\
x_{t+1,2} &= \phi_2 x_{t,2} + \sigma_2(d_t\rho(a_{\omega_t}^* + b_{\omega_t}^* v_{\omega_t} u_{t,1})\times \\
&\quad \exp(m_{\omega_t}/2) + \sigma_2\sqrt{1-\rho^2}u_{t,3}) + J_t Z_t^v, && (11)
\end{aligned}$$

where $\hat{p}_t = \tilde{p}_t - s_t - a_t$, and $(u_{t,1}, u_{t,2}, u_{t,3})' \sim \mathcal{N}(0, I)$. Omori et al. (2007) computed the probabilities pr_j and the mixture component parameters a_j, b_j, m_j, and ν_j^2, for $j = 1, ..., 10$, which we reproduced in Table 4. This representation allows us to block-sample the latent volatility states $\mathbf{x}_i = (x_{1,i}, ..., x_{n,i})$, for $i = 1, 2$, through the linear Gaussian state space simulation smoother of De Jong and Shephard (1995), and Durbin and Koopman (2002).

Table 4: Mixture component parameters $(pr_j, m_j, v_j^2, a_j^*, b_j^*)$

Index j	pr_j	m_j	v_j^2	a_j^*	b_j^*
1	0.00609	1.92677	0.11265	1.01418	0.50710
2	0.04775	1.34744	0.17788	1.02248	0.51125
3	0.13057	0.73504	0.26768	1.03403	0.51701
4	0.20674	0.02266	0.40611	1.05207	0.52604
5	0.22715	-0.85173	0.62699	1.08153	0.54076
6	0.18842	-1.97278	0.98583	1.13114	0.56557
7	0.12047	-3.46788	1.57469	1.21754	0.60877
8	0.05591	-5.55246	2.54498	1.37454	0.68728
9	0.01575	-8.68384	4.16591	1.68327	0.84163
10	0.00115	-14.65000	7.33342	2.50097	1.25049

NOTE: This table lists the selection of $pr_j = Pr(\omega_t = j)$, where ω_t is the mixture indicator at time t, and the mixture component parameters (m_j, v_j, a_j^*, b_j^*) for $j = 1, \ldots, 10$ from Omori et al. (2007), which are used to accurately approximate the bivariate density $\zeta_t, \eta_{t,2} \,|\, d_t, \rho, \sigma_2$.

4.3 MCMC Algorithm

For notational conveniences, denote, for each security, $\mathbf{p} = \{p_t\}_{t=1}^n$, $\mathbf{p}^* = \{p_t^*\}_{t=1}^n$, $\tilde{\mathbf{p}} = \{\tilde{p}_t\}_{t=1}^n$, $\mathbf{d} = \{d_t\}_{t=1}^n$, $\mathbf{Z}^p = \{Z_t^p\}_{t=1}^n$, $\mathbf{Z}^v = \{Z_t^v\}_{t=1}^n$, $\mathbf{J} = \{J_t\}_{t=1}^n$, $\boldsymbol{\lambda} = \{\lambda_t\}_{t=1}^n$, all unknown parameters in a vector $\boldsymbol{\theta} = (\phi_1,\ \phi_2,\ \sigma_1,\ \sigma_2,\ \rho,\ \mu,\ \sigma_r,\ \nu,\ \kappa,\ \mu_p,\ \sigma_p,\ \mu_v,\ \sigma_v,\ \tau_s,\ \tau_a)'$, $\boldsymbol{\beta} = (\beta_1, ..., \beta_K)'$, $\boldsymbol{\alpha} = (\alpha_1', ..., \alpha_X')'$, and denote the prior probability density function for variable $\bullet$ as $\pi(\bullet)$. The variables τ_s and τ_a correspond to the smoothing parameters, which determine the spline's smoothness for the seasonal and Monday open volatility effects, respectively. We take a Bayesian approach and use an MCMC algorithm to simulate from the posterior distribution

$$\pi(\boldsymbol{\theta},\ \mathbf{z},\ \boldsymbol{\beta},\ \boldsymbol{\alpha},\ |\ \mathbf{p}) \propto \prod_{t=1}^{T} \pi(p_t \mid z_t,\ \boldsymbol{\beta},\ \boldsymbol{\alpha},\ \boldsymbol{\theta})\ \pi(z_t \mid z_{t-1},\ \boldsymbol{\theta})\ \pi(\boldsymbol{\beta} \mid \boldsymbol{\theta})\ \pi(\boldsymbol{\alpha} \mid \boldsymbol{\theta})\ \pi(\boldsymbol{\theta}), \tag{12}$$

where $z_t = (x_{t,1},\ x_{t,2},\ \lambda_t,\ J_t,\ Z_t^p,\ Z_t^v,\ p_t^*)$, $\mathbf{z} = \{z_t\}_{t=1}^n$, and where $\pi(b \mid a)$ denotes the probability density function of b conditional on a. We make use of conjugate priors where possible or, in all other cases, proper, but not too strong, prior distributions. An overview of our proposed Extended Unobserved Components model and the details of its priors can be found in Appendix E. The model is estimated by means of the following MCMC algorithm, where the starting values are set to the prior

mean or mode:

1. Initialise $\boldsymbol{\theta}$, $\mathbf{x}_1$, $\mathbf{x}_2$, $\boldsymbol{\omega}$, $\boldsymbol{\lambda}$, $\mathbf{J}$, $\mathbf{Z}^p$, $\mathbf{Z}^v$, $\boldsymbol{\alpha}$, $\boldsymbol{\beta}$ and $\mathbf{p}^*$.
2. Sample $(\phi_1, \phi_2, \sigma_1, \sigma_2, \rho, \mu, \mathbf{x}_1, \mathbf{x}_2) \,|\, \boldsymbol{\omega}, \tilde{\mathbf{p}}, \mathbf{d}, \boldsymbol{\beta}, \boldsymbol{\alpha}$ by
   (a) Sampling $(\phi_1, \phi_2, \sigma_1, \sigma_2, \rho) \,|\, \boldsymbol{\omega}, \tilde{\mathbf{p}}, \mathbf{d}, \boldsymbol{\beta}, \boldsymbol{\alpha}$, and
   (b) Sampling $(\mu, \mathbf{x}_1, \mathbf{x}_2) \,|\, \phi_1, \phi_2, \sigma_1, \sigma_2, \rho, \boldsymbol{\omega}, \tilde{\mathbf{p}}, \mathbf{d}, \boldsymbol{\beta}, \boldsymbol{\alpha}$.
3. Sample $(\boldsymbol{\beta}, \tau_s^2) \,|\, \tilde{\mathbf{p}}, \boldsymbol{\omega}, \mathbf{x}_1, \mathbf{x}_2, \boldsymbol{\alpha}, \boldsymbol{\theta}, \mathbf{p}^*$.
4. Sample $(\boldsymbol{\alpha}, \tau_a^2) \,|\, \tilde{\mathbf{p}}, \boldsymbol{\omega}, \mathbf{x}_1, \mathbf{x}_2, \boldsymbol{\beta}, \boldsymbol{\theta}, \mathbf{p}^*$.
5. Sample $\boldsymbol{\omega} \,|\, \tilde{\mathbf{p}}, \boldsymbol{\theta}, \mathbf{x}_1, \mathbf{x}_2, \boldsymbol{\alpha}, \boldsymbol{\beta}, \mathbf{J}, \mathbf{Z}^p, \mathbf{Z}^v, \boldsymbol{\lambda}, \mathbf{p}^*$.
6. Sample $(\boldsymbol{\lambda}, \nu) \,|\, \boldsymbol{\theta}, \mathbf{p}, \mathbf{x}_1, \mathbf{x}_2, \mathbf{J}, \mathbf{Z}^p, \mathbf{Z}^v, \boldsymbol{\beta}, \boldsymbol{\alpha}, \boldsymbol{\omega}, \mathbf{p}^*$ by
   (a) Sampling $\nu \,|\, \boldsymbol{\theta}, \mathbf{p}, \nu, \mathbf{x}_1, \mathbf{x}_2, \mathbf{J}, \mathbf{Z}^p, \mathbf{Z}^v, \boldsymbol{\beta}, \boldsymbol{\alpha}, \boldsymbol{\omega}, \mathbf{p}^*$, and
   (b) $\boldsymbol{\lambda} \,|\, \nu, \boldsymbol{\theta}, \mathbf{p}, \nu, \mathbf{x}_1, \mathbf{x}_2, \mathbf{J}, \mathbf{Z}^p, \mathbf{Z}^v, \boldsymbol{\beta}, \boldsymbol{\alpha}, \boldsymbol{\omega}, \mathbf{p}^*$.
7. Sample $(\mathbf{J}, \mathbf{Z}^p, \mathbf{Z}^v) \,|\, \mathbf{p}, \mathbf{x}_1, \mathbf{x}_2, \boldsymbol{\lambda}, \kappa, \mu_p, \mu_v, \sigma_p, \sigma_v, \mathbf{p}^*$.
8. Sample $(\kappa, \mu_p, \mu_v, \sigma_p, \sigma_v) \,|\, \mathbf{J}, \mathbf{Z}$.
9. Sample $\mathbf{p}^* \,|\, \mathbf{p}, \mathbf{x}_1, \mathbf{x}_2, \sigma_r, \mu, \boldsymbol{\lambda}, \mathbf{J}, \mathbf{Z}^p, \mathbf{Z}^v, \boldsymbol{\beta}, \boldsymbol{\alpha}$.
10. Sample $\sigma_r^2 \,|\, \mathbf{p}^*$.

Note that we sample from the approximated models (9)-(11) through the approximation of the true density $\pi(\zeta, \eta_{t,2}|d_t, \rho, \sigma_2)$ by a mixture of ten normal distributions, as in Equation (8). Although the differences are rather small, we re-weight the drawn samples to obtain estimated parameters of the true SV model discussed in Section 4.1, as we will show in Section 4.3.5. In the following subsections, we briefly discuss the above-mentioned sampling steps separately (see Appendix F for the details).

4.3.1 Sampling Volatility Parameters and Latent States

For notational conveniences, let us define $\boldsymbol{\vartheta} = (\phi_1, \phi_2, \sigma_1, \sigma_2, \rho)'$. The conditional distribution of $(\boldsymbol{\vartheta}, \mu, \mathbf{x}_1, \mathbf{x}_2) \,|\, \boldsymbol{\omega}, \tilde{\mathbf{p}}, \mathbf{d}, \boldsymbol{\beta}, \boldsymbol{\alpha}$ is given by

$$\pi(\boldsymbol{\vartheta}, \mu, \mathbf{x}_1, \mathbf{x}_2 \,|\, rest) \propto \pi(\boldsymbol{\vartheta} \,|\, rest) \times \pi(\mu, \mathbf{x}_1, \mathbf{x}_2 \,|\, \boldsymbol{\vartheta}, rest),$$

where

$$\pi(\boldsymbol{\vartheta} \,|\, rest) \propto f(\tilde{\mathbf{p}} \,|\, \boldsymbol{\vartheta}, \boldsymbol{\omega}, \mathbf{d}, \boldsymbol{\beta}, \boldsymbol{\alpha}) \pi(\boldsymbol{\vartheta}),$$
$$\pi(\mu, \mathbf{x}_1, \mathbf{x}_2 \,|\, \boldsymbol{\vartheta}, rest) \propto \pi(\mu \,|\, \boldsymbol{\vartheta}, rest) \pi(\mathbf{x}_1, \mathbf{x}_2 \,|\, \mu, \boldsymbol{\vartheta}, rest),$$

and $f(\bullet)$ denotes the conditional likelihood function of the approximated models (9)-(11). Throughout the remainder of this paper, we use *rest* for the full conditional parameters as stated in each of the MCMC steps. The posterior distribution $\pi(\boldsymbol{\vartheta}, \mu, \mathbf{x}_1, \mathbf{x}_2 \,|\, rest)$ is marginalised over μ, which supports fast convergence of the full procedure. Consequently, we can determine the conditional likelihood $f(\tilde{\mathbf{p}} \,|\, \boldsymbol{\vartheta}, \boldsymbol{\omega}, \mathbf{d}, \boldsymbol{\beta}, \boldsymbol{\alpha})$ by means of an Augmented Kalman Filter, proposed by De Jong (1991), applied on the models (9)-(11) (see Appendix G for the details). To sample the volatility parameters $\boldsymbol{\vartheta}$, we make use of a Metropolis-Hastings algorithm with a truncated Gaussian approximation of $\pi(\boldsymbol{\vartheta}|rest)$ as proposal density, proposed by Chib and Greenberg (1994). We define $\hat{\boldsymbol{\vartheta}}$ as the volatility estimates that maximises the posterior density $\pi(\boldsymbol{\vartheta} \,|\, rest)$, and draw a candidate $\boldsymbol{\vartheta}^*$ from the truncated normal distribution on region R, $\mathcal{TN}_R(\boldsymbol{\vartheta}_*, \boldsymbol{\Sigma}_*)$, where

$$\boldsymbol{\vartheta}_* = \hat{\boldsymbol{\vartheta}} + \boldsymbol{\Sigma}_* \frac{\partial \log \pi(\boldsymbol{\vartheta} \,|\, rest)}{\partial \boldsymbol{\vartheta}}\bigg|_{\boldsymbol{\vartheta}=\hat{\boldsymbol{\vartheta}}}, \qquad \boldsymbol{\Sigma}_*^{-1} = -\frac{\partial^2 \log \pi(\boldsymbol{\vartheta} \,|\, rest)}{\partial \boldsymbol{\vartheta} \partial \boldsymbol{\vartheta}'}\bigg|_{\boldsymbol{\vartheta}=\hat{\boldsymbol{\vartheta}}}, \tag{13}$$

and $R = \{\gamma : |\phi_1|, |\phi_2| < 1, \phi_2 < \phi_1, \sigma_1^2, \sigma_2^2 > 0, |\rho| < 1\}$. This candidate $\boldsymbol{\vartheta}^*$ is accepted or rejected according to the Metropolis-Hastings accepting probabilities. To ensure, or increase the speed of, convergence towards the posterior mode we manipulate the optimisation algorithm to find $\hat{\boldsymbol{\vartheta}}$. The first (approximately) 50 MCMC iterations maximise the likelihood function until the change in likelihood is small in an absolute and relative sense. For the following MCMC draws, we compute $\hat{\boldsymbol{\vartheta}}$ by decreasing the number of optimisation iterations and function calls. This reduces the accuracy of $\hat{\boldsymbol{\vartheta}}$ and "increases" its variance parameters $\boldsymbol{\Sigma}_*$. This enables the algorithm to re-position its volatility parameter estimates if the posterior mode is distant from the current "optimal" $\hat{\boldsymbol{\vartheta}}$. This algorithm is robust to find the posterior mode and decreases the path and time of the MCMC algorithm to reach it.

Sampling $\pi(\mu, \mathbf{x}_1, \mathbf{x}_2 \,|\, \boldsymbol{\vartheta}, rest)$ is rather straightforward. The parameter μ can be sampled from the normal distribution with mean and variance that are associated with the Augmented Kalman filter in Appendix G. Furthermore, we can sample the volatility states from its full conditional $\pi(\mathbf{x}_1, \mathbf{x}_2 \,|\, \mu, \boldsymbol{\vartheta}, rest)$ by means of the Gaussian simulation smoother, implemented by Frühwirth-Schnatter (1994), Carter and Kohn (1994), and Durbin and Koopman (2002) to cite only the earliest papers.

4.3.2 Sampling Seasonal and Monday Open States

To sample the seasonal and Monday open effects, we use a state space framework for polynomial smoothing splines, following the theory of Kohn and Ansley (1987). Define $\mathbf{g} = (g_1, ..., g_K)'$ as the latent coefficients $\boldsymbol{\beta}$ or $\boldsymbol{\alpha}$, where K equals the number of periods within a trading day or $K = 5$, respectively. We assume that the components in $\mathbf{g}$ follow a modified cubic smoothing spline prior of the form $\nabla^2 g_k \sim \mathcal{N}(0, c_k^2 \tau_j^2)$, where ∇^2 is the second difference operator, τ_j^2 is the smoothing parameter with j equal to s or α for either season or Monday open effect consideration, respectively, and c_k's are prespecified scale factors, given by

$$c_k = \begin{cases} 100 & \text{if } k = 1, K \\ 1 & \text{otherwise,} \end{cases} \tag{14}$$

if the seasonal components $\boldsymbol{\beta}$ are considered and $c_k = 1$ for all $k = 1, ..., 5$ if the $\boldsymbol{\alpha}$ effects are considered. We observe the following data series:

$$\hat{y}_k = \hat{v}_k^2 \sum_{t:H_{tk}=1} (\tilde{p}_t - x_{t,1} - x_{t,2} - a_t - m_{\omega_t}) v_{\omega_t}^{-2} \qquad \text{and} \qquad \hat{v}_k^2 = \left(\sum_{t:H_{tk}=1} v_{\omega_t}^{-2} \right)^{-1}, \tag{15}$$

if seasonal components $\mathbf{g} = \boldsymbol{\beta}$ are considered and

$$\hat{y}_l = \hat{v}_l^2 \sum_{t:I_{tl}=1} (\tilde{p}_t - x_{t,1} - x_{t,2} - s_t - m_{\omega_t}) v_{\omega_t}^{-2} \qquad \text{and} \qquad \hat{v}_l^2 = \left(\sum_{t:I_{tl}=1} v_{\omega_t}^{-2} \right)^{-1}, \tag{16}$$

if Monday open effects $\mathbf{g} = \boldsymbol{\alpha}$ are considered. For notational conveniences, we denote both data series by $\hat{y}_k \sim \mathcal{N}(g_k, \hat{v}_k^2)$ for $k = 1, ..., K$, where $K = 5$ for $\boldsymbol{\alpha}$. Following Weinberg et al. (2007), we define the latent state vector $z_k = (g_k, \partial g_k / \partial k)'$, which enables us to write the entire model in the following Gaussian state space form:

$$\begin{aligned} \hat{y}_k &= h' z_k + \varepsilon_{k,1}, \quad & \varepsilon_{k,1} &\sim \mathcal{N}(0, \hat{\nu}_k^2) \\ z_{k+1} &= F z_k + \varepsilon_{k,2}, \quad & \varepsilon_{k,2} &\sim \mathcal{N}(0, \tau_j^2 c_k^2 U) \end{aligned}, \text{ where } h = \begin{pmatrix} 1 \\ 0 \end{pmatrix}, \; F = \begin{pmatrix} 1 & 1 \\ 0 & 1 \end{pmatrix}, \; U = \begin{pmatrix} 1/3 & 1/2 \\ 1/2 & 1 \end{pmatrix},$$

$\varepsilon_{k,1}$ and $\varepsilon_{k,2}$ are, both serial and mutual, independent, and $z_1 \sim \mathcal{N}(0, c_1^2 I)$, with c_1 sufficient large and I being a (2×2) identity matrix. To draw the states and smoothing parameter, we sample from the following posterior bivariate distribution:

$$\pi(\mathbf{z}, \tau^2 \,|\, \hat{\mathbf{y}}) = \prod_{k=1}^{K} \pi(\hat{y}_k \,|\, z_k) \pi(z_{k+1} \,|\, z_k, \tau^2),$$

where $\mathbf{z} = \{z_k\}_{k=1}^K$ and $\hat{\mathbf{y}} = \{\hat{y}_k\}_{k=1}^K$. We jointly generate the coefficients $\mathbf{z}$ and τ^2 by means of a Metropolis step. Consider $\tau^{2(i)}$ as τ^2 at i-th step of the MCMC algorithm, we then draw a proposal estimate $\tau^{2(*)}$ from the Normal distribution with mean $\tau^{2(i)}$ and variance w, which we accept with probability

$$\min\Big\{1, \frac{\pi(\mathbf{y} \,|\, \tau^{2(*)})\pi(\tau^{2(*)})}{\pi(\mathbf{y} \,|\, \tau^{2(i)})\pi(\tau^{2(i)})}\Big\}, \tag{17}$$

and where $w = \sum_{k=2}^K (z_k - Fz_{k-1})' U^{-1} (z_k - Fz_{k-1})/c_k^2$. Both $\pi(\hat{\mathbf{y}} \,|\, \tau^2)$ and $\mathbf{z}$ in w are obtained by the Kalman filter. If the proposal coefficient is accepted, set $\tau^{2(i+1)} = \tau^{2(*)}$ and sample $\mathbf{z}^{(i+1)}$ from $\pi(\mathbf{z}|\tau^{2(i+1)}, \hat{\mathbf{y}})$ by means of the simulation smoother. Then, $\mathbf{g}$ is directly obtained from $\mathbf{z}$ by definition. A zero-sum constraint on the seasonal parameters is imposed by re-normalising the draws, instead of constraining the Gaussian state space model, which would become infeasible.

4.3.3 Sampling the Scale Mixture Components and Degrees of Freedom

To sample $(\boldsymbol{\lambda}, \nu)$ jointly from its posterior, we follow the sampling scheme of Stroud and Johannes (2014). Note that the conditional posterior can be written as $\pi(\boldsymbol{\lambda}, \nu \,|\, rest) = \pi(\nu \,|\, rest)\pi(\boldsymbol{\lambda} \,|\, \nu, rest)$. We define $w_t = (p_t - p_t^* - J_t Z_t^p)/\exp(h_t/2)$, such that $(w_t \,|\, \nu, rest) \sim t_\nu(0,1)$. Under the discrete uniform prior distribution for $\nu \sim \mathcal{DU}(a_\nu, b_\nu)$, the posterior distribution follows a multinomial $(\nu \,|\, \mathbf{w}, rest) \sim \mathcal{M}(l_{a_\nu}, ..., l_{b_\nu})$, where $\mathbf{w} = \{w_t\}_{t=1}^n$, and with probabilities

$$l_\nu \propto \prod_{t=1}^n p_\nu(w_t), \quad \nu = a_\nu, ..., b_\nu,$$

where we denote $p_\nu(w_t)$ as the Student-t probability density function with ν degrees of freedom. As the computation of all individual multinomial probabilities is computational heavy, Stroud and Johannes (2014) propose a Metropolis step to draw a new ν coefficient. We define the width parameters as δ and, given the current value $\nu^{(i)}$, we draw a candidate value $\nu^{(*)} \sim \mathcal{DU}(\nu^{(i)} - \delta, \nu^{(i)} + \delta)$, which is accepted with probability

$$\min\left\{1, \frac{\prod_{t=1}^n p_{\nu^{(*)}}(w_t)}{\prod_{t=1}^n p_{\nu^{(i)}}(w_t)}\right\}. \tag{18}$$

The width δ is determined by allowing the acceptance probability to vary between 20% and 50%. Subsequently, given the degrees of freedom, we can draw the scale factors. Note that $\epsilon_t^* = (p_t - p_t^* - J_t Z_t^p)/\exp(h_t/2)$, which is, given ν, normally distributed with mean zero and variance λ_t, that is, $(\epsilon_t^* \,|\, \lambda_t, \nu, rest) \sim \mathcal{N}(0, \lambda_t)$. Assuming the conjugate prior $(\lambda_t \,|\, \nu) \sim \mathcal{IG}(\nu/2, \nu/2)$, it is straightforward

to see that the full conditional follows

$$(\lambda_t \,|\, \nu, rest) \sim \mathcal{IG}\Big(\frac{\nu+1}{2}, \frac{\nu+(\epsilon_t^*)^2}{2}\Big). \tag{19}$$

4.3.4 Sampling of Remainder

Throughout the rest of the sampling algorithm, the steps are rather straightforward. More details about means and variances for the upcoming distributions are given in Appendix F. Sampling the jump states and parameters is simple if we assume conjugate priors $J_t \sim Bern(\kappa)$ and $Z_t \sim \mathcal{N}(\boldsymbol{\mu}_z, \boldsymbol{\Sigma}_z)$, where $\boldsymbol{\mu}_z = (\mu_p, \mu_v)'$ and $\boldsymbol{\Sigma}_z = \text{diag}(\sigma_p^2, \sigma_v^2)$. The jump indicators J_t, given the other parameters, are Bernoulli distributed. Furthermore, the size parameters Z_t^p and Z_t^v can be drawn from a joint normal distribution.

For the jump parameters $(\kappa, \mu_p, \sigma_p, \mu_v, \sigma_v)$, conjugate priors are available. We assume that $\kappa \sim \mathcal{B}(a_\kappa, b_\kappa)$ and $(\mu_j, \sigma_j^2) \sim \mathcal{NIG}(m_j, c_j, a_j, b_j)$, for $j = p, v$, such that we can draw $(\kappa \,|\, rest)$ from the beta distribution, and $(\mu_p, \sigma_p^2 \,|\, rest)$ and $(\mu_v, \sigma_v^2 \,|\, rest)$ from the normal-inverse Gamma distribution.

We sample the mixture indicators ω_t for $t = 1, ..., n$, from its discrete conditional posterior distribution. We perform the inverse transform method to sample the conditional indicators.

Given all other parameters and mixture components, equations (3)-(4) can be seen as a traditional Gaussian state space model. Therefore, the latent states p_t^* can be sampled by means of the simulation smoother of Durbin and Koopman (2002). Moreover, conditional on the remaining parameters and the states p_t^*, the parameter σ_r can be sampled from the inverse gamma distribution if we assume a conjugate prior $\sigma_r \sim \mathcal{IG}(a_r/2, b_r/2)$.

4.3.5 Auxiliary Re-weighting Approximated Samples

Omori et al. (2007) show that the mixture of normal distributions is an accurate approximation of the true distribution of ζ_t. However, minor errors are still made, which we correct to obtain samples from the true distribution. Let us denote

$$\zeta_t^{(i)} = \tilde{p}_t - h_t^{(i)}, \quad \eta_{2,t}^{(i)} = [(x_{t+1,2}^{(i)} - \mu^{(i)}) - \phi_2^{(i)}(x_{t,2}^{(i)} - \mu^{(i)}) - J_t^{(i)} Z_t^{v(i)}]/\sigma_2^{(i)},$$

where (i) denotes the i-th sample from the MCMC algorithm, for $i = 1, ..., M$, where M is the number of MCMC draws. In order to re-sample the obtained approximated samples, we compute the weights

$$w_i^* = \prod_{t=1}^{n} \frac{\pi(\zeta_t^{(i)}, \eta_t^{(i)} \,|\, d_t, \mu^{(i)}, \boldsymbol{\vartheta}^{(i)})}{g(\zeta_t^{(i)}, \eta_t^{(i)} \,|\, d_t, \mu^{(i)}, \boldsymbol{\vartheta}^{(i)})}, \quad w_i = \frac{w_i^*}{\sum_{k=1}^{M} w_k^*}, \quad \text{for } i = 1, ..., M.$$

We can now require a sample from $\pi(\boldsymbol{\theta}, \mathbf{z}, \boldsymbol{\beta}, \boldsymbol{\alpha} \mid \mathbf{p})$ by re-weighting the sampled coefficients and states proportional to the weights w_i.

4.4 Simulation Study

In this subsection, we present a simulation study to validate our proposed model and estimation algorithm. This also shows that our Extended Unobserved Components model is identifiable under informative, but weak priors. We illustrate our estimation procedure and its performance by simulating from our model given by (3)-(7). We generate 74 data points per day over a sample of 130 days, resulting in a total of 9620 observations, which is similar to the ASX sample data. The true parameters are given in the second column of Table 5, which are a combination of multiple empirical studies (see e.g. Omori et al., 2007 and Stroud and Johannes, 2014). Additionally, we simulate $\boldsymbol{\alpha}$ and $\boldsymbol{\beta}$ by means of cubic smoothing splines.

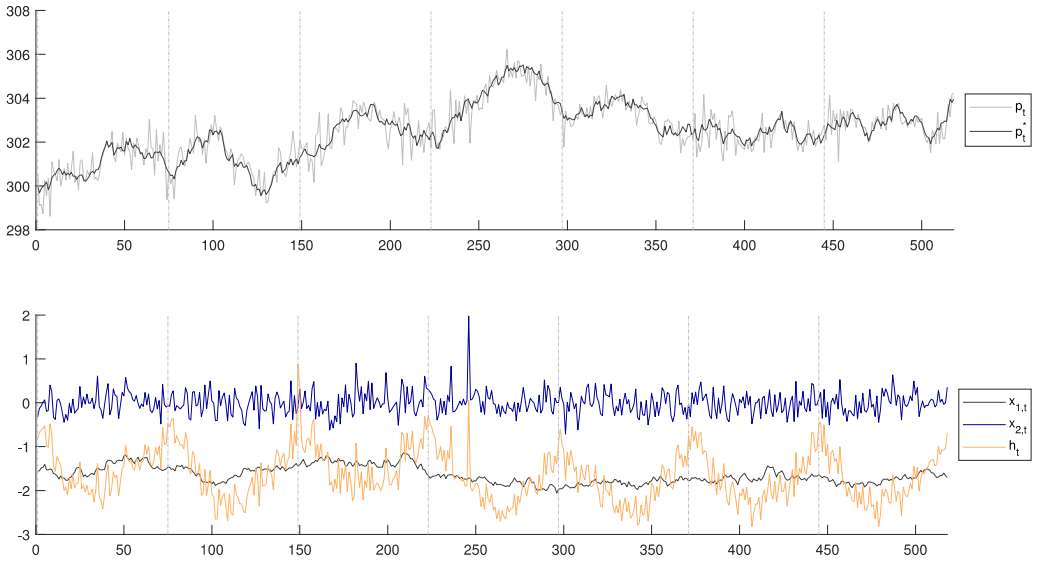

Figure 4: This figure plots the simulated data. The upper panel illustrates the noisy price dynamics with its underlying market price. The lower panel shows the true unobserved volatility states.

Figure 4 plots the simulated data for the 7 days, where the dashed-dotted lines indicate the first observation of the day. The third day corresponds to the Monday open. The upper panel shows the price dynamics with its true underlying log spot price. The lower panel displays the volatility states. By construction, the long-term volatility variable is more consistent over time than the short-term volatility. Moreover, the total volatility state h_t shows an obvious daily pattern and an increase in Monday open volatility. For evaluation, we draw 10,500 samples from our full estimation algorithm and regard 500 of the MCMC draws as burn-in sample. We efficiently program our sampling algorithm

from scratch in base SAS and proc IML SAS. The biggest burden arises due to the optimisation of the likelihood function in the second step of the algorithm (Section 4.3.1), for which we use standard non-linear optimisation packages. This, however, reduces as we decrease the number of iterations and function calls.

The results are based on the priors given in Appendix E. Table 5 reports the true values, posterior means, standard deviations, 95% credible intervals, and inefficiency factors. The inefficiency factor is defined as $1 + 2\sum_{i=1}^{\infty} \hat{\rho}_i$, where $\hat{\rho}_i$ denotes the sample autocorrelation at lag i. This quantity can be interpreted as the ratio of the numerical variance of the posterior mean from our MCMC chain to the hypothetical variance of the posterior mean based on independent draws. Theoretically, it is the inverse of the relative numerical efficiency defined in Geweke et al. (1991).

Table 5: Simulation Results

Parameter	True value	Mean	St. dev.	95% interval	Inefficiency
ϕ_1	0.97	0.9771	0.0060	[0.9665, 0.9858]	1.8408
ϕ_2	0	0.0182	0.0691	[-0.0949, 0.1341]	1.4375
σ_1	0.05	0.0453	0.0053	[0.0373, 0.0544]	1.0771
σ_2	0.25	0.2566	0.0200	[0.2234, 0.2899]	1.7397
ρ	-0.20	−0.1466	0.0382	[-0.2096, -0.0845]	1.1229
$\exp(\mu/2)$	0.45	0.4528	0.0057	[0.4434, 0.4621]	1.0718
ν	20	23.4979	3.7779	[18, 30]	18.7476
κ	0.008	0.0099	0.0016	[0.0076, 0.0128]	2.0284
μ_p	-1.5	−1.5382	0.1224	[-1.7299, -1.3271]	5.4892
μ_v	1.1	0.9894	0.0886	[0.8542, 1.1249]	1.2935
σ_p	0.85	0.8715	0.0902	[0.7300, 1.0268]	4.5355
σ_v	0.80	0.7673	0.0528	[0.6847, 0.8562]	1.8357
σ_r	0.20	0.2053	0.0051	[0.1971, 0.2140]	12.0544

NOTE: This table presents summary statistics for our simulation experiment using our sampling algorithm on models (3)-(7). The table reports the true parameter values, posterior means, standard deviations, 95% credible intervals, and inefficiency factors. The sample size included a total of 9620 observations over 130 trading days. The results are based on 10,000 MCMC draws, after discarding the first 500.

All posterior means are relatively close to their true values and their standard deviations are small. Moreover, the true values are contained in the 95% credible intervals. The inefficiency factors take low values, except for ν and σ_r. For ν, this is possibly caused by the Metropolis step. Its acceptance probability is quite low, resulting in a highly-correlated sample. The variable σ_r, on the other hand, does not depend on a Metropolis step. However, it only depends on the underlying latent price process p_t^*, which remains very consistent over all draws. Therefore, it results in a highly-correlated sample. Appendix H illustrates the sampled draws and posterior distributions. Moreover, it reports the autocorrelation of the draws over 20 lags for all parameters. The first lag is significantly positive for all coefficients. However, this decays sharply over the lags (except for ν and σ_r as mentioned before). All things considered, it suggests that we are successful in efficiently sampling from the true

posterior distributions.

For illustrative purposes, Figure 5 plots the posterior mean and true $\boldsymbol{\beta}$ and $\boldsymbol{\alpha}$ series, including 95% confidence intervals. The sampled means are close to the true values and the true values are encompassed in their corresponding 95% credible intervals. The remaining volatility states show similar results. Therefore, we conclude that our estimation algorithm efficiently samples from the true posterior distributions.

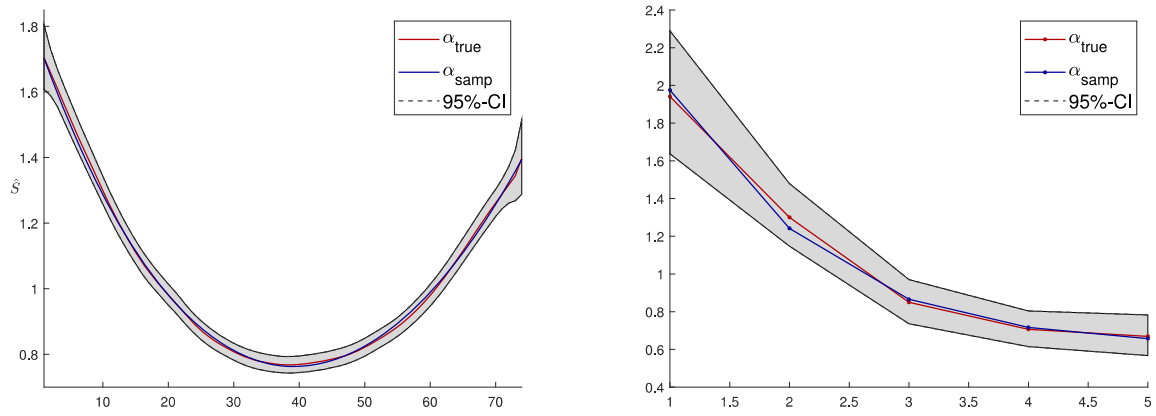

Figure 5: This figure presents the true simulated values, posterior means, and 95% confidence intervals for the seasonal effects $\boldsymbol{\beta} = (\beta_1, \ldots, \beta_{74})$ (left panel) and the Monday open effects $\boldsymbol{\alpha} = (\alpha_1, \ldots, \alpha_5)$ (right panel). Results are illustrated on a standard deviation scale, that is $\hat{S} = \exp(\boldsymbol{\beta}/2)$ and $\hat{S} = \exp(\boldsymbol{\alpha}/2)$, respectively. For example, $\hat{S} = 2$ means that the underlying volatility is twice its original baseline.

4.5 Empirical Analysis

We apply the same approach to the intraday log prices for each stock in our sample. We record 10,000 samples, after we discard the first 500 MCMC iterations, for each parameter and state across all stocks. We are interested in average volatility dynamics within each exchange and, therefore, we compute average posteriors. For each draw, we take the average across all stocks within the specific market. Throughout the remainder of this paper, each aforementioned parameter now denotes the average posterior distribution. For example, $\boldsymbol{\beta}$ denotes the average posterior distribution for the daily volatility pattern across all sample stocks within either the ASX or JSE.

Table 6 summarises the average posterior distributions and reports inefficiency factors for both the Australian and South-African markets. The SV factors indeed correspond to a slow-moving intraday factor and a fast-moving interday determinant. The mean of ϕ_1 is 0.9985 and 0.9981, corresponding to a day-to-day AR(1) coefficient of 0.89 and 0.83 for the ASX and JSE, respectively. These estimates imply a half-life, $\log(0.5)/\log(\phi_1)$, between approximately 4 and 7 days, relatively lower than other studies that examine daily returns. The rapidly moving intraday factor $x_{t,2}$ has mean coefficients of

0.9810 and 0.9848, generating a daily AR(1) coefficient of 0.24 and 0.23, both consistent with a half-life of around half their trading day, for the ASX and JSE, respectively. Note that both ϕ_2 and σ_2 are significantly different from zero, giving evidence for high-frequency shocks in volatility and supports the use of a two-factor SV model.

Table 6: Estimation Results ASX and JSE

Parameter	Mean		St. dev.		95% interval	
	ASX	JSE	ASX	JSE	ASX	JSE
ϕ_1	0.9985	0.9981	0.0010	0.0011	[0.9964, 0.9999]	[0.9955, 0.9999]
ϕ_2	0.9810	0.9848	0.0056	0.0036	[0.9680, 0.9900]	[0.9769, 0.9906]
σ_1	0.0469	0.0446	0.0264	0.0217	[0.0266, 0.1277]	[0.0262, 0.1214]
σ_2	0.0511	0.0454	0.0043	0.0088	[0.0336, 0.1152]	[0.0345, 0.0661]
ρ	−0.0004	0.0045	0.0525	0.0423	[-0.1046, 0.1026]	[-0.0784, 0.0873]
$\exp(\mu/2)$	0.6333	0.5122	8.1982	0.0913	[0.3998, 0.6405]	[0.3788, 0.6759]
ν	52.5912	46.6473	4.9731	4.3378	[41.422, 57.261]	[37.988, 50.992]
κ	0.0112	0.0132	0.0173	0.0186	[0.0001, 0.0472]	[0.0001, 0.0513]
μ_p	−1.4838	−1.3207	6.7119	5.4608	[-14.475, 11.618]	[-10.268, 7.8402]
μ_v	0.4551	0.4573	0.2200	0.1806	[0.0987, 0.8171]	[0.1560, 0.7579]
σ_p	0.2796	0.2931	0.2983	0.3104	[0.1813, 0.6447]	[0.2021, 0.6831]
σ_v	0.3349	0.3171	0.3667	0.3301	[0.3018, 0.3827]	[0.3331, 0.3986]
σ_r	0.0020	0.0021	0.0001	0.0001	[0.0019, 0.0021]	[0.0020, 0.0022]

NOTE: This table presents the posterior means, standard deviations, and 95% credible intervals for the average ASX and JSE sample stocks. The results are based on 10,000 MCMC draws, after the first 500 are discarded.

Estimations of ρ are small negative, indicating that the leverage effect is weak. Estimates of ν are about 52 and 46 for the ASX and JSE, respectively. This indicates rather mild non-normal price shocks and implying very modest higher probabilities of larger shocks in our samples. Note that abundant price shocks are also captured by $J_t Z_t^p$. Moreover, this result is based on the average of all considered stocks. Individual price series display divergent estimates. Few stocks show the importance of using heavy-tailed error distributions, while others can be modelled by a normal model. For consistency and robustness, we use the t-distributed errors for all stock prices. Mean price jumps μ_p are not significantly different from zero, but do have a large 95% range, indicating that both large positive and negative jump sizes occur. The arrivals of such jumps occur with $\kappa = 0.0112$ and $\kappa = 0.0132$, which is equal to a daily rate of 0.83 and 1.25 for the ASX and JSE, respectively. The price jumps are relatively small as σ_p is approximately 0.28, which is considerably smaller than the modal non-jump volatility of $\exp(\mu/2) \approx 0.63$ (ASX) and 0.51 (JSE). Similarly, volatility jumps are quite high, increasing the volatility by a factor $\exp(\mu_v/2) = 1.40$ and 1.37, that is an increase of around 40% and 37%, for the ASX and JSE, respectively. The inefficiency factor of the slowest mixing parameters ϕ_1 is around 60. Although it is considerably higher than for the simulated data, our sampling algorithm still works reasonably well for empirical researches.

5 The Efficiency of Auction Mechanisms

In this section, we test the auction efficiency. We first analyse the opening price stability, by implementing variance ratios, measured by our model-based volatility patterns. Second, we examine price discovery during the auction process by conducting weighted price ratios. Lastly, we consider auction price efficiency by measuring how accurate the determined opening price reflects the true underlying market price. All three things considered encompass a measure for the efficiency of opening auctions. A sufficient operative mechanism (i) obviates an increase in opening price volatility, (ii) covers a large proportion of price discovery during the pre-open session, and (iii) produces efficient opening prices. In addition, we test which of the two call designs is superior in the three auction efficiency targets.

5.1 Opening Price Stability

We obtain an average measure that defines the consistent increase in price volatility at the market open through the posterior mean of $\boldsymbol{\beta}$. Note again that $\boldsymbol{\beta}$ now denotes the average posterior distribution across all stocks, within a particular exchange, for each $k = 1, \ldots, K$. By definition, β_1 corresponds to the opening price volatility increase relative to the basis level of a trading day. We link a significant increase to the deficiency of market depth during the auction book-building phase. Au contraire, no significant increase would imply that the opening price absorbed all necessary overnight information, such that the call preserved price stability.

We denote $\boldsymbol{\beta}_{ASX}$ and $\boldsymbol{\beta}_{JSE}$ as the average beta posterior for the ASX and JSE sample stocks, respectively. Note that the daily volatility pattern is imposed by the density zero-sum constraint. Therefore, the ASX and JSE average seasonal dynamics are of the same scale, which makes comparisons between the two simple. For statistical inference, we compute the difference posterior distribution for $k = 1, \ldots, 36$ and $k = K - 12, \ldots, K$. That is, $\beta_{diff,k} = \beta_{JSE,k} - \beta_{ASX,k}$, for each MCMC draw, during the first three hours and the final hour of continuous trading. We repeat the above analysis for high and low tertile stocks. That is, within a particular exchange, we compute the difference posterior distribution between high and low tertile stocks. Mathematically, we then denote $\beta_{diff,k} = \beta_{low,k} - \beta_{high,k}$ for all $k = 1, \ldots, K$, for either the ASX or JSE listed stocks. Furthermore, we use similar volatility difference distributions, based on the Monday open series $\boldsymbol{\alpha}$, and compute statistical tests analogously.

Our method enables us to evaluate the differences in price volatility across different markets. In addition, we try to capture the increased volatility that is exclusively caused by (inefficient) auction processes through $\boldsymbol{\beta}$. By contrast, existing literature has frequently exploited variance ratios to test the impact of auction mechanisms on price or return volatility within specific markets, see for example

Comerton-Forde and Rydge (2006) and Amihud and Mendelson (1991). In their approach, they calculate the open-to-same day 11:00 returns, which is the log of the midpoint price at 11:00 minus the log of the openings price on the same day.[4] The variance of these returns can be analysed and compared across different periods for the same security, which is convenient to examine the effect of changes in auction mechanisms within a specific market. Compared to these studies, we argue that our method is more robust for auction efficiency tests and comparisons across markets.

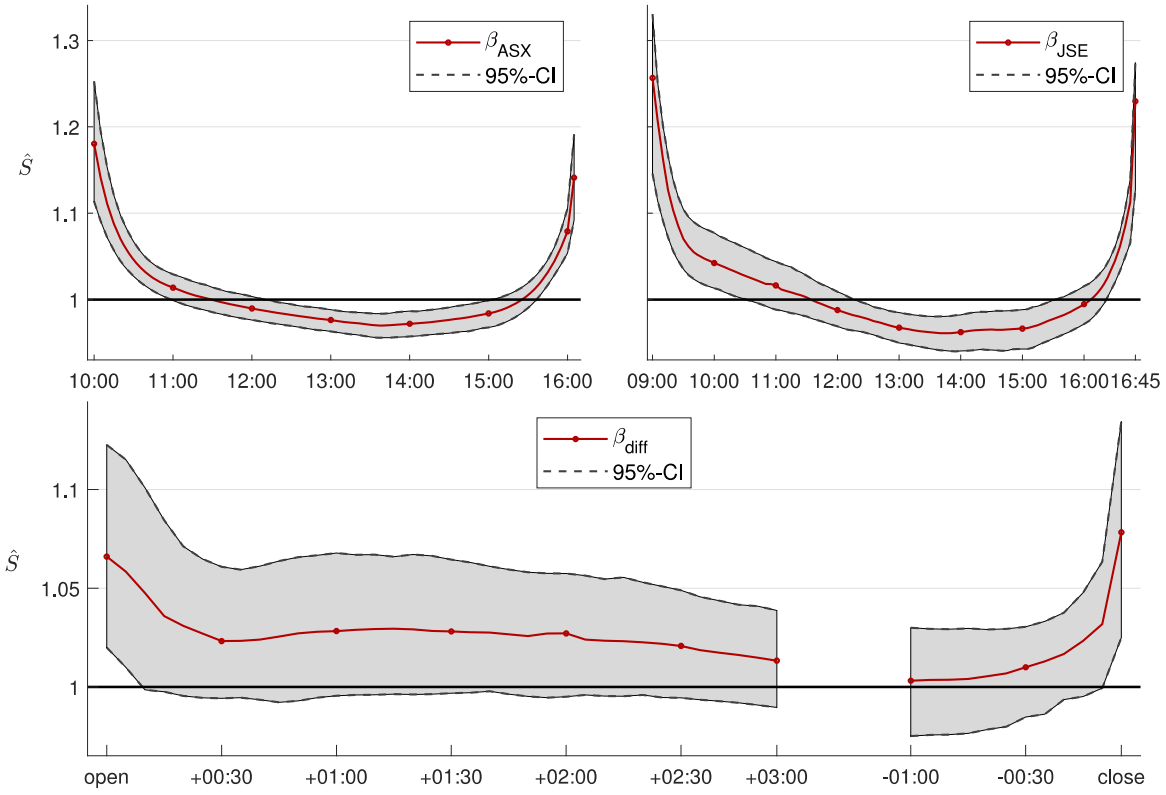

Figure 6: This figure shows the posterior means and 95% intervals for the daily intraday patterns. Results are presented on a standard deviation scale, that is $\hat{S} = \exp(\boldsymbol{\beta}/2)$. The upper panels summarise β_k, for $k = 1, \ldots, K$, considering the ASX (left) and the JSE (right). The lower panel charts the posterior mean for $\exp(\beta_{k,diff}/2)$, where $\beta_{k,diff} = \beta_{k,JSE} - \beta_{k,ASX}$. The variable k includes two subsets. The first runs for 3 hours from market opening and the second contains the last hour of continuous trading.

Figure 6 summarises the posterior distribution of $\hat{S}_k$, where $\hat{S}_k = \exp(\beta_k/2)$ denotes the standard deviation scale of β_k. So, $\hat{S}_k = 1$ corresponds to the average 5-minute volatility and, therefore, $\hat{S}_k = 2$ would imply that the volatility is approximately twice its baseline level. The left and right upper panel corresponds to the ASX and JSE market, respectively. There is a clear "U"-shaped pattern present in the intraday volatility. Both figures show the importance of including a daily pattern component in price volatility models, as $\hat{S}_k$ fluctuates by a factor 1.3. At the market open, $\hat{S}_k$ spikes to roughly 1.18 and 1.25 for the ASX and JSE, respectively. Both are highly significant, implying that the average opening price volatility is substantially higher than the remainder of the trading day. Similar results

[4]The price at 11:00 is assumed to be the security's true value, as suggested by Ciccotello and Hatheway (2000)

are found for the closing price, which, however, is rather due to market participants willing to trade at this price to beat benchmarks, increasing price fluctuations. This is in line with the relative high trading volumes closing the market closure.

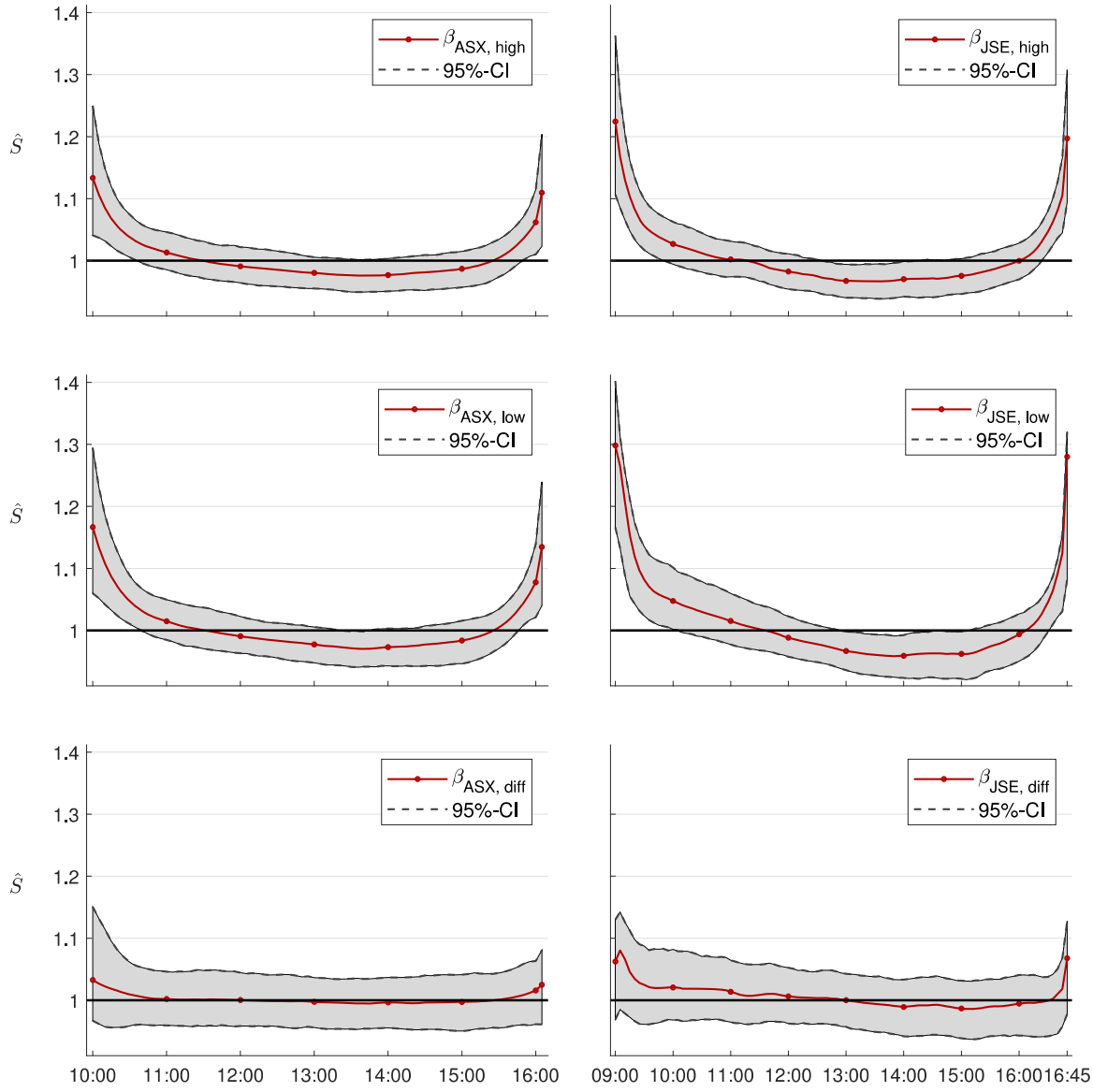

Figure 7: This figure shows the posterior means and 95% intervals for the daily intraday patterns. Results are presented on a standard deviation scale, that is $\hat{S} = \exp(\boldsymbol{\beta}/2)$. The left panels correspond to the ASX and the right panels to the JSE. The upper panels denote the high tertile stocks, while the middle figures correspond to the low tertile stocks. The lower panels chart the difference between low and high tertile daily pattern estimates.

The lower panel of Figure 6 charts the posterior distribution of the standard deviation scale of $\beta_{diff,k}$. The average opening price volatility is significantly higher for the South-African market. This significant increase remains during the first 10 minutes of the continuous session. The Australian market needs approximately one hour to find a stable consensus price, while the JSE needs roughly one hour and a half. Hence, the ASX has a significant 7% lower opening price volatility than the JSE

and its convergence to price stability is around 30 minutes faster. At the market close, there is again a substantial volatility discrepancy, which is conform to the large increase in closing price benchmark traders participating at the Johannesburg Stock Exchange.

Figure 7 reports the posterior distributions for $\boldsymbol{\beta}$ for the low and high tertiles and its difference, for each market. There is a small, however not significant, improvement in reducing opening price volatility and increasing price stability speed if auction participation is higher. The lack of significant evidence for volatility reduction and the increase in price stability speed could occur due to two reasons. First, the lack of data considering many auction participants reduces the strength in tertile differences. Although the ASX high tertile stocks contain almost 3 times more volume than low tertile stocks during the auction phase, it has only a relative value of 2.27. Second, our tertiles are based on incoming order volume rather than the number of participants. Therefore, the auction could have a relatively high order volume, but which is all entered by only a few active participants. A deficit of price informativeness occurs and price stability delays.

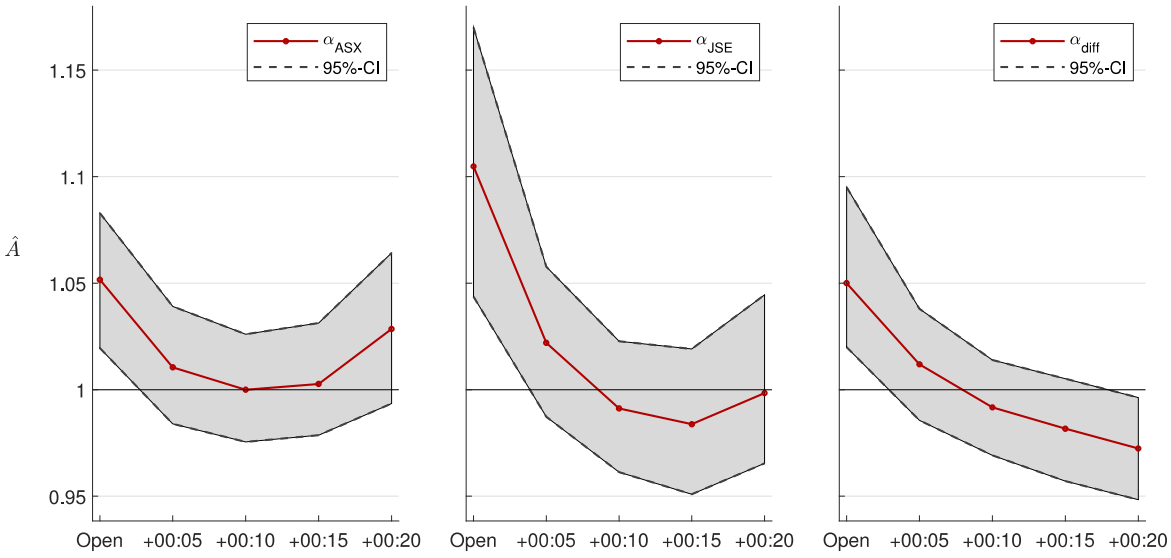

Figure 8: This figure shows the posterior means and 95% intervals for the Monday open effects, $\boldsymbol{\alpha} = (\alpha_1, \ldots, \alpha_5)$. Results are presented on a standard deviation scale, that is $\hat{A} = \exp(\boldsymbol{\alpha}/2)$. The left and middle panel correspond to the ASX and JSE Monday open effects, respectively. The last panel summarises the posterior distribution of $\exp(\boldsymbol{\alpha}_{diff}/2)$, where $\boldsymbol{\alpha}_{diff} = \boldsymbol{\alpha}_{JSE} - \boldsymbol{\alpha}_{ASX}$.

The Monday open effects posterior means and 95% confidence intervals are given in Figure 8. Note that the results are shown on the standard deviation scale, that is, $\hat{A} = \exp(\boldsymbol{\alpha}/2)$. We report our distribution summary for both the ASX and JSE, as well as JSE's $\hat{A}$ divided into ASX' $\hat{A}$ posterior distribution outline. The over-weekend uncertainty significantly increases the opening price volatility, intensifying the uncertainty by a factor 1.05 and 1.11 for the ASX and JSE, respectively. However, the Monday open effect fades away within five minutes and, therefore, only increases the opening price volatility. The Monday opening price volatility increases significantly higher for the JSE listed stocks

than those of the ASX.

As for $\boldsymbol{\beta}$, Figure 9 reports the posterior distributions for $\boldsymbol{\alpha}$, considering the low and high tertiles and its difference on standard deviations scale, for each market. An interesting result occurs with this analysis. Conditional on relatively high market participation, the ASX market does, on average, not suffer from an increase in opening price volatility after the weekend-closure. This implies that increasing auction participants diminishes long market closure uncertainty. Relevant information over the weekend is incorporated by the participants and does not increase price instability at the market open.

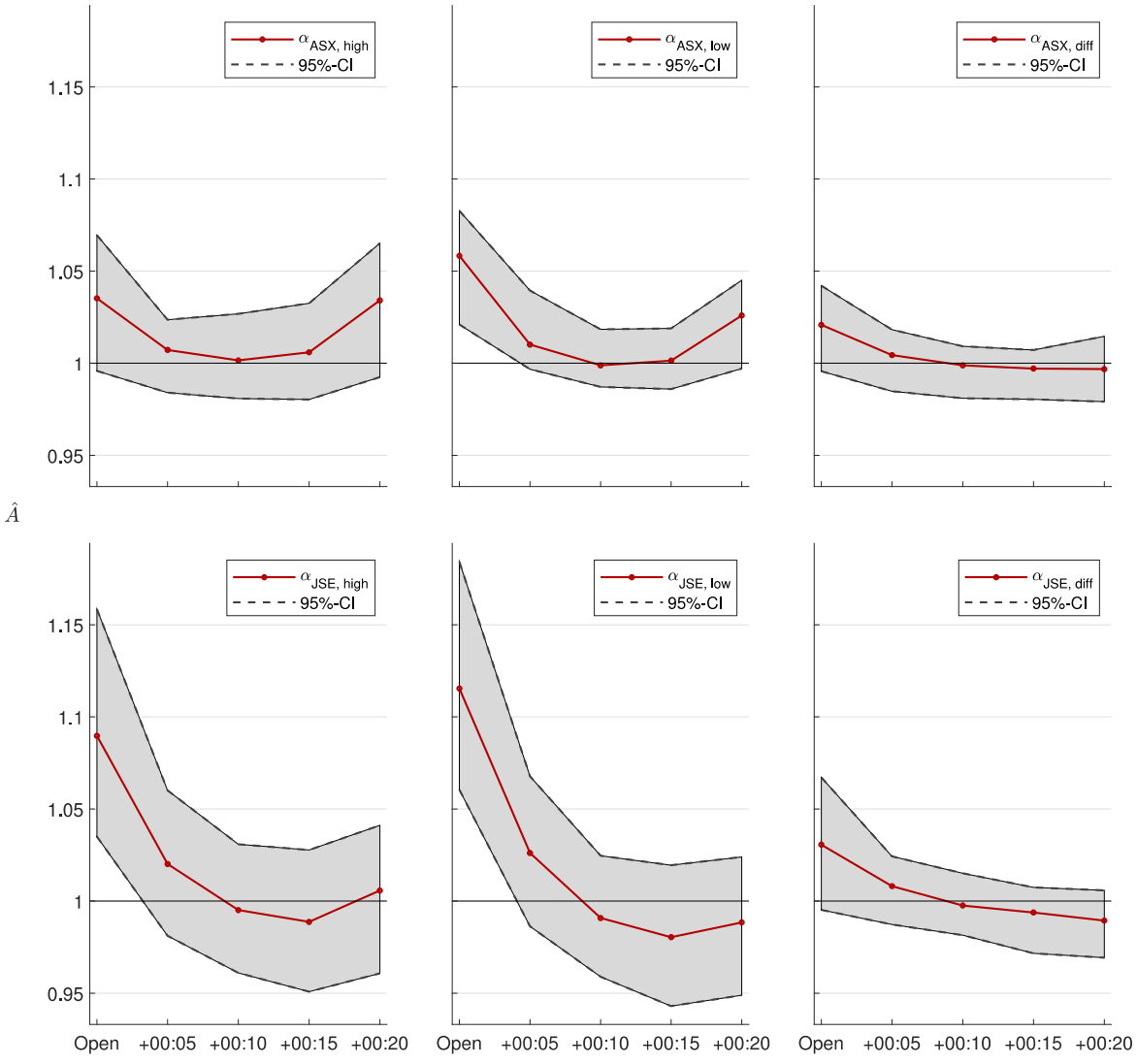

Figure 9: This figure shows the posterior means and 95% intervals for the daily intraday patterns. Results are presented on a standard deviation scale, that is $\hat{A} = \exp(\boldsymbol{\alpha}/2)$. The upper panels correspond to the JSE and the lower panels to the ASX. The left panels denote the high tertile stocks, while the middle figures correspond to the low tertile stocks. The right panels chart the difference between low and high tertile Monday open effects.

The high tertile stocks perform (slightly) better than the low tertile stocks in both markets in

means of opening price stability. That is, increasing auction participants decreases price volatility shortly after the market open and diminishes Monday open price uncertainty. However, the relative difference is insignificant. The rate of decrease for the Monday open effects is similar across the two tertiles, consistent with equal digestion times.

5.2 Price Discovery

Additional to the dispatch of market price stabilisation, measured by the variance ratios, we compare the level of information absorbency in security prices around the open. Since we are mainly interested in information efficiency of price discovery at the market open, we examine the intraday price discovery process during the full trading day by making use of weighted price contributions (WPC). We estimate the fraction of close-to-close price evolution ascertained for different periods within a trading day. The intraday periods for which we estimate the percentage of close-to-close price discovery are the following. The first period runs from 07:00 up to the opening auction start-off. From there, we include 10-minute periods up to the first hour in the normal trading session. We then add a block from 10:00 to 16:00 and 11:00 to 15:00 for the JSE and ASX, respectively. Subsequently, we divide the extent of time until 15 minutes and 30 minutes prior to the start of the closing auction into 10-minute intervals for the JSE and ASX, respectively. We then include the last period until the closing auction and the auction process itself. A clear overview of all intraday time periods for the JSE listed stocks is given in Table 7. For each trading day, exchange, and above mentioned period τ, we define the WPC statistic as

$$\mathrm{WPC}_\tau = \sum_{s=1}^{S} \left(\frac{|r_s|}{\sum_{s=1}^{S} |r_s|} \right) \times \left(\frac{r_{\tau,s}}{r_s} \right), \tag{20}$$

where r_s denotes the close-to-close log return for stock s and $r_{\tau,s}$ corresponds to the logarithmic return for period τ for stock s. Hence, r_s defines the daily return of stock s, that is the log closing price of today minus the closed log price of yesterday. Likewise, $r_{\tau,s}$ denotes the difference between the log price at time $t+\tau$ and time t for stock s. Note that we consider S stocks, where S is the number of sample stocks for either the ASX or JSE sample. The second term in Equation (20) measures the relative proportion of the day's return for stock s. A value close to one implies that the day's return, for stock s, is almost fully discovered in period τ. The latter fraction of Equation (20) is standardised by the first component, which weights each stock proportionally to the absolute value of r_s. Hence, smaller weights are given to stocks that have absolute smaller day returns r_s, which assumes that large close-to-close returns are more informative.

We compute the WPCs for each day and exchange. In a similar manner as Fama and MacBeth (1973), we obtain statistical inference by the Fama-Macbeth procedure. That is, we average the cross-

sectional computed WPCs across time and employ the time-series standard errors for significance testing procedures. The weighted price contribution is a model-free and well-documented measure to evaluate period by period price discovery. A similar approach is done by Cao et al., 2000 and Ibikunle, 2015, where they compute the proportion of close-to-close price discovery of each 10-minute-period. A major advantage of the statistic is its simplicity and non-model based structure, which avoids any assumptions on the sample data. Statistical validation of its performance is done by Van Bommel (2011) and Wang and Yang (2015).

Table 7: Price Discovery per Time Period

Time periods	High		Low		Overall		
	JSE	ASX	JSE	ASX	JSE	ASX	Diff.
Pre-open/opening auction							
07:00-08:30	0.036	0.052	0.006	0.003	0.026	0.060*	0.034
08:30-08:40	−0.038	0.004	0.011	0.000	−0.023	0.019	0.042
08:40-08:50	0.042	0.010	0.038	0.094*	0.060	0.046	−0.014
08:50-09:00	0.186*	0.416*	0.149*	0.283*	0.139*	0.322*	0.183*
Total	0.225*	0.481*	0.205*	0.380*	0.202*	0.446*	0.244*
Continuous session							
09:00-09:10	0.065*	0.082*	0.037*	0.082*	0.058*	0.077*	0.019
09:10-09:20	0.031*	0.056*	0.050*	0.063*	0.042*	0.053*	0.011
09:20-09:30	0.030*	0.024*	0.035*	0.025*	0.033*	0.024*	−0.009
09:30-09:40	0.036*	0.020*	0.024*	0.028*	0.035*	0.024*	−0.012
09:40-09:50	0.041*	0.010	0.038*	0.022*	0.039*	0.015*	−0.024*
09:50-10:00	0.034*	0.024*	0.026*	0.022*	0.027*	0.024*	−0.003
10:00-16:00	0.466*	0.266*	0.495*	0.325*	0.475*	0.289*	−0.186*
16:00-16:10	0.013*	0.004	0.004	0.002	0.007	0.007	0.000
16:10-16:20	0.006	0.005	0.006	0.014*	0.004	0.011*	0.007
16:20-16:30	0.021*	0.009*	0.024*	0.007	0.025*	0.005*	−0.020*
16:30-16:45	0.020*	0.033*	0.038*	0.031*	0.026*	0.031*	0.005
Total	0.763*	0.532*	0.774*	0.621*	0.770*	0.560*	−0.210*
Closing auction							
16:45-17:00	0.012	−0.012	0.021*	−0.001	0.027*	−0.006	−0.033*

NOTE: This table presents the average weighted price contribution (WPC) for both the JSE and ASX listed stocks. Additional to WPC computations based on all stocks within an exchange, the WPCs for both the high and low pre-open order entry quintiles are computed. The last column shows the difference between the ASX and JSE computed WPCs, based on all stocks. The time periods in the first column are based on the JSE opening times. For the ASX, the first period runs from 07:00 to 09:30. From there, we add one hour to all periods up to 10:00-16:00. This period is replaced by 11:00-15:00. Subsequently, the periods afterwards follow: 15:00-15:10, 15:10-15:20, 15:20-15:30, 15:30-16:00, and the closing auction from 16:00 to 16:10. The data covers all trading days between 3rd January 2019 and 17th July 2019. The symbol *indicates the WPCs that are significantly different from zero at the 0.05 level.

Table 7 reports the WPCs for the high and low order flow entry tertiles and all stocks combined within one of the two markets. The last column presents the difference between the ASX and JSE, considering all stocks. Approximately 20 and 45 per cent of the daily price discovery occurs during the pre-open market phase for all JSE and ASX listed stocks, respectively. This presents that information assembled overnight, for example, due to major American market opening hours, is reasonably incor-

porated into the stock price evolution during the opening auction. In addition, corporate-information released overnight also shows an impact on the after-hours trading session, see for example Jiang et al. (2012). Well-informed traders use the first opportunity to incorporate new information into the stock prices, which is during the opening auction.

The ASX is superior in relative price discovery during the pre-open hours. Before the market opens, the ASX discovers a significant 24.4% more of the total daily price evolution than the JSE. A considerable 18.8 per cent occurs during the final 10 minutes of the opening auction. Approximately 80 per cent of total JSE listed stocks price discovery still does not occur before market open. Therefore, a large proportion of, approximately, 77% and 3% shifts to the continuous trading session and closing auction, respectively. Both fractions are significantly larger than the ASX listed stocks. This suggests that the call design of the ASX aids better in discovering a consensus price before actual trading starts.

Additionally, four side results arise from this analysis. First, there is a vast disparity between the high and low tertile stocks in the fraction of price evolution discovered during the total pre-open phase. This difference is most compelling during the final 10 minutes of the opening auction and for the ASX listed stocks. The contrast equals 3.7% for the JSE listed stocks and even 13.3% for the ASX stocks. This clearly illustrates that more participants during an opening auction are favoured to enhance price discovery before the market opens. The general lack of price informativeness, due to a scarce amount of active participants, results in opening prices that poorly discovers daily price evolution.

Although the absolute pre-open phase runs for several hours, the largest proportion of price discovery is exposed during the final 10 minutes of the closing auction (13.9% and 32.2% for the JSE and ASX, respectively). This leads to our second noticeable result, there is no significant price discovery until 10 minutes prior to market open. This refers back to the point that some market participants are suspicious about entered orders, which can still be amended or cancelled until a few minutes prior to market open. Approaching the market opening increases price information and more market participants feel at ease to place orders based on the indicative opening price. Furthermore, the first 10 to 20 minutes in continuous trading also contains a large, and significant, part of the total price discovery process. Approximately 10% and 13% is discovered through the first 20 minutes, for the JSE and ASX, respectively. This reflects the phenomenon that some market participants withhold information during the auction process to benefit from mispriced stocks. Their information gets included in the stock price once they start trading at the market open, resulting in a large proportion of total price discovery during these first minutes.

Lastly, there is a low average price discovery during the closing auction. For the ASX listed stocks,

the proportion of price discovery is even negative, while for the JSE stocks a small, but significant, 2.7 per cent. This result is rather striking, as we have seen in our earlier analysis of Section 3, that the largest relative order flow entry occurs during this period. Figure 6 shows that there is an increase of 15% and 23% in price volatility during the closing auction for the ASX and JSE, respectively. There is, however, no consensus price discovery during this phase, which supports the claim that traders prefer to execute against the closing price to achieve benchmark results. The negative value for the ASX listed stocks records that a small correction of prices involves during the closing auction. After the normal trading hours, market participants have the opportunity to revise the valuation of stocks downwards, especially for the high tertile stocks.

Table 8: Price Discovery per Time Period for Mondays

Time periods	High		Low		Overall		
	JSE	ASX	JSE	ASX	JSE	ASX	Diff.
Pre-open/opening auction							
07:00-08:30	0.116	0.097	0.049	0.067	0.024	0.111	0.087
08:30-08:40	−0.065	0.066	−0.038	0.040	−0.023	0.046*	0.070
08:40-08:50	0.139*	0.013	0.043	0.085	0.196*	0.024	−0.172
08:50-09:00	0.048*	0.329*	0.170*	0.268*	−0.026	0.318*	0.344*
Total	0.238*	0.505*	0.224*	0.460*	0.171*	0.499*	0.328*
Continuous session							
09:00-09:10	0.041	0.099*	−0.041	0.104*	0.019	0.083*	0.064*
09:10-09:20	0.031	0.049*	0.112*	0.054*	0.078*	0.053*	−0.025
09:20-09:30	0.065*	0.037*	0.029	0.050*	0.046*	0.033*	−0.013
09:30-09:40	0.024	0.007	0.003	0.023	0.038*	0.017	−0.021
09:40-09:50	0.030	0.025	0.019	0.018	0.022	0.019*	−0.003
09:50-10:00	0.026	0.015	0.050*	0.010	0.022	0.026	0.004
10:00-16:00	0.460*	0.205*	0.527*	0.246*	0.494*	0.232*	−0.262*
16:00-16:10	0.006	0.004	−0.005	−0.009	0.010	−0.001	−0.011
16:10-16:20	0.002	−0.010	0.000	0.014	0.003	0.007	0.004
16:20-16:30	0.017	0.013	0.001	0.011	0.023*	0.008	−0.016
16:30-16:45	0.010	0.068*	0.046*	0.029	0.028*	0.040*	0.012
Total	0.709*	0.510*	0.740*	0.549*	0.783*	0.517*	−0.266*
Closing auction							
16:45-17:00	0.053	−0.015	0.036	−0.009	0.046*	−0.016	−0.062

NOTE: This table presents the average weighted price contribution (WPC) for both the JSE and ASX listed stocks. Additional to WPC computations based on all stocks within an exchange, the WPCs for both the high and low pre-open order entry tertiles are computed. The last column shows the difference between the ASX and JSE computed WPCs, based on all stocks. The time periods in the first column are based on the JSE opening times. The data covers Monday trading days only between the 3rd of January 2019 and 17th July 2019. The symbol *indicates the WPCs that are significantly different from zero at the 0.05 level.

We conduct an identical analysis for Monday trading days only. Prior to the Monday open, there is a large time frame where price-sensitive revelations can take place. On the other hand, there is no preceding price discovery by large American exchanges, such as the New York Stock Exchange (NYSE) or the NASDAQ, who open several hours postliminary the ASX and JSE open. Table 8 reports the average WPC statistic, similarly structured as Table 7, but for Monday trading days only.

The main and side results from the previous analysis still apply overall. There are two specifics worth mentioning. The key aspect is that the superior price discovery during the ASX' opening auction is rather due to its auction mechanism than the available price information on other exchanges. On Mondays, there is still a large percentage of price discovery explained by the opening auction. Despite both exchanges have no current information from other large exchanges (especially the ASX, which is one of the first markets to open), approximately 50% and 17% of the ASX and JSE stock daily prices are discovered before the market open. Second, a large proportion of JSE's price discovery during the opening auction is shifted to a 10-minute earlier period. This appearance might be the consequence of its time ordering priority during the opening auction. Market participants bear a higher probability of getting their orders filled if entered betimes.

The analyses show that a large proportion of the daily return is revealed during the opening call. The question that remains is whether it is due to the appearance that individual pre-open orders reveal more information than orders entered during normal trading hours on the one hand, or if the number of orders (participants) causes the large price evolution revelation. As shown in Section 3, the relative order flow is reasonably constant over an average trading day (except for periods that approach the market close). Therefore, one could expect that individual orders reveal more information for stocks in the pre-open phase than during the continuous session. On the other hand, low tertile stocks contain half of the relative pre-open order entry, but the proportion of price discovery for these stocks is not half the fraction of the high tertile stocks. To examine this we construct the weighted price contribution per order entry (WPCO), which measures the amount of periodic price return per ratio of incoming orders in that specific period. We compute the WPCO by dividing each WPC, for all τ, by the weighted ratio of incoming orders during that interval. We define $io_{\tau,s}$ as the number of incoming orders during time period τ for stock s, and io_s as the total orders entered during the full trading day. Then we define WPCO_τ as:

$$\text{WPCO}_\tau = \frac{\sum_{s=1}^{S} \left(|r_s| / \sum_{s=1}^{S} |r_s| \right) \times (r_{\tau,s}/r_s)}{\sum_{s=1}^{S} \left(|r_s| / \sum_{s=1}^{S} |r_s| \right) \times (io_{\tau,s}/io_s)}, \tag{21}$$

By definition, the measure approximates one if all orders include similar information levels. Table 9 reports the WPCO statistic for each period. The table shows that not all available information is incorporated into the auction price for both the ASX and JSE. The orders entered during the final 10 minutes of the call are very informative and all significantly different from zero. However, the first 20 to 40 minutes into the continuous session are quite informative too, for which the individual order informativeness diminishes afterwards. This implies that, as the day progresses, orders become less informative after the accumulated information from the previous day's close gets incorporated during

Table 9: Price Discovery per Incoming Order and per Time Period

Time periods	High		Low		Overall		
	JSE	ASX	JSE	ASX	JSE	ASX	Diff.
Pre-open/opening auction							
07:00-08:30	331.91	78.79	−510.21	134.44	155.40	156.76*	1.36
08:30-08:40	−720.06	79.63	1028.62	−106.81	−695.70	19.00	714.70
08:40-08:50	−98.64	−58.77	4087.48	984.08*	1128.13	108.79	−1019.34
08:50-09:00	27.50*	28.05*	20.79*	37.12*	30.27*	34.44*	4.17
Total	−459.29	127.70	4626.68	1048.83	618.10	318.99*	−299.11
Continuous session							
09:00-09:10	8.24*	2.51*	5.21	5.78*	7.45*	3.62*	−3.83
09:10-09:20	3.06*	2.24*	7.81*	4.06*	5.53*	2.57*	−2.96*
09:20-09:30	2.36	1.09*	4.06*	1.47*	3.13*	1.20*	−1.93*
09:30-09:40	3.37*	0.91*	4.06	1.70*	4.45*	1.24*	−3.21*
09:40-09:50	4.01*	0.52	6.38*	1.31*	4.55*	0.81*	−3.73*
09:50-10:00	2.60*	0.95*	2.05	1.18*	2.08*	1.13*	−0.95
10:00-16:00	1.16*	0.50*	1.40*	0.58*	1.33*	0.52*	−0.81*
16:00-16:10	1.00*	0.08	1.11	0.06	1.33	0.19	−1.14
16:10-16:20	0.08	0.17	0.07	0.39*	−0.17	0.30*	0.46
16:20-16:30	0.88	0.20*	1.23*	0.15	1.39*	0.13*	−1.26*
16:30-16:45	0.46	0.17*	1.04*	0.14*	0.70*	0.15*	−0.55*
Total	27.21*	9.35*	34.47*	16.81*	31.77*	11.87*	−19.90*
Closing auction							
16:45-17:00	0.04	−3.56	0.05	−0.08	0.08*	−1.74	−1.81

NOTE: This table presents the average weighted price contribution per incoming order (WPCO) for both the JSE and ASX listed stocks. Additional to WPCO computations based on all stocks within an exchange, the WPCOs for both the high and low pre-open order entry tertiles are computed. The last column shows the difference between the ASX and JSE computed WPCOs, based on all stocks. The time periods in the first column are based on the JSE opening times. The data covers all trading days between 3rd January 2019 and 17th July 2019. The symbol *indicates the WPCOs that are significantly different from zero at the 0.05 level.

the pre-open and early trading sessions. Still, orders shortly after the market open are very informative and, hence, not all information was absorbed into the opening price. Perhaps traders avoid trading in an environment which is dominated by informed traders. Some market participants prefer to wait until they know at which the market price opens and to respond on the subsequent dynamics.

Second, it is most likely that the ASX' superior price discovery process during the pre-open hours is since market participants find it more appealing to participate in their auction. None of the pre-open periods shows evidence that individual orders are more informative for either the ASX or JSE. Therefore, ASX pre-open orders are not significantly more informed than these of the JSE.

Lastly, enhanced price discovery in pre-open sessions mainly occurs due to the rise in auction participation. During the pre-open, there is no clear pattern or significant difference between high and low tertile stocks within one of the two exchanges. This rejects that individual orders of low tertile stocks are more informative than high tertile stocks. Surprisingly is that low tertile stock orders, through the total pre-open hours, have a large, but very noisy, informativeness level. The

WPCO statistic is roughly 10 times larger than for high tertile stock orders. In combination with its large spread, it suggests that when there are relatively few auction orders, the impact on price efficiency is large but inconsistent. Hence, a market participant could influence the opening price fairly easy, which can be truly price discovering or obscuring. Curiously, the informativeness of the opening auction orders improves, at least on average, the level of price discovery according to Table 7. Despite their wide spreads, these are informative driven orders. In the short term, these prices are unlikely to be reversed and the wide spreads during the auction is a result of market makers responding to the impact of these auction orders. Hence, enticing auction participants shows its importance in consistent price discovery after the overnight close. To avoid cluttering the reader with many tables, we exclude Monday tradings days only WPCO's, as results are very similar to our full sample analysis.

5.3 Price Discovery Efficiency

Although the previous section shows that price discovery is relatively large during the pre-open and the start of normal trading, we also expect that the spreads around these periods are large as well. This implies the existence of price reversals, such that prices at the end have negative price contributions. Potential price reversals and non-convergence of observed prices could cause noisy prices and, hence, inefficiency. In order to evaluate the efficiency of security prices in specific inter-day periods, we compute unbiasedness regressions. That is, for each stock s, intraday period τ, and each day in our sample period, we estimate the following regression:

$$r_s^* = a + b\, r_{close \to \tau} + \epsilon_{close \to \tau}, \tag{22}$$

where r_s^* denotes the log observed close-to- underlying one hour after market open return for stock s. That is the difference between the previous' day log closing price (observed) and the log of today's true underlying price at open time + 01:00 (model-based). The parameter a corresponds to the regression intercept, b defines the slope coefficient and measures the ratio of signal to noise, $r_{close \to \tau}$ denotes the observed logarithmic return from previous' market close to today's end of period τ, and $\epsilon_{close \to \tau}$ is the corresponding noise term. We consider periods τ for each day up to one hour after the opening of the market. A regression slope b different from 1 implies that the period's price is biased and does not converge to fundamental values. Different from existing studies, we do not assume that the observed exchange prices converge to fundamental values. We do so by using r_s^* in the regression, which is based on the true underlying market price, instead of observed returns r_s. For the true market price, we make use of p_t^*, which we assume to be the best quote available.

Analogously to Biais et al. (1999), we compute confidence intervals by using the time series' stan-

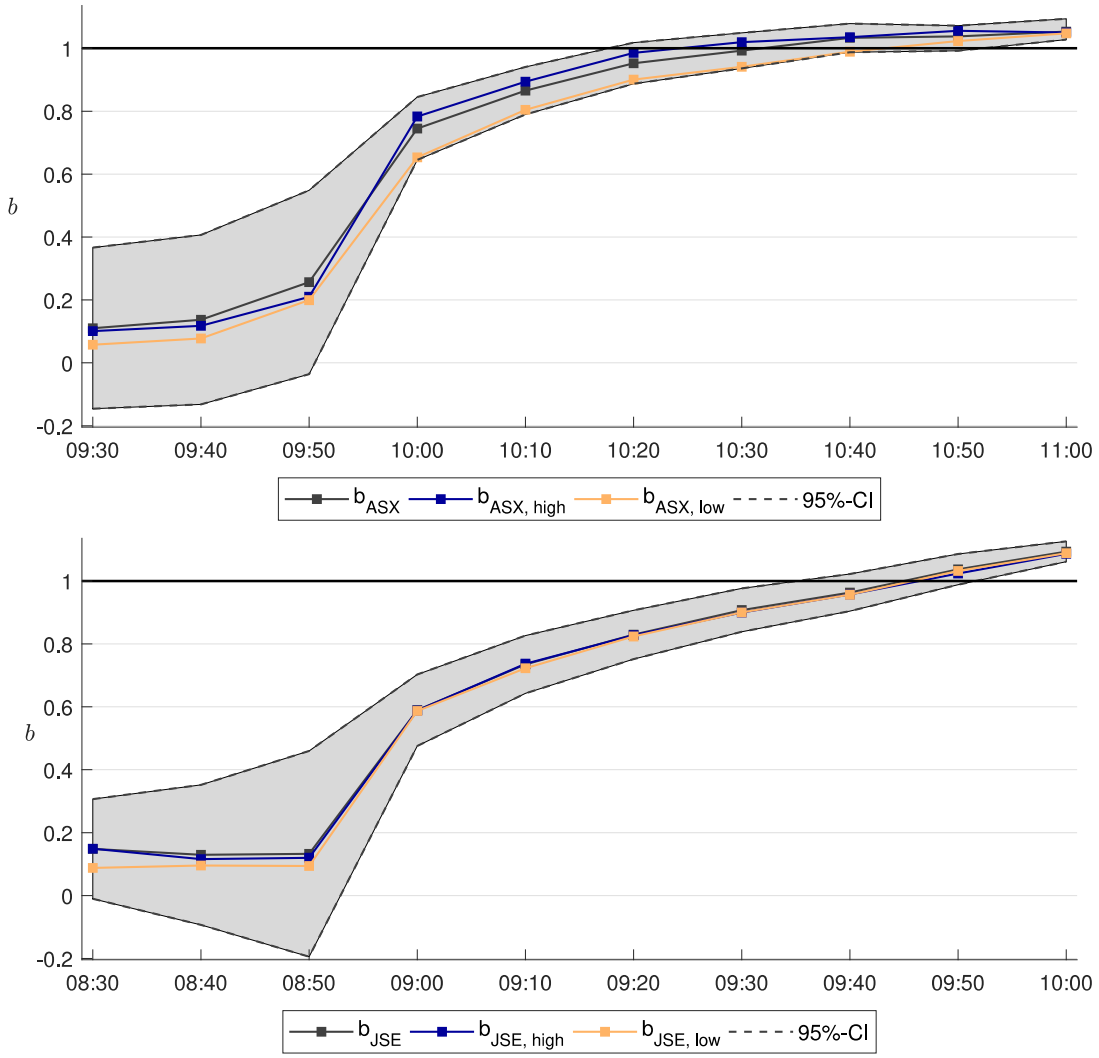

Figure 10: This figure shows the auction and one hour after market open price efficiency by time periods. The signal to noise ratio is computed by estimating the following regression for each stock and each time interval: $r_s^* = a + b\, r_{close \to \tau} + \epsilon_{close \to \tau}$. The upper panel corresponds to the mean of the ASX listed stocks and the lower panel to the average JSE listed stocks. A coefficient less (greater) than one implies an underestimated (overestimated) average price.

dard errors of the average slope coefficient estimates. Figure 10 charts the mean coefficient estimates across all stocks, within a specific market, along with the 95% confidence bands. The upper panel corresponds to the ASX, while the lower panel corresponds to the JSE listed stocks. Additionally, the average b estimates are presented for the low and high relative pre-open order volume tertiles. Two main results emerge from this analysis. The first main aspect is that the average opening price is inefficient for both the ASX and JSE and, therefore, does not accurately reflect the true underlying security price. The informational efficiency in stock prices is particularly low during the first phase of the call auction. During the last 10 minutes prior to market open, it rises dramatically. An average increase from 0.2 to 0.75 and from 0.15 to 0.6 is registered for the ASX and JSE listed stocks, respectively. However, both estimates are significantly different from one at the market open, implying

inefficient opening prices. Second, the clearing price efficiency is higher for the Australian market. The average b_{ASX} coefficient is significantly higher than b_{JSE} at the market open. Moreover, the level of price efficiency becomes satisfactory between 15 and 30 minutes after the open for the ASX, while this is only after approximately 45 minutes for the JSE. Therefore, in means of opening price efficiency and its convergence speed to fundamental values, the ASX auction process is superior.

There are two additional results worth mentioning. First, note that the observed one hour after market open returns are significantly different from the true underlying returns. This suggests that there is still a considerable amount of noise in security prices while continuous trading has already proceeded for one hour. Second, increasing auction participants shows to increase opening price efficiency. Although this effect seems rather negligible for the JSE listed stocks, which could be due to the lack in sufficient discrepancies of auction participants involvement across the two tertiles, it is significant for the ASX listed stocks. Hence, expanding participation increases opening price informativeness and efficiency.

6 Conclusion

This paper examined the auction efficiency of two important call designs implemented by, among others, the Australian Stock Exchange and the Johannesburg Securities Exchange. Although a call auction is a time-disciplined approach to price evolution, it has certain dynamics that are different from the continuous market. During the pre-open process, there is an interplay of active participants who compete for primacy in the order book. Its main goal is to find a true and stable consensus price before the normal trading hours start. We analysed opening price variances, price discovery during the pre-open session, and auction price efficiency.

In order to measure price stability and to test price efficiency, we developed a multi-factor stochastic volatility model of intraday stock prices. We presented direct usage of Markov chain Monte Carlo methods for parameter and state estimation. We find evidence for multi-scale volatility dynamics, where we distinct fast and slow factors, and for correlated jumps (both in prices and volatility). The proposed model in this article is key in extracting the true underlying market price, to derive a consistent intraday volatility pattern, and to model Monday opening effects. The first is used to test whether auction prices converge to fundamental values. The second as a measure of opening price stability, as it reveals the increased volatility during the market opening session, relatively to the remainder of the trading day. The latter is used in a similar fashion, which enables us to analyse the increased volatility after the market being closed for the weekend.

Our analysis indicates that auction algorithms are important, but not sufficient in producing stable

and efficient opening prices. First, price volatility during the market open increases between 18 and 25 per cent, relative to the normal baseline level. Second, over-weekend price uncertainty increases the opening price instability significantly. Third, still a large proportion of daily price discovery occurs during the first phase of continuous trading, which suggests that not all available information is incorporated into the opening price. Lastly, we showed that the call's determined opening price does not converge to fundamental values, which suggests an inaccurate reflection of the true underlying market price. All of these aspects claim current auction processes to be inefficient.

The instability and inefficiency of opening prices are due to the lack of market depth. If all active participants would compete during the call, then all relevant information would be absorbed in the auction price, suggesting the discovery of a true consensus price. Moreover, unexecuted orders roll over to the continuous session, leaving a deep order book. Accordingly, new incoming orders would not excessively impact the exchange prices, which preserves price stability.

Our analyses showed that increasing auction participants significantly enhance the pre-open price discovery process and price efficiency. Moreover, it decreases the opening price volatility and, for the ASX, it ceases the Monday open effect. Relatively many auction participants may be key, along with the basic principles of the ASX, in producing an efficient auction process. The relative high pre-open incoming orders tertile for the ASX already covers approximately 50 per cent of the total daily price discovery during the call period.

The Australian Securities Exchange auction process is superior above the call of the Johannesburg Stock Exchange. The ASX encourages more active participants to build the pre-open order book. The pre-open relative order flow and relative volume traded at the auction price are significantly higher. This results in an enhanced price discovery process, a decrease in opening price volatility, a decrease on Monday open effect, and an increase in auction price efficiency.

Although the ASX runs the superior call design, it is still unsuccessfully in producing stable and efficient opening prices, which implies that current auction mechanisms are still not sufficient. The key improvement in call designs is getting the book building started in a more timely fashion and to create additional market depth. Enticing active participants, which increases natural order matching, aids in aligning a true consensus price. This is, stimulating a broad public to participate. One could, therefore, consider reducing commission rates for early order entry, delay the random open if still a sufficient stream of orders is entered, prohibit market orders and order cancellation during the auction process, and restrict order amending.

This study finds that including the latter three basic principles and introducing a random open, conducted by the ASX, slightly improves price stability and increases price efficiency. More sophisticated research can be done if one has access to a more detailed data sample. For example, if individual

buy and sell orders are obtained, a true distinction between all principles for opening price determination could be made. This would enable the researcher to examine the effect on opening price efficiency for each of the four principles. Second, it would enable the analyst to compute more accurate auction participation divisions, without the assumption that volume during the pre-open is an indicator for the number of participants. One could then test auction performances, conditional on the number of auction participants, more accurately. This paper has, however, shown sufficient evidence suggesting the inefficiency of current call auction designs. This anomaly does not necessarily involve the execution algorithm, but rather the encouragement of broad and active auction participation.

References

Yakov Amihud and Haim Mendelson. Volatility, efficiency, and trading: Evidence from the Japanese stock market. *Journal of Finance*, 46(5):1765–1789, 1991.

Torben G Andersen and Tim Bollerslev. Intraday periodicity and volatility persistence in financial markets. *Journal of Empirical Finance*, 4(2-3):115–158, 1997.

Torben G Andersen and Tim Bollerslev. Deutsche mark–dollar volatility: intraday activity patterns, macroeconomic announcements, and longer run dependencies. *Journal of Finance*, 53(1):219–265, 1998.

Torben G Andersen, Luca Benzoni, and Jesper Lund. An empirical investigation of continuous-time equity return models. *Journal of Finance*, 57(3):1239–1284, 2002.

Michael J Barclay and Terrence Hendershott. Price discovery and trading after hours. *Review of Financial Studies*, 16(4):1041–1073, 2003.

Michael J Barclay and Terrence Hendershott. A comparison of trading and non-trading mechanisms for price discovery. *Journal of Empirical Finance*, 15(5):839–849, 2008.

David S Bates. Post-'87 crash fears in the S&P 500 futures option market. *Journal of Econometrics*, 94(1-2):181–238, 2000.

Mascia Bedendo and Stewart D Hodges. A Parsimonious Continuous Time Model Of Equity Index Returns: Inferred From High Frequency Data. *International Journal of Theoretical and Applied Finance*, 7(8):997–1030, 2004.

Bruno Biais, Pierre Hillion, and Chester Spatt. Price discovery and learning during the preopening period in the Paris Bourse. *Journal of Political Economy*, 107(6):1218–1248, 1999.

Charles Cao, Eric Ghysels, and Frank Hatheway. Price discovery without trading: Evidence from the Nasdaq preopening. *Journal of Finance*, 55(3):1339–1365, 2000.

Chris K Carter and Robert Kohn. On Gibbs sampling for state space models. *Biometrika*, 81(3): 541–553, 1994.

Siddhartha Chib and Edward Greenberg. Bayes inference in regression models with ARMA (p, q) errors. *Journal of Econometrics*, 64(1-2):183–206, 1994.

Siddhartha Chib, Federico Nardari, and Neil Shephard. Markov chain Monte Carlo methods for stochastic volatility models. *Journal of Econometrics*, 108(2):281–316, 2002.

Conrad S Ciccotello and Frank M Hatheway. Indicating ahead: Best execution and the Nasdaq preopening. *Journal of Financial Intermediation*, 9(2):184–212, 2000.

Carole Comerton-Forde and James Rydge. The influence of call auction algorithm rules on market efficiency. *Journal of Financial Markets*, 9(2):199–222, 2006.

Piet De Jong. The diffuse Kalman filter. *Annals of Statistics*, 19(2):1073–1083, 1991.

Piet De Jong and Neil Shephard. The simulation smoother for time series models. *Biometrika*, 82(2): 339–350, 1995.

Pierre Del Moral. Non-linear filtering: interacting particle resolution. *Markov Processes and Related Fields*, 2(4):555–581, 1996.

Ian Domowitz and Ananth Madhavan. Open sesame: alternative opening algorithms in securities markets. In *The Electronic Call Auction: Market Mechanism and Trading*, volume 7, pages 375–393. Springer, 2001.

Darrell Duffie, Jun Pan, and Kenneth Singleton. Transform analysis and asset pricing for affine jump-diffusions. *Econometrica*, 68(6):1343–1376, 2000.

James Durbin and Siem Jan Koopman. A simple and efficient simulation smoother for state space time series analysis. *Biometrika*, 89(3):603–616, 2002.

Nicholas Economides and Robert A Schwartz. Electronic call market trading. *Journal of Portfolio Management*, 21(3), 1995.

Andrew Ellul, Hyun Song Shin, and Ian Tonks. Opening and closing the market: Evidence from the London Stock Exchange. *Journal of Financial and Quantitative Analysis*, 40(4):779–801, 2005.

Robert F Engle and Magdalena E Sokalska. Forecasting intraday volatility in the us equity market. multiplicative component garch. *Journal of Financial Econometrics*, 10(1):54–83, 2012.

Bjørn Eraker, Michael Johannes, and Nicholas Polson. The Impact of Jumps in Volatility and Returns. *Journal of Finance*, 58(3):1269–1300, 2003.

Eugene F Fama and James D MacBeth. Risk, return, and equilibrium: Empirical tests. *Journal of political economy*, 81(3):607–636, 1973.

Sylvia Frühwirth-Schnatter. Data augmentation and dynamic linear models. *Journal of Time Series Analysis*, 15(2):183–202, 1994.

John Geweke et al. *Evaluating the accuracy of sampling-based approaches to the calculation of posterior moments*, volume 196. Federal Reserve Bank of Minneapolis, Research Department Minneapolis, MN, 1991.

Andrew Harvey, Esther Ruiz, and Neil Shephard. Multivariate stochastic variance models. *Review of Economic Studies*, 61(2):247–264, 1994.

Gbenga Ibikunle. Opening and closing price efficiency: Do financial markets need the call auction? *Journal of International Financial Markets, Institutions and Money*, 34:208–227, 2015.

Christine X Jiang, Tanakorn Likitapiwat, and Thomas H McInish. Information content of earnings announcements: Evidence from after-hours trading. *Journal of Financial and Quantitative Analysis*, 47(6):1303–1330, 2012.

Sangjoon Kim, Neil Shephard, and Siddhartha Chib. Stochastic volatility: likelihood inference and comparison with ARCH models. *Review of Economic Studies*, 65(3):361–393, 1998.

Masahito Kobayashi. Testing for volatility jumps in the stochastic volatility process. *Asia-Pacific Financial Markets*, 12(2):143–157, 2005.

Robert Kohn and Craig F Ansley. A new algorithm for spline smoothing based on smoothing a stochastic process. *SIAM Journal on Scientific and Statistical Computing*, 8(1):33–48, 1987.

Ananth Madhavan. Trading mechanisms in securities markets. *Journal of Finance*, 47(2):607–641, 1992.

Ananth Madhavan and Venkatesh Panchapagesan. Price discovery in auction markets: A look inside the black box. *Review of Financial Studies*, 13(3):627–658, 2000.

Martin Martens, Yuan-Chen Chang, and Stephen J Taylor. A comparison of seasonal adjustment methods when forecasting intraday volatility. *Journal of Financial Research*, 25(2):283–299, 2002.

Philippe Masset. Properties of high frequency DAX returns: Intraday patterns, Jumps and their impact on subsequent volatility. *SSRN Electronic Journal*, 1:1–28, 2008.

D Timothy Mccormick. Considering execution performance in electronic call market design. In *The Electronic Call Auction: Market Mechanism and Trading*, pages 113–123. Springer, 2001.

Luis Angel Medrano and Xavier Vives. Strategic behavior and price discovery. *RAND Journal of Economics*, pages 221–248, 2001.

Jouchi Nakajima and Yasuhiro Omori. Leverage, heavy-tails and correlated jumps in stochastic volatility models. *Computational Statistics & Data Analysis*, 53(6):2335–2353, 2009.

Daniel B Nelson. *The time series behavior of stock market volatility and returns*. Unpublished Doctoral Dissertation, Massachusetts Institute of Technology, 1988.

Yasuhiro Omori, Siddhartha Chib, Neil Shephard, and Jouchi Nakajima. Stochastic volatility with leverage: Fast and efficient likelihood inference. *Journal of Econometrics*, 140(2):425–449, 2007.

Marco Pagano and Ailsa Röell. Transparency and liquidity: A comparison of auction and dealer markets with informed trading. *Journal of Finance*, 51(2):579–611, 1996.

Michael S Pagano and Robert A Schwartz. A closing call's impact on market quality at Euronext Paris. *Journal of Financial Economics*, 68(3):439–484, 2003.

Aldo Rustichini, Mark A Satterthwaite, Steven R Williams, et al. Convergence to efficiency in a simple market with incomplete information. *Econometrica*, 62:1041–1041, 1994.

Jonathan R Stroud and Michael S Johannes. Bayesian modeling and forecasting of 24-hour high-frequency volatility. *Journal of the American Statistical Association*, 109(508):1368–1384, 2014.

Viktor Todorov. Econometric analysis of jump-driven stochastic volatility models. *Journal of Econometrics*, 160(1):12–21, 2011.

Jos Van Bommel. Measuring price discovery: The variance ratio, the R2, and the weighted price contribution. *Finance Research Letters*, 8(3):112–119, 2011.

Jianxin Wang and Minxian Yang. How well does the weighted price contribution measure price discovery? *Journal of Economic Dynamics and Control*, 55:113–129, 2015.

Jonathan Weinberg, Lawrence D Brown, and Jonathan R Stroud. Bayesian forecasting of an inhomogeneous Poisson process with applications to call center data. *Journal of the American Statistical Association*, 102(480):1185–1198, 2007.

A Example of the ASX Opening Price Settlement Process

In this appendix, we give a detailed, but very simple, example of the ASX opening price settlement procedure. We make use of the four principles that the ASX uses to determine the opening price during the auction process. Note that observation times are given in GMT time.

Situation 1: Principle 1 can determine the opening price.

Consider the following order book:

Table A.1: Situation 1

Time Stamp	Buy/Sell	Quantity	Price	Time Stamp	Buy/Sell	Quantity	Price
23:50.00	Buy	40	48	23:56.33	Sell	1	49
23:50.23	Buy	30	49	23:57.21	Sell	100	46
23:51.02	Sell	90	45	23:58.11	Sell	100	50
23:51.05	Sell	25	48	23:58.57	Buy	100	45
23:52.55	Buy	10	51	23:59.21	Buy	70	46
23:54.12	Buy	50	47	23:59.44	Sell	1	47

NOTE: This table illustrates an example of a pre-market order book. Before the ASX opens at 00:00.00, orders can be placed. This table exemplify such incoming orders. Time Stamp denotes the time of the incoming order and the flag Buy/Sell shows whether the incoming order was a bid or offer. The table also includes the quantity and the desired price of the incoming orders. Based on these bids and offers, the exchange determines an opening price. Note that this example is fabricated to describe principal 1.

We compute a bid/offer box, such that we order the price in decreasing order. We include the cumulative sum of bids and offers. Hence, we get:

Table A.2: Maximum Volume Matching

Time Stamp	Sum Bids	Bid Quantity	Price	Ask Quantity	Sum Offers	Time stamp
23:52.55	10	10	51	0	317	–
–	10	0	50	100	317	23:58.11
23:50.23	40	30	49	1	217	23:56.33
23:50.00	80	40	48	25	216	23:51.05
23:54.12	130	50	47	1	191	23:59.44
23:59.21	200	70	46	100	190	23:57.21
23:58.57	300	100	45	90	90	23:51.02

NOTE: This table reproduces the price settlement procedure, based on principle 1. Sum Bids and Sum Offers denote the cumulative sum of buy and sell orders, respectively. We sort all the order book data in decreasing price level. Note that, therefore, cumulative bids are increasing and cumulative offers decreasing.

The largest cumulative quantity of bids and offers that can be executed is at a price level of 46. The 190 offers can be matched with the 200 bids that are available at the price of 46, providing the greatest number of securities matched of 190. Hence, the opening price is 46. If principle 1 can not

produce a single opening price, then principle 2 is included.

Situation 2: Principle 2 can determine the opening price.

Consider the following order book:

Table A.3: Situation 2

Time Stamp	Buy/Sell	Quantity	Price	Time Stamp	Buy/Sell	Quantity	Price
23:50.00	Buy	40	48	23:56.33	Sell	1	49
23:50.23	Buy	30	49	23:57.21	Sell	100	46
23:51.02	Sell	90	45	23:58.11	Sell	100	50
23:51.05	Sell	25	48	23:58.57	Buy	100	45
23:52.55	Buy	10	51	23:59.21	Buy	110	47
23:54.12	Buy	10	46	23:59.44	Sell	10	451

NOTE: This table illustrates an example of a pre-market order book. Before the ASX opens at 00:00.00, orders can be placed. This table exemplify such incoming orders. Time Stamp denotes the time of the incoming order and the flag Buy/Sell shows whether the incoming order was a bid or offer. The table also includes the quantity and the desired price of the incoming orders. Based on these bids and offers, the exchange determines an opening price. Note that this example is fabricated to describe principal 2.

We compute a bid/offer box, such that we order the price in decreasing order. We include the cumulative sum of bids and offers. Hence, we get:

Table A.4: Minimum Non-Matching Quantity

Time Stamp	Sum Bids	Bid Quantity	Price	Ask Quantity	Sum Offers	Time stamp
23:52.55	10	10	51	10	336	23:59.44
–	10	0	50	100	326	23:58.11
23:50.23	40	30	49	1	226	23:56.33
23:50.00	80	40	48	25	225	23:51.05
23:59.21	190	110	47	0	190	–
23:54.12	200	10	46	100	190	23:57.21
23:58.57	300	100	45	90	90	23:51.02

NOTE: This table reproduces the price settlement procedure, based on principle 2. Sum Bids and Sum Offers denote the cumulative sum of buy and sell orders, respectively. We sort all the order book data in decreasing price level. Note that, therefore, cumulative bids are increasing and cumulative offers decreasing.

In this situation, there are multiple prices that maximise the trading volume. At the price levels 46 and 47 there is an equal number of securities that can match, 190 at both price levels. At a price level of 47, the non-matching quantity equals 190 bids - 190 offers = 0. At a price level of 46, the non-matching quantity equals 200 bids - 190 offers = 10. Hence, the opening price is 47, where the the least number of order imbalances take place. If neither principle 1 or principle 2 produce a single opening price, then principle 3 is included.

Situation 3: Principle 3 can determine the opening price.

In this example, we consider an order book that the order-imbalance is on the buy side. Therefore, the price is set on the highest price. In case of an order-imbalance on the sell side, the price would be set on the lowest price. Consider the following order book:

Table A.5: Situation 3

Time Stamp	Buy/Sell	Quantity	Price	Time Stamp	Buy/Sell	Quantity	Price
23:50.00	Buy	40	48	23:56.33	Sell	1	49
23:50.23	Buy	30	49	23:57.21	Sell	100	46
23:51.02	Sell	90	45	23:58.11	Sell	100	50
23:51.05	Sell	25	48	23:58.57	Buy	100	45
23:52.55	Buy	10	51	23:59.21	Buy	10	50
23:54.12	Buy	110	47	23:59.44	Sell	10	451

NOTE: This table illustrates an example of a pre-market order book. Before the ASX opens at 00:00.00, orders can be placed. This table exemplify such incoming orders. Time Stamp denotes the time of the incoming order and the flag Buy/Sell shows whether the incoming order was a bid or offer. The table also includes the quantity and the desired price of the incoming orders. Based on these bids and offers, the exchange determines an opening price. Note that this example is fabricated to describe principal 3.

We compute a bid/offer box, such that we order the price in decreasing order. We include the cumulative sum of bids and offers. Hence, we get:

Table A.6: Highest Price

Time Stamp	Sum Bids	Bid Quantity	Price	Ask Quantity	Sum Offers	Time stamp
23:52.55	10	10	51	10	336	23:59.44
23:59.21	20	10	50	100	326	23:58.11
23:50.23	50	30	49	1	226	23:56.33
23:50.00	90	40	48	25	225	23:51.05
23:54.12	200	110	47	0	190	–
–	200	0	46	100	190	23:57.21
23:58.57	300	100	45	90	90	23:51.02

NOTE: This table reproduces the price settlement procedure, based on principle 3. Sum Bids and Sum Offers denote the cumulative sum of buy and sell orders, respectively. We sort all the order book data in decreasing price level. Note that, therefore, cumulative bids are increasing and cumulative offers decreasing.

In this situation, both the price levels 46 and 47 maximise the trading volume with a matching quantity of 190. Moreover, both have an order imbalance of 200 bids - 190 offers = 10. Under these circumstances, there is a surplus in buy order. Therefore, the price is set on the highest price by means of principle 3. Hence, the opening price is 47, because the unmatched securities are bid securities. If principles 1 to 3 are insufficient in determining a single opening price, principle 4 is included.

Situation 4: Principle 4 can determine the opening price.

In this situation, the previous closing price is 45. Therefore, 45 is considered as the reference price. Consider the following order book:

Table A.7: Situation 4

Time Stamp	Buy/Sell	Quantity	Price	Time Stamp	Buy/Sell	Quantity	Price
23:50.00	Buy	40	48	23:56.33	Sell	1	49
23:50.23	Buy	30	49	23:57.21	Sell	110	46
23:51.02	Sell	90	45	23:58.11	Sell	100	50
23:51.05	Sell	25	48	23:58.57	Buy	100	45
23:52.55	Buy	10	51	23:59.21	Buy	10	50
23:54.12	Buy	110	47	23:59.44	Sell	10	451

NOTE: This table illustrates an example of a pre-market order book. Before the ASX opens at 00:00.00, orders can be placed. This table exemplify such incoming orders. Time Stamp denotes the time of the incoming order and the flag Buy/Sell shows whether the incoming order was a bid or offer. The table also includes the quantity and the desired price of the incoming orders. Based on these bids and offers, the exchange determines an opening price. Note that this example is fabricated to describe principal 4.

We compute a bid/offer box, such that we order the price in decreasing order. We include the cumulative sum of bids and offers. Hence, we get:

Table A.8: Reference Price

Time Stamp	Sum Bids	Bid Quantity	Price	Ask Quantity	Sum Offers	Time stamp
23:52.55	10	10	51	10	336	23:59.44
23:59.21	20	10	50	100	326	23:58.11
23:50.23	50	30	49	1	226	23:56.33
23:50.00	90	40	48	25	225	23:51.05
23:54.12	200	110	47	0	200	–
–	200	0	46	110	200	23:57.21
23:58.57	300	100	45	90	90	23:51.02

NOTE: This table reproduces the price settlement procedure, based on principle 4. Sum Bids and Sum Offers denote the cumulative sum of buy and sell orders, respectively. We sort all the order book data in decreasing price level. Note that, therefore, cumulative bids are increasing and cumulative offers decreasing.

Note that, in this situation, both the price levels 46 and 47 (i) maximise the trading volume, (ii) minimise the non-matching quantity, and (iii) have an equivalent bid and offer surplus of 0. Therefore, the price is settled by principle 4, which sets the price on the one in the subset closest to the reference price of 45. Hence, the opening price is 46.

B Example of the JSE Opening Price Settlement Process

In this appendix, we give a simple example of the HSE opening price settlement procedure. We skip the first principle, which is given in Appendix A. Consider again situation 2 of Appendix A. This order book gives us two price equilibria by maximising trading volume. The bid and offer box is given in Table B.1. Note that, both the price levels 46 and 47 maximise the trading volume. The buy order

Table B.1: JSE's Time Priority

Time Stamp	Sum Bids	Bid Quantity	Price	Ask Quantity	Sum Offers	Time stamp
23:52.55	10	10	51	10	336	23:59.44
–	10	0	50	100	326	23:58.11
23:50.23	40	30	49	1	226	23:56.33
23:50.00	80	40	48	25	225	23:51.05
23:59.21	190	110	47	0	190	–
23:54.12	200	10	46	100	190	23:57.21
23:58.57	300	100	45	90	90	23:51.02

NOTE: This table reproduces the price settlement procedure, based on the time priority procedure of the JSE. Sum Bids and Sum Offers denote the cumulative sum of buy and sell orders, respectively. We sort all the order book data in decreasing price level. Note that, therefore, cumulative bids are increasing and cumulative offers decreasing. Note that the Time Stamp is rather different in GMT time for the Johannesburg Stock Exchange. However, for comparison conveniences, we pretend similar Time Stamps between the ASX and JSE.

of 10 instruments for 46 has been the first order in the auction process in this subset. Therefore, the JSE's auction process sets the opening price on 46. Note that this is different from the ASX, whom includes the second principle and would set its price on 47.

C Individual Stock Summary Statistics

Table C.1: Summary Statistics JSE Stocks

		Pre-open orders			Volume traded 9:00-9:30		
Category	Ticker	Median	Mean	Rel. (%)	Median	Mean	Rel. (%)
Large	NPN	402.22	557.82	1.17	80.265	91.228	9.80
	EXX	238.24	360.84	1.11	25.970	40.200	3.22
	BTI	387.70	575.81	0.97	24.233	35.008	3.11
	APN	296.40	420.68	0.94	59.572	103.02	5.42
	BID	180.02	217.89	0.93	26.280	33.540	4.21
	CFR	2603.5	3372.6	0.91	145.43	221.19	4.48
	MRP	272.70	336.52	0.86	41.394	72.593	4.14
	AMS	63.850	82.515	0.84	8.9750	11.202	3.34
	AGL	666.28	879.65	0.82	75.720	87.984	5.20
	DSY	261.41	320.44	0.79	40.349	61.428	3.71
Middle	NED	252.21	293.17	0.79	62.430	81.475	5.35
	SHP	324.04	384.74	0.79	119.35	69.469	4.66
	ABG	540.83	591.62	0.78	100.50	159.11	4.60
	SBK	680.02	739.56	0.77	156.62	194.80	5.44
	SOL	284.66	381.19	0.77	60.979	104.25	5.51
	TBS	120.07	185.69	0.75	18.018	25.707	3.59
	BVT	199.47	268.84	0.75	42.622	56.463	5.18
	RMH	430.88	511.93	0.74	70.404	84.589	4.39
	VOD	307.35	394.70	0.69	63.915	100.34	4.64
	REM	185.63	251.39	0.67	31.203	37.914	3.69
Small	FSR	1728.3	2043.6	0.65	601.47	721.79	6.66
	MTN	765.67	979.66	0.63	161.19	258.97	4.10
	GRT	1312.6	1566.7	0.61	234.94	280.32	3.67
	BHP	680.80	1334.6	0.60	80.883	89.167	5.61
	SLM	711.05	790.31	0.58	178.26	260.03	4.82
	CPI	43.773	71.891	0.58	6.4610	9.3869	3.54
	OMU	2183.1	2725.6	0.51	545.25	755.47	5.05
	MNP	268.67	331.55	0.46	19.312	27.605	4.15
	RDF	2448.2	2780.3	0.46	461.99	603.11	4.01
	INP	283.35	462.14	0.38	37.723	47.978	4.38

NOTE: This table presents summary statistics for pre-open order volume and volume traded during the first 30 minutes of the continuous trading session for the JSE listed stocks. We report the Median, mean and relative percentage of incoming orders or volume traded. We divide the sample in three subsets, based on its relative incoming order median. The relative order entering is computed by dividing the total incoming orders during the pre-open hours by the remainder of total incoming orders that day.

Table C.2: Summary Statistics ASX Stocks

		Pre-open orders			Volume traded 10:00-10:30		
Category	Ticker	Median	Mean	Rel. (%)	Median	Mean	Rel. (%)
Large	MQG	229.06	331.91	3.38	84.472	115.85	14.23
	RIO	400.67	517.89	2.23	183.44	236.77	15.61
	RHC	66.658	89.793	2.03	32.929	42.636	10.68
	CSL	109.71	157.42	1.88	79.557	98.039	13.49
	COH	27.582	45.416	1.83	19.208	23.875	14.26
	ASX	54.015	79.017	1.66	28.206	36.815	9.59
	GMG	1532.0	1850.4	1.16	368.79	463.18	11.96
	WES	675.70	1023.7	1.15	243.08	312.51	13.23
	WPL	680.75	859.16	1.14	255.71	304.60	14.63
	WOW	694.93	1007.0	1.05	273.14	385.05	12.13
	SHL	294.06	363.05	1.04	104.78	126.58	12.29
	BHP	2102.4	3466.2	1.03	907.77	1027.3	17.94
	MGR	13386	18070	1.00	1447.1	1808.4	13.08
Middle	WBC	2259.1	3756.3	1.00	715.28	1038.3	14.31
	TCL	1868.8	2314.3	0.99	497.83	592.87	11.67
	TWE	860.74	1029.6	0.99	321.46	409.40	12.91
	NCM	805.66	1068.7	0.96	399.83	459.17	18.27
	CBA	431.15	780.80	0.93	313.69	415.62	13.88
	AMC	1281.9	1961.8	0.92	400.03	579.12	12.68
	ALL	379.51	449.89	0.82	185.51	230.91	10.87
	NAB	1940.0	2500.6	0.78	725.65	945.84	14.07
	AGL	467.85	586.69	0.73	219.42	262.31	13.29
	ANZ	1107.6	1791.4	0.73	532.70	737.77	12.48
	S32	20046	25220	0.73	2648.0	3183.1	17.27
	FMG	8822.9	10016	0.72	2818.7	3511.7	19.84
	GPT	2641.9	3389.8	0.72	527.32	680.10	9.89
	SYD	2057.8	2813.8	0.71	533.56	684.04	11.81
Small	APA	478.87	680.16	0.69	158.09	209.65	9.07
	TLS	33464	47330	0.66	3264.2	4260.1	14.13
	STO	2084.6	2810.4	0.65	618.05	714.94	13.28
	SUN	723.89	978.38	0.64	249.18	327.74	10.17
	BXB	814.60	1148.7	0.62	343.56	439.37	11.05
	QBE	870.50	1332.8	0.62	350.37	422.55	11.05
	DXS	586.80	913.00	0.61	294.10	391.09	11.01
	SCG	6641.8	9647.0	0.54	1178.6	1505.4	9.69
	IAG	1275.4	1755.6	0.52	382.38	488.22	9.34
	OSH	1035.0	1359.2	0.51	364.60	478.54	11.02
	COL	429.53	658.28	0.48	270.08	370.82	12.35
	ORG	1234.7	1515.9	0.40	533.37	608.77	10.76
	AZJ	1627.4	2288.4	0.30	452.82	590.32	7.59

NOTE: This table presents summary statistics for pre-open order volume and volume traded during the first 30 minutes of the continuous trading session for the ASX listed stocks. We report the Median, mean and relative percentage of incoming orders or volume traded. We divide the sample in three subsets, based on its relative incoming order median. The relative order entering is computed by dividing the total incoming orders during the pre-open hours by the remainder of total incoming orders that day.

D Reformulation Steps of Bivariate Conditional Density

To motivate our technique, recall that we have the following observations:

$$\begin{aligned} d_t &= I(\epsilon_t \geq 0) - I(\epsilon_t < 0) \\ \zeta_t &= \log(\epsilon_t^2) \\ \tilde{p}_t &= \log(p_t - p_t^* - J_t Z_t^p)^2 - \log\lambda_t = h_t + \zeta_t. \end{aligned}$$

Alternatively, we have the map $p_t = d_t\sqrt{\lambda_t}\exp(\tilde{p}_t/2) + p_t^* + J_t Z_t^p$. The variable ζ_t is $\log\chi^2$ distributed. The main idea is to approximate ζ_t by a mixture of normals. That is

$$g(\zeta_t) = \sum_{j=1}^{10} pr_j \mathcal{N}(\zeta_t | m_j, v_j^2).$$

Furthermore, $\eta_{t,2} \sim \mathcal{N}(0, \sigma_2^2)$. Given ϵ_t, we use the Lemma of conditional distributions to show that $\eta_{t,2}|\epsilon_t$ is normally distributed with mean $\rho\sigma_2\epsilon_t$ and variance $\sigma_2^2 - (\rho\sigma)^2 = \sigma^2(1-\rho^2)$. Note that $\zeta_t = \log(\epsilon_t^2)$ and hence, $\epsilon_t = \text{sign}(\epsilon_t)\exp(\zeta_t/2) = d_t\exp(\zeta_t/2)$. Thus, $\eta_{t,2}|d_t, \zeta_t, \rho, \sigma \sim \mathcal{N}(d_t\rho\sigma_2\exp(\zeta_t/2), \sigma_2^2(1-\rho^2))$. By Bayes' theorem we have that

$$\begin{aligned} f(\zeta_t, \eta_{t,2}|d_t, \rho, \sigma_2) &= f(\zeta_t|d_t) f(\eta_{t,2}|\zeta_t, \rho, \sigma_2) \\ &= f(\zeta_t) f(\eta_{t,2}|\zeta_t, \rho, \sigma_2) \end{aligned}$$

So using the normal mixture approximation for $f(\zeta)t)$, this yields:

$$g(\zeta_t, \eta_{t,2} \,|\, d_t, \rho, \sigma_2) = \sum_{j=1}^{10} pr_j \mathcal{N}(\zeta_t \,|\, m_j, \nu_j^2) \mathcal{N}\Big[\eta_t \,|\, d_t\rho\sigma_2 \exp(\zeta_t/2), \sigma_2^2(1-\rho^2)\Big]$$

Now we follow Omori et al. (2007), where they approximate $\exp(\zeta_t/2)$ by $\exp(m_j/2)(a_j^* + b_j^*(\zeta_t - m_j))$, which is argued that it does not depend upon ρ. Inserting this expression in the above stated formula gives the desired expression for the bivariate conditional density.

E Extended Unobserved Components Model

Our total proposed Extended Unobserved Components Model, for each security s, can be written as:

Log prices:	$p_t = p_t^* + \exp\left(\frac{h_t}{2}\right)\sqrt{\lambda_t}\epsilon_t + J_t Z_t^p$
Latent prices:	$p_t^* = p_{t-1}^* + \sigma_r r_{t-1}$
Total volatility:	$h_t = x_{t,1} + x_{t,2} + H_t'\boldsymbol{\beta} + I_t'\boldsymbol{\alpha}$
Slow volatility:	$x_{t,1} = \mu + \phi_1(x_{t-1,1} - \mu) + \sigma_1 u_{t-1,1}$
Fast volatility:	$x_{t,2} = \phi_2 x_{t-1,2} + \sigma_2(\rho\epsilon_{t-1} + \sqrt{1-\rho^2}u_{t-1,2}) + J_{t-1}Z_{t-1}^v$
Seasonal:	$\boldsymbol{\beta} \sim \mathcal{N}(0, \tau_s^2 U_s) \cdot \mathbb{1}(\boldsymbol{\iota}'\boldsymbol{\beta} = 0)$
Announcements:	$\boldsymbol{\alpha}_i \sim \mathcal{N}(0, \tau_\alpha^2 U_\alpha)$
Scale factor:	$\lambda_t \sim \mathcal{IG}\left(\frac{v}{2}, \frac{v}{2}\right)$
Jump times:	$J_t \sim \mathcal{B}ernoulli(\kappa)$
Price jumps:	$Z_t^p \sim \mathcal{N}(\mu_p, \sigma_p^2)$
Volatility jumps:	$Z_t^v \sim \mathcal{N}(\mu_v, \sigma_v^2)$

where $H_t = (H_{t,1}, ..., H_{t,K})'$, $I_t = (I_{1t}', ..., I_{nt}')'$, $I_{lt} = (I_{lt1}, ..., I_{ltX})'$, $\boldsymbol{\alpha} = (\alpha_1', ..., \alpha_n')'$, τ_s^2 and τ_α^2 are smoothing parameters used for the cubic smoothing splines (see Section 4.3) for the seasonal and announcements components, respectively, and, similarly, U_s and U_α are matrices implied by the cubic smoothing spline priors, explained in Section 4.3. For identification purposes, a zero-sum restriction is imposed on the seasonal coefficients, noted by $\mathbb{1}(\boldsymbol{\iota}'\boldsymbol{\beta} = 0)$, where $\boldsymbol{\iota}$ denotes a column vector containing ones. Similar to Weinberg et al. (2007), who do not find problems with parameter convergence, we consider the following prior distributions: $\sigma_r \sim \mathcal{IG}(0.001, 0.001)$, $\mu \sim \mathcal{N}(-6.2, 1)$, $\left(\frac{\phi_j+1}{2}\right) \sim \mathcal{B}eta(20, 1.5)$, for $j = 1, 2$ and $\phi_1 > \phi_2 > 0.5$, as proposed by Chib et al. (2002). Furthermore, $\sigma_j^2 \sim \mathcal{IG}(0.001, 0.001)$, for $j = 1, 2$, $v \sim \mathcal{DU}(2, 128)$, $\rho \sim \mathcal{U}(-1, 1)$, $\kappa \sim \mathcal{B}eta(1, 1000)$, $(\mu_p, \sigma_p^2) \sim \mathcal{NIG}(0.50, 10, 10, 1)$, $(\mu_v, \sigma_v^2) \sim \mathcal{NIG}(0.50, 10, 10, 1)$, and $\tau_j \sim \mathcal{IG}(0.001, 0.001)$, for $j = s, a$, where $\mathcal{DU}$ is the discrete uniform distribution, $\mathcal{IG}$ is the inverse gamma distribution, and $\mathcal{NIG}$ is denoted as the normal-inverse gamma distribution.

F Full MCMC Algorithm for the EUC Model

In this appendix, we show additional details of the sampling scheme discussed in Section 4.3. The sampling procedure applies on the Extended Unobserved Components model, for which a full outline is given in Appendix E. The algorithm is as fvfollows.

1. Initialise $\boldsymbol{\theta}$, $\mathbf{x}_1$, $\mathbf{x}_2$, $\boldsymbol{\omega}$, $\boldsymbol{\lambda}$, $\mathbf{J}$, $\mathbf{Z}^p$, $\mathbf{Z}^v$, $\boldsymbol{\alpha}$, $\boldsymbol{\beta}$ and $\mathbf{p}^*$.

2. Sampling $(\boldsymbol{\vartheta}, \mu, \mathbf{x}_1, \mathbf{x}_2) \,|\, \boldsymbol{\omega}, \tilde{\mathbf{p}}, \mathbf{d}, \boldsymbol{\beta}, \boldsymbol{\alpha}$ by

   (a) Sampling $\boldsymbol{\vartheta} \,|\, \boldsymbol{\omega}, \tilde{\mathbf{p}}, \mathbf{d}, \boldsymbol{\beta}, \boldsymbol{\alpha}$.

   We sample $\boldsymbol{\vartheta}$ from its conditional posterior $\pi(\boldsymbol{\vartheta} \mid rest) \propto f(\tilde{\mathbf{p}} \mid \boldsymbol{\vartheta}, \boldsymbol{\omega}, \mathbf{d}, \boldsymbol{\beta}, \boldsymbol{\alpha})\pi(\boldsymbol{\vartheta})$ by means of a Metropolis-Hastings algorithm. We compute the likelihood function $f(\tilde{\mathbf{p}} \mid \boldsymbol{\vartheta}, \boldsymbol{\omega}, \mathbf{d}, \boldsymbol{\beta}, \boldsymbol{\alpha})$ by making use of the Augmented Kalman filter in Appendix G. We estimate $\boldsymbol{\vartheta}_*$ and $\boldsymbol{\Sigma}_*$ as in Equation (13) and propose the estimator $\boldsymbol{\vartheta}^*$ from the truncated normal distribution $\mathcal{TN}_R(\boldsymbol{\vartheta}_*, \boldsymbol{\Sigma}_*)$, where $R = \{\gamma : |\phi_1|, |\phi_2| < 1, \phi_2 < \phi_1, \sigma_1^2, \sigma_2^2 > 0, |\rho| < 1\}$. However, evaluating the marginal likelihood is computational excessive due the inclusion of six heavy constraints. We, therefore, generate a proposal coefficient from the normal distribution $\mathcal{N}(\boldsymbol{\vartheta}_*, \boldsymbol{\Sigma}_*)$ after transforming the parameters $\vartheta_1 = \log(1+\phi_1) - \log(1-\phi_1)$, $\vartheta_2 = \log(1+\phi_2) - \log(\phi_1 - \phi_2)$, $\vartheta_3 = \log(\sigma_1^2)$, $\vartheta_4 = \log(\sigma_2^2)$, $\vartheta_5 = \log(1+\rho) - \log(1-\rho)$, to impose the restrictions on the parameters. Let $\boldsymbol{\vartheta}^{(i)}$ be the current point in the algorithm. We accept the proposal $\boldsymbol{\vartheta}^*$ with probability $\alpha(\boldsymbol{\vartheta}^{(i)}, \boldsymbol{\vartheta}^* | rest)$, where

$$\alpha(\boldsymbol{\vartheta}^{(i)}, \boldsymbol{\vartheta}^* | rest) = \min\left\{1, \frac{\pi(\boldsymbol{\vartheta}^* | rest) f_{TN}(\boldsymbol{\vartheta}^{(i)} | \boldsymbol{\vartheta}_*, \boldsymbol{\Sigma}_*)}{\pi(\boldsymbol{\vartheta}^{(i)} | rest) f_{TN}(\boldsymbol{\vartheta}^* | \boldsymbol{\vartheta}_*, \boldsymbol{\Sigma}_*)}\right\}.$$

   The function $f_{TN}(\bullet \mid \bullet)$ implies the truncated normal density for the proposal estimator $\boldsymbol{\vartheta}_*$. If the proposal candidate is rejected, we pick the current point $\boldsymbol{\vartheta}^{(i)}$ as the next draw.

   (b) Sampling $(\mu, \mathbf{x}_1, \mathbf{x}_2) \,|\, \boldsymbol{\vartheta}, \boldsymbol{\omega}, \tilde{\mathbf{p}}, \mathbf{d}, \boldsymbol{\beta}, \boldsymbol{\alpha}$.

   We first sample $\pi(\mu | \boldsymbol{\vartheta}, rest) \sim \mathcal{N}(Q_{n+1}^{-1} q_{n+1}, Q_{n+1}^{-1})$, where the variables Q_{n+1} and q_{n+1} are outputs from the augmented Kalman filter, described in Appendix G. Subsequently, we block sample from $\pi(\mathbf{x}_1, \mathbf{x}_2 | \mu, \boldsymbol{\vartheta}, rest)$ using the simulation smoother of Durbin and Koopman (2002), based on the Gaussian state space model in equations (9) - (11). Additional variable selection for the Kalman filter recursion is explicated in Appendix G.

3. Sampling $(\boldsymbol{\beta}, \tau_s^2) \,|\, \tilde{\mathbf{p}}, \boldsymbol{\omega}, \mathbf{x}_1, \mathbf{x}_2, \boldsymbol{\alpha}, \boldsymbol{\theta}, \mathbf{p}^*$.

   Given the states and parameters, we shape the seasonal coefficients in a Gaussian state space form. Accordingly, we define a state vector $\boldsymbol{\beta}_k^* = (\beta_k, \hat{\beta}_k)'$, where $\hat{\beta}_k$ is by definition the derivative of β_k,

and write

$$\begin{aligned} \hat{y}_k &= h'\boldsymbol{\beta}_k^* + \varepsilon_{k,1}, \quad \varepsilon_{k,1} \sim \mathcal{N}(0, \hat{\nu}_k^2) \\ \boldsymbol{\beta}_{k+1}^* &= F\boldsymbol{\beta}_k^* + \varepsilon_{k,2}, \quad \varepsilon_{k,2} \sim \mathcal{N}(0, \tau_s^2 c_k^2 U_k) \end{aligned}, \text{ where } h = \begin{pmatrix} 1 \\ 0 \end{pmatrix}, \; F = \begin{pmatrix} 1 & 1 \\ 0 & 1 \end{pmatrix}, \; U_k = \begin{pmatrix} 1/3 & 1/2 \\ 1/2 & 1 \end{pmatrix},$$

for $k = 1, ..., K_i$, where $\hat{y}_k$ and $\hat{\nu}_k^2$, and c_k are given in Equation (15) and (14), respectively. We then take the Metropolis step in Equation (17) and sample $\tilde{\boldsymbol{\beta}}$ by means of the simulation smoother. Hence, we sample $(\tilde{\boldsymbol{\beta}}, \tau_s^2)$ as a block from its unconstrained posterior. To impose the density zero-sum constraint, we set $\beta_k = \tilde{\beta}_k - (\sum_{k=1}^K \tilde{\beta}_k)/K$.

4. Sampling $(\boldsymbol{\alpha}, \tau_a^2) \,|\, \tilde{\mathbf{p}}, \boldsymbol{\omega}, \mathbf{x}_1, \mathbf{x}_2, \boldsymbol{\beta}, \boldsymbol{\theta}, \mathbf{p}^*$.

   We shape the Monday open coefficients in a Gaussian state-space form. We define the state vector $\alpha_l^* = (\alpha_l, \hat{\alpha}_l)'$, where $\hat{\alpha}_l$ is the derivative of α_l, by definition. We write

$$\begin{aligned} \hat{y}_l &= h'\boldsymbol{\alpha}_l^* + \varepsilon_{l,1}, \quad \varepsilon_{l,1} \sim \mathcal{N}(0, \hat{\nu}_l^2) \\ \boldsymbol{\alpha}_{l+1}^* &= F\boldsymbol{\alpha}_l^* + \varepsilon_{l,2}, \quad \varepsilon_{l,2} \sim \mathcal{N}(0, \tau_\alpha^2 U_\alpha) \end{aligned}, \text{ where } h = \begin{pmatrix} 1 \\ 0 \end{pmatrix}, \; F = \begin{pmatrix} 1 & 1 \\ 0 & 1 \end{pmatrix}, \; U_\alpha = \begin{pmatrix} 1/3 & 1/2 \\ 1/2 & 1 \end{pmatrix},$$

   for $l = 1, ..., 5$, where $\hat{y}_l$ and $\hat{\nu}_l^2$ are given in Equation (16). We then use the Metropolis algorithm from Section 4.3.2 to sample $(\boldsymbol{\alpha}, \tau_\alpha^2)$ as a block from its posterior.

5. Sampling $\boldsymbol{\omega} \,|\, \tilde{\mathbf{p}}, \boldsymbol{\theta}, \mathbf{x}_1, \mathbf{x}_2, \boldsymbol{\alpha}, \boldsymbol{\beta}, \mathbf{J}, \mathbf{Z}^p, \mathbf{Z}^v, \boldsymbol{\lambda}, \mathbf{p}^*$.

   For the purpose to sample ω_t, we compute the following posterior distributions:

$$\pi(\omega_t = j | rest) \propto \frac{p_j}{\nu_j} \exp\Big\{ - \frac{(\hat{p}_t - x_{t,1} - x_{t,2} - m_j)^2}{2\nu_j^2} \Big\} \exp\Big\{ - \frac{[(x_{t+1,2} - \mu) - \phi_2(x_{t,2} - \mu) - R_{j,t}]^2}{2\sigma_2^2(1 - \rho^2)} \Big\}$$

   for $j = 1, ..., 10$ mixture distributions, where $\hat{p}_t = \tilde{p}_t - s_t - a_t$ and $R_{j,t} = d_t \rho \sigma_2 [a_j + b_j(\hat{p}_t - x_{t,1} - x_{t,2} - m_j)] \exp(m_j/2)$. We sample the discrete coefficients ω_t by the inverse transformation method, implied on the above stated equation, for $t = 1, ..., n-1$. For the case of $t = n$, we replace the second exponential term by one.

6. Sampling $(\boldsymbol{\lambda}, \nu) \,|\, \boldsymbol{\theta}, \mathbf{p}, \mathbf{x}_1, \mathbf{x}_2, \mathbf{J}, \mathbf{Z}^p, \mathbf{Z}^v, \boldsymbol{\beta}, \boldsymbol{\alpha}, \boldsymbol{\omega}, \mathbf{p}^*$ by

   (a) Sampling $\nu \,|\, \boldsymbol{\theta}, \nu, \mathbf{x}_1, \mathbf{x}_2, \mathbf{J}, \mathbf{Z}^p, \mathbf{Z}^v, \boldsymbol{\beta}, \boldsymbol{\alpha}, \boldsymbol{\omega}, \mathbf{p}^*$.

   We use the Metropolis step of Stroud and Johannes (2014) to sample from $\pi(\nu | rest)$, given in Equation (18).

   (b) $\boldsymbol{\lambda} \,|\, \nu, \boldsymbol{\theta}, \nu, \mathbf{x}_1, \mathbf{x}_2, \mathbf{J}, \mathbf{Z}^p, \mathbf{Z}^v, \boldsymbol{\beta}, \boldsymbol{\alpha}, \boldsymbol{\omega}, \mathbf{p}^*$.

   Given ν and the rest of the parameters and states, we can individually sample the scale mixture components from $\pi(\lambda_t | \nu, rest)$ for $t = 1, ..., n$. We draw $(\lambda_t | \nu, rest)$ directly from its posterior,

which is inverse gamma distributed, as given in Equation (19).

7. Sampling $(\mathbf{J}, \mathbf{Z}^p, \mathbf{Z}^v) \,|\, \mathbf{p}, \mathbf{x}_1, \mathbf{x}_2, \boldsymbol{\lambda}, \kappa, \mu_p, \mu_v, \sigma_p, \sigma_v, \mathbf{p}^*$.

Conditional on the other states and parameters, we could write that $(w_t \mid J_t, Z_t, rest) \sim \mathcal{N}(J_t Z_t, \Sigma_t)$, where

$$w_t = \begin{pmatrix} p_t - p_t^* \\ x_{t+1,2} - \mu - \phi_2(x_{t,2} - \mu) \end{pmatrix}, \; Z_t = \begin{pmatrix} Z_t^p \\ Z_t^v \end{pmatrix}, \; \Sigma_t = \begin{pmatrix} \lambda_t \exp(h_t) & \rho\sigma_2\sqrt{\lambda_t}\exp(h_t/2) \\ \rho\sigma_2\sqrt{\lambda_t}\exp(h_t/2) & (1-\rho^2)\sigma_2^2 \end{pmatrix}.$$

We use conjugate priors for J_t and Z_t, as specified in Section 4.3.4. The entire conditional for jump indicators J_t and the jumps sizes Z_t are

$$\begin{aligned} Pr(J_t = 1 \mid rest) &= \frac{\kappa\phi(w_t; \mu_z, \Sigma_t + \Sigma_z)}{(1-\kappa)\phi(w_t; 0, \Sigma_t) + \kappa\phi(w_t; \mu_z, \Sigma_t + \Sigma_z)}, \\ (Z_t \mid J_t = 1, rest) &\sim \mathcal{N}((\Sigma_t^{-1} + \Sigma_z^{-1})^{-1}(\Sigma_t^{-1} w_t + \Sigma_z^{-1}\mu_z), (\Sigma_t^{-1} + \Sigma_z^{-1})^{-1}). \end{aligned}$$

8. Sampling $(\kappa, \mu_p, \mu_v, \sigma_p, \sigma_v) \,|\, \mathbf{J}, \mathbf{Z}$.

To draw from $\pi(\kappa, \mu_p, \mu_v, \sigma_p, \sigma_v \mid \mathbf{J}, \mathbf{Z})$, we assume conjugate priors, as specified in Section 4.3.4. The full conditional for the aforementioned jump parameters are

$$\begin{aligned} (\kappa \mid \mathbf{J}, \mathbf{Z}) &\sim \mathcal{B}(a_\kappa^*, b_\kappa^*), \\ (\mu_p, \sigma_p^2 \mid \mathbf{J}, \mathbf{Z}) &\sim \mathcal{NIG}(m_p^*, c_p^*, a_p^*, b_p^*), \\ (\mu_v, \sigma_v^2 \mid \mathbf{J}, \mathbf{Z}) &\sim \mathcal{NIG}(m_v^*, c_v^*, a_v^*, b_v^*), \end{aligned}$$

where, for j either p or v for notational conveniences,

$$\begin{aligned} a_\kappa^* &= a_\kappa + \sum_{t=1}^n J_t, & b_\kappa^* &= b_\kappa + n - \sum_{t=1}^n J_t & c_j^* &= c_j + \sum_{t=1}^n J_t, \\ c_j^* m_j^* &= c_j m_j + \sum_{t=1}^n J_t Z_t^j, & a_j^* &= a_j + \sum_{t=1}^n J_t, & b_j^* &= b_j + c_j m_j^2 + \sum_{t=1}^n (J_t Z_t^j)^2 - c_j^* m_j^{*2}. \end{aligned}$$

9. Sampling $\mathbf{p}^* \,|\, \mathbf{p}, \mathbf{x}_1, \mathbf{x}_2, \sigma_r, \mu, \boldsymbol{\lambda}, \mathbf{J}, \mathbf{Z}^p, \mathbf{Z}^v, \boldsymbol{\beta}, \boldsymbol{\alpha}$.

Given all the other states and parameters, we can write equations (3)-(4) as a Gaussian linear state space model. We can write the model as

$$\begin{aligned} \hat{y}_t &= p_t^* + u_{t,1}, \quad u_{t,1} \sim \mathcal{N}(0, \Gamma_t), \\ p_{t+1}^* &= p_t^* + u_{t,2}, \quad u_{t,2} \sim \mathcal{N}(0, \sigma_r^2), \end{aligned}$$

where $\hat{y}_t = p_t - J_t Z_t^p$, $\Gamma_t = \exp(h_t)\lambda_t$, and σ_r^2 is fixed. We, therefore, can use the simulation smoother of Durbin and Koopman (2002) to sample the latent market price p_t^* from its full conditional. For this purpose, we initialise $p_1^* \sim \mathcal{N}(0, c_{p^*}\sigma_r^2)$, where c_{p^*} is a large constant.

10. Sampling $\sigma_r^2 \,|\, \mathbf{p}^*$.

    For σ_r^2, we assume the conjugate prior $\sigma_r^2 \sim \mathcal{IG}(a_r/2, b_r/2)$. We can sample from the full posterior distribution $\pi(\sigma_r^2|\mathbf{p}^*)$ by retrieving a draw from

$$\sigma_r^2 \sim \mathcal{IG}\Big(a_r + n/2, \Big[b_r + c_{p^*}^{-1} p_1^* + \sum_{t=1}^{n-1}(p_{t+1}^* - p_t^*)^2\Big]/2\Big).$$

G Augmented Kalman Filter

In order to find $\boldsymbol{\vartheta}$ that maximises the conditional posterior $\pi(\boldsymbol{\vartheta} \mid rest)$, we require to evaluate the likelihood function $f(\tilde{\mathbf{p}} \mid \boldsymbol{\vartheta}, \boldsymbol{\omega}, \mathbf{d}, \boldsymbol{\beta}, \boldsymbol{\alpha})$. For this purpose, we make use of an Augmented Kalman Filter and perform likelihood computations, based on the study of De Jong (1991). Interim, assume fixed parameters $\boldsymbol{\vartheta} = (\phi_1, \phi_2, \sigma_2, \sigma_2, \rho)'$ and consider the state space model

$$\begin{aligned} y_t &= X_t\Lambda + Z_t'\xi_t + G_t u_t, \quad \text{for} \quad t = 1, ..., n, \\ \xi_{t+1} &= W_t\Lambda + T_t\xi_t + H_t u_t, \quad \text{for} \quad t = 0, 1, ..., n, \end{aligned}$$

where X_t, Z_t, W_t, T_t, G_t, H_t, for $t = 1, ..., n$, X_0, H_0 are constants, and where

- $\Lambda = l + L\mu$, $\mu \sim \mathcal{N}(c, C)$,
- $u_t \overset{i.i.d}{\sim} \mathcal{N}(0, I)$ for $t = 0, 1, ..., n$,
- $\alpha_0 = 0$, and μ is uncorrelated with the innovation terms u_t's.

In our approximated linear Gaussian state space model, given by equations (9)-(11), we fix $Z_t = (1, 1)'$,

$$G_t = (\nu_{\omega_t}, 0, 0), \;\; T_t = \begin{bmatrix} \phi_1 & 0 \\ 0 & \phi_2 \end{bmatrix}, \;\; H_t = \begin{bmatrix} 0 & \sigma_1 & 0 \\ \sigma_2 d_t \rho b^*_{\omega_t} \nu_{\omega_t} exp(m_{\omega_t}/2) & 0 & \sigma_2\sqrt{1-\rho^2} \end{bmatrix}, \;\; l = (1, 1, 0)',$$

$$W_t = \begin{bmatrix} 0 & 0 & 0 \\ J_t Z_t^v & \sigma_2 d_t \rho a^*_{\omega_t} exp(m_{\omega_t}/2) & 1 \end{bmatrix}, \;\; X_t = (m_{\omega_t}, 0, 0), \;\; L = (0, 0, 1-\phi_2)' \text{ for } t = 1, ..., n \text{ and, as}$$

initialisation, $W_0 = \begin{bmatrix} 0 & 0 & 0 \\ 0 & 0 & 1/(1-\phi_2) \end{bmatrix}$. Moreover, $\mu \sim \mathcal{N}(\mu_0, \sigma_{\mu_0}^2)$, where the priors μ_0 and $\sigma_{\mu_0}^2$

are hyperparameters. Also note that y_t corresponds to $\tilde{p}_t$ and $\xi_t = (x_{t,1}, x_{t,2})'$. When we fix μ, we can apply the standard Kalman filter. We initialise $\hat{\xi}_{1|0} = W_0\Lambda$ and $P_{1|0} = H_0H_0'$. The Kalman filter recursion follows

$$\begin{aligned} D_t &= Z_t'P_{t|t-1}Z_t + G_tG_t', & K_t &= (T_tP_{t|t-1}Z_t + H_tG_t')D_t^{-1} \\ L_t &= T_t - K_tZ_t', & P_{t+1|t} &= T_tP_{t|t-1}L_t' + H_t(H_t - K_tG_t)' \\ e_t &= y_t - X_t\Lambda - Z_t'\hat{\xi}_{t|t-1}, & \hat{\xi}_{t+1|t} &= W_t\Lambda + T_t\hat{\xi}_{t|t-1} + K_te_t, \end{aligned}$$

for $t = 1, ..., n$. Additionally, we consider the following equations to extent towards the Augmented Kalman filter:

$$\begin{aligned} f_t &= y_t - X_tl - Z_t'\xi^*_{t|t-1}, & \xi^*_{t+1|t} &= W_tl + T_t\xi^*_{t|t-1} + K_tf_t \\ F_t &= X_tL - Z_t'\Xi^*_{t|t-1}, & \Xi^*_{t+1|t} &= -W_tL + T_t\Xi^*_{t|t-1} + K_tF_t, \end{aligned}$$

for $t = 1, ..., n$, where $\xi^*_{1|0} = W_0l$ and $\Xi^*_{1|0} = -W_0L$. It is computational efficient to note that

$$e_t = f_t - F_t\mu, \qquad \xi_{t+1|t} = \xi^*_{t+1|t} - \Xi^*_{t+1|t}\mu.$$

In order to find the parameters $\boldsymbol{\vartheta}$ that optimise the posterior density $\pi(\boldsymbol{\vartheta} \mid rest)$, we have to maximise the (log) likelihood function. Note that the the log likelihood function, given μ, can be written as

$$\log f(y \mid \mu) = -\frac{1}{2}\Big\{n\log 2\pi + \sum_{t=1}^{n}\log|D_t| + \sum_{t=1}^{n}f_t'D_tf_t - 2\Big(\sum_{t=1}^{n}F_t'D_t^{-1}f_t\Big)'\mu + \mu'\Big(\sum_{t=1}^{n}F_t'D_t^{-1}F_t\Big)\mu\Big\}.$$

Furthermore, the posterior distribution of μ, conditionally on y, is normally distributed with mean $Q_{n+1}^{-1}q_{n+1}$ and variance Q_{n+1}^{-1}, so that is $\mu \sim \mathcal{N}(Q_{n+1}^{-1}q_{n+1}, Q_{n+1}^{-1})$, where

$$q_{t+1} = q_t + F_t'D_t^{-1}f_t, \quad q_1 = C^{-1}c, \quad Q_{t+1} = Q_t + F_t'D_t^{-1}F_t, \quad Q_1 = C^{-1},$$

for $t = 1, ..., n$. Hence, to obtain the full likelihood of y, we can write

$$\begin{aligned} \log f(y) &= \log f(y \mid \mu) + \log\pi(\mu) - \log\pi(\mu \mid y) \\ &= \text{constant} - \frac{1}{2}\Big\{\sum_{t=1}^{n}\log|D_t| + \sum_{t=1}^{n}f_t'D_t^{-1}f_t + c'C^{-1}c + \log|Q_{n+1}| - q_{n+1}'Q_{n+1}^{-1}q_{n+1}\Big\}. \end{aligned}$$

H Simulation Samples

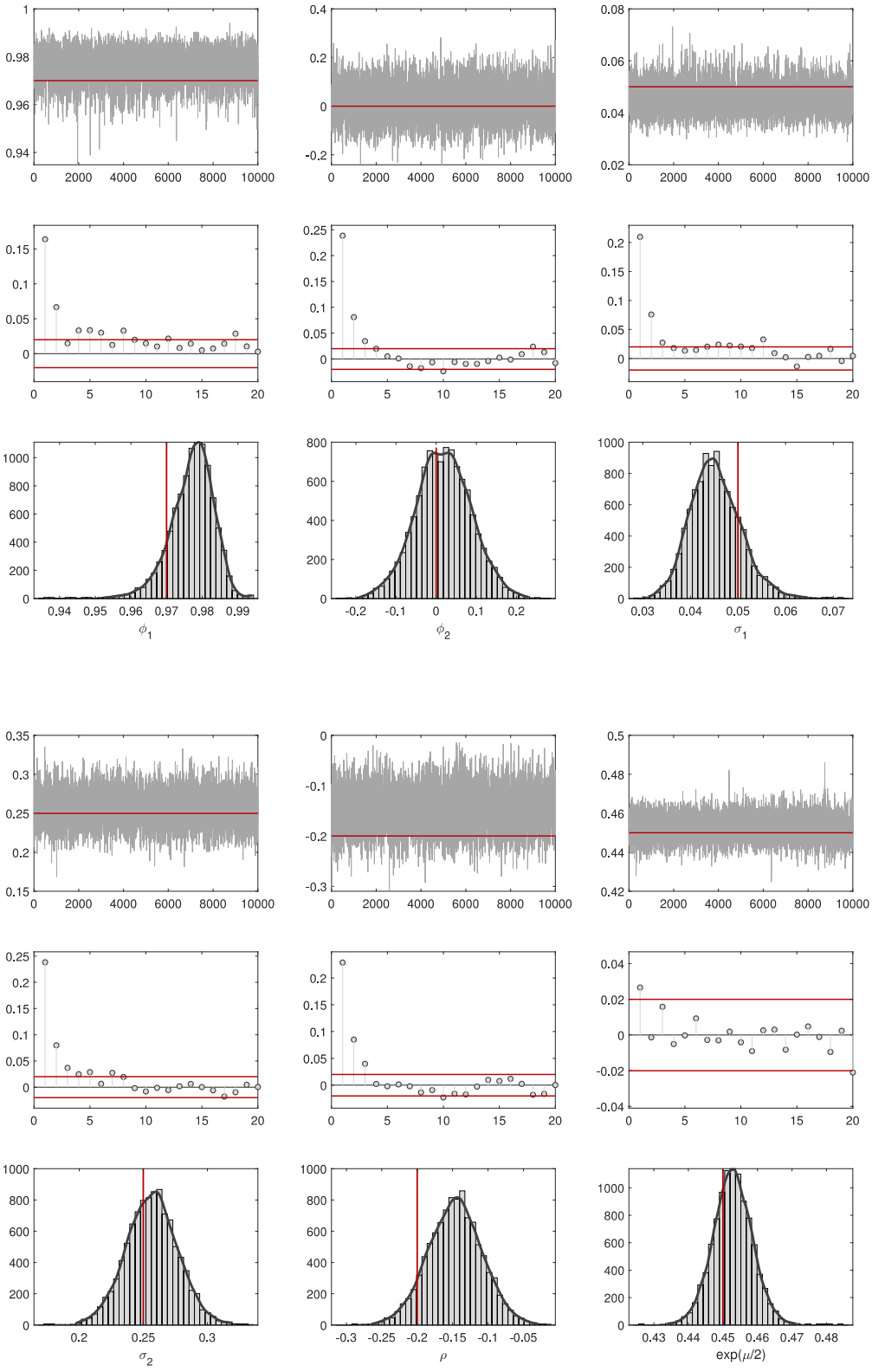

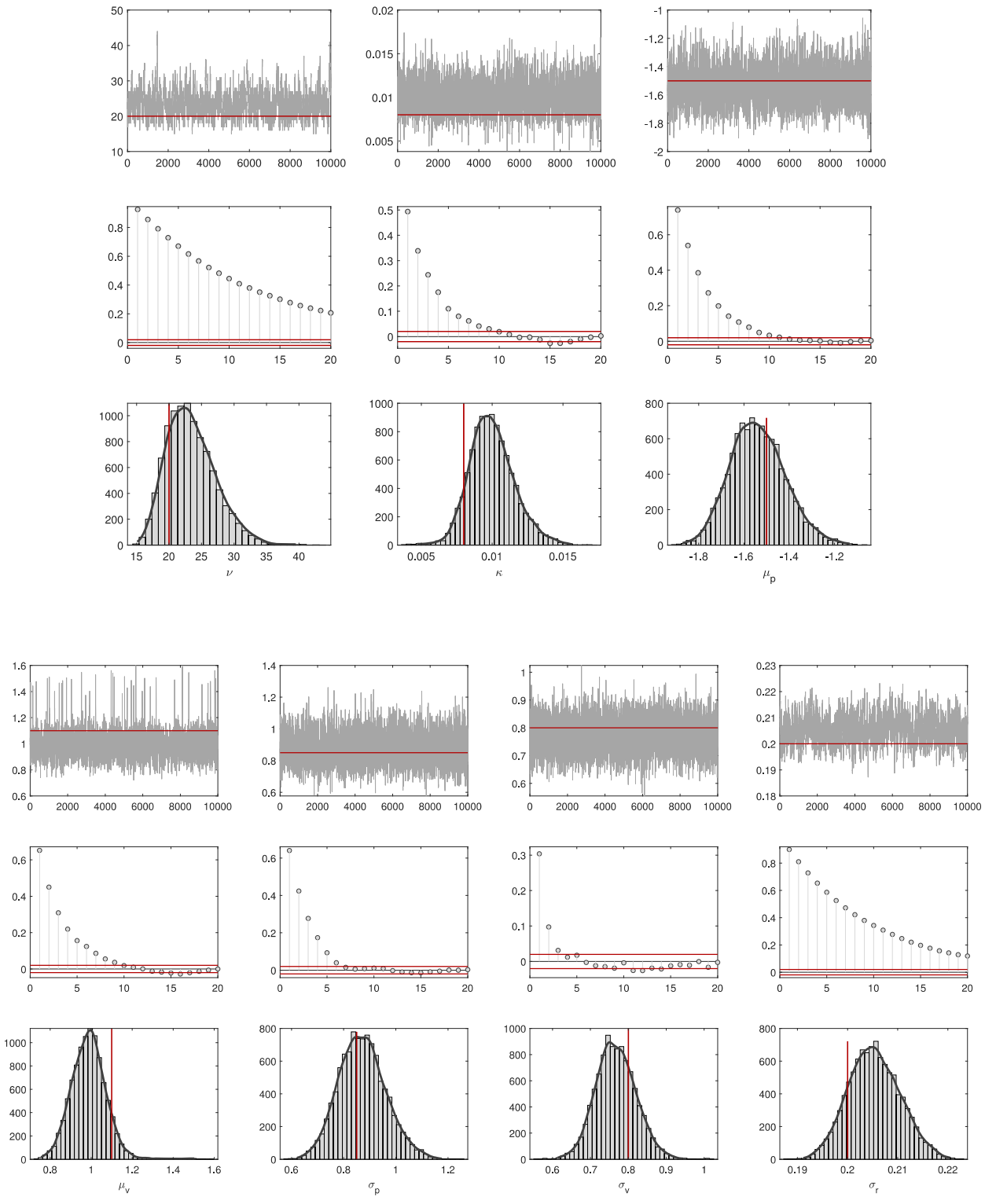

Figure 11: This figure presents samples from the posterior distributions, based on our simulation study. For each parameters, we report the sample paths (top), sample autocorrelations (middle), and posterior density functions (bottom). The red line in the top and bottom figures represents the true parameter value. The red lines in the autocorrelograms correspond to the 95% confidence intervals.